Diffusion in Aggregated Soil

CENTRALE LANDBOUWCATALOGUS
0000 0478 5586

Promotoren: dr. ir. C.T. de Wit,
emeritus hoogleraar in de theoretische teeltkunde

ir. J.H.G. Verhagen,
toegevoegd docent, vakgroep Theoretische Produktie Ecologie

pUDC201, 1992

C. Rappoldt

Diffusion in Aggregated Soil

Proefschrift

ter verkrijging van de graad van
doctor in de landbouw- en milieuwetenschappen,
op gezag van de rector magnificus,
dr. H.C. van der Plas,
in het openbaar te verdedigen
op vrijdag 6 maart 1992
des namiddags te vier uur in de Aula
van de Landbouwuniversiteit te Wageningen

BIBLIOTHEEK
LANDBOUWUNIVERSITEIT
WAGENINGEN

Omslagontwerp: Hans van der Linde, Nijmegen
Omslag illustratie: "Grond", olieverf op doek, Hans van der Linde, 1990
Druk: Van Denderen B.V., Groningen

NN08201, 1476

Stellingen

1. De beschrijving van microbiologische processen in de bodem in samenhang met transportprocessen vereist een model dat op meetbare statistische eigenschappen van de bodemstruktuur is gebaseerd.
   Dit proefschrift

2. Voor het verkrijgen van een representatief beeld van de bodemstruktuur is het efficiënter om van een groot aantal bodemmonsters een doorsnede te analyseren dan om van een klein aantal monsters de ruimtelijke struktuur te bepalen.
   Dit proefschrift

3. Indien geen onderscheid te maken is tussen macroporiën enerzijds en de bodemmatrix anderzijds, dan hebben modellen voor een enkel bodemaggregaat geen betekenis voor de betreffende bodem.
   Dit proefschrift

4. Een heterogene verdeling van activiteit in een bodemaggregaat kan leiden tot processen die kwalitatief verschillen van die in een homogeen aggregaat.
   Dit proefschrift

5. Het toekennen van een invloedssfeer aan elke wortel van een wortelstelsel, zoals voorgesteld door Barley, leidt tot een onnodig gecompliceerde beschrijving van het nutriëntentransport naar de wortels.
   Barley, K.P., 1970. The configuration of the root system in relation to nutrient uptake. Adv. Agron. 22:159-201.
   Dit proefschrift

6. De bestaande programmeertalen voor het beschrijven van continue processen hebben een grote educatieve betekenis, maar schieten tekort in het onderzoek.

7. De door Ingold en Gregory geponeerde electrostatische kracht, die een spore op de as van een buisje van een buisjeszwam houdt, bestaat niet.
   Ingold, C.T., 1957. Spore liberation in the higher fungi. Endeavour 16:78-83.
   Gregory, P.H., 1973. The microbiology of the atmosphere. Leonard Hill Ltd. London. (2-nd edition)

8. Voordat een fysicus kritiek uitoefent op het ontbreken van opgegeven foutenmarges in het kwantitatieve werk van een bioloog, dient hij zich eerst af te vragen hoe hij zèlf de temperatuur op een warme zomerdag zou opgeven.

9. De druk op onderzoekers om in ambtelijk beoordeelde projektvoorstellen onrealistische verwachtingen te wekken leidt tot een zichzelf in stand houdend systeem van onderzoeksfinanciering gebaseerd op wederzijds zelfbedrog, tot het gebruik van ongeteste modellen en tenslotte tot het bedrijven van wat Feynman heeft genoemd "Cargo Cult Science".
   Feynman, R.P. , 1986. Surely you are joking Mr. Feynman. Bantam Books. New York.

10. De constatering van Russell: "The most elementary failure in Russia is in regard to food" heeft niets aan actualiteit ingeboet.
    Bertrand Russell in "Why Russian Communism has Failed", Chapter VI from "The practice and theory of bolshevism", Unwin Books, London, 1920.

11. Het handhaven van tariefmuren tegen de invoer van produkten uit de vroegere satellietstaten van de Sowjetunie naar de Europese Gemeenschap is, behalve immoreel, ook gevaarlijk.

12. Je moet schaatsen als er ijs is.

Stellingen behorend bij het proefschrift van C. Rappoldt: Diffusion in aggregated soil. Wageningen, 6 maart 1992.

Abstract

Rappoldt, C., 1992. Diffusion in aggregated soil. Doctoral thesis, Wageningen Agricultural University, Wageningen, The Netherlands

The structure of an aggregated soil is characterized by the distribution of the distance from an arbitrary point in the soil to the nearest macropore or crack. From this distribution an equivalent model system is derived to which a diffusion model can be more easily applied. The model system consists of spherical, or cylindrical or plane aggregates, which do not represent the individual aggregates of the soil, however. The radii of the spheres, cylinders or plane sheets represent different length scales occurring in the soil structure and the relative abundance of each radius is expressed as a weight factor. These weight factors are derived by conserving the distance distribution of the soil: the real soil and the model system have the same distance distribution. This implies that the length scales occurring in the two systems are the same and that diffusion processes take place in approximately the same way. A model of diffusion in soil aggregates is evaluated by solving a differential equation for a spherical, a cylindrical or a plane geometry. The overall result for the soil is then found as a weighted sum of the results for the various length scales or radii.

In case of an isotropic soil structure, the weight factors for a cylinder system can also be obtained from distances measured in a cross section of the soil. The measurements may be carried out by means of image analysis.

The "scale method" is also applied to root systems with a non-regular root distribution. Theoretically calculated nutrient uptakes show good agreement with exact results in the literature obtained with an electrical analogue.

For a cracked clayey soil, the crack pattern observed in the field is compared with the distribution of anoxic soil. In case of a uniform soil activity, anoxic soil is expected to occur in the centres of the crumbs only. Part of the anoxic soil, however, was found within 1 mm from a crack. From the measured local diffusivity of oxygen it is concluded that the anaerobiosis near cracks is caused by a local soil activity exceeding the overall soil respiration by at least a factor 100. The presence of highly active and anoxic "hot spots" near macropores or cracks implies that denitrification may take place by the flow of water through the hot spots and without nitrate diffusion.

Key words:

soil structure, image analysis, model soil, soil aggregates, oxygen diffusion, anaerobiosis, denitrification, plant roots, worm burrows

Dankwoord

Dit proefschrift is tot stand gekomen met hulp van velen. Mijn beide promotoren C.T. de Wit en J.H.G. Verhagen wil ik bedanken voor de gelegenheid die ik heb gehad om in een bijzonder veelzijdige onderzoeksomgeving aan een fysisch onderwerp te werken. Ik dank hen voor de talloze gesprekken over moeilijkheden, resultaten en manuscripten en voor de vrijheid bij het op eigen wijze uitwerken van het onderwerp. Jan Verhagen wil ik ook bedanken voor het nalopen van alle wiskundige afleidingen en voor het mij bijbrengen van een wat grotere netheid. De begeleiding door Kees de Wit vond plaats tegen de achtergrond van kameraadschappelijke bijeenkomsten van het "promotieteam", waarvan verder deel uitmaakten Daniël van Kraalingen, Gerrie van de Ven, Sanderine Nonhebel, Martin Kropff, Radha Ranganathan en Niek van Duivenboode. Het van zo nabij volgen van onze tegenslagen en vorderingen op heel verschillende vakgebieden was heel bijzonder en ik heb daar meer van geleerd dan ik hier kan zeggen. Een bron van inspiratie waren ook de vragen en opmerkingen van Jan Goudriaan en Pieter Raats.

Het onderzoek is grotendeels uitgevoerd op de vakgroep Theoretische Productie Ecologie (TPE) van de Landbouwuniversiteit en het werd gefinancierd door de Programmacommissie Basiskennis Bodemonderzoek. Peter Leffelaar wil ik bedanken voor de faciliteiten die hij mij bood in zijn laboratorium op het Centrum voor Agrobiologisch Onderzoek (CABO), voor al zijn adviezen in bodemfysische zaken en voor het indertijd opstellen van een ruime begroting. De directie van het Instituut voor Bodemvruchtbaarheid, alsmede Pieter Raats, Klaas Harmanny, Bram de Vos en Marius Heinen van de afdeling Bodemfysica ben ik erkentelijk voor de mogelijkheid mijn proefschrift in Haren af te ronden.

Velen hebben bijgedragen aan het experimentele werk. Toon Helmink heeft gedurende anderhalf jaar als assistent voor mij gewerkt. Hij heeft zich in het bijzonder beziggehouden met het kleuren van zuurstofloze grond en met het meten van bodemrespiratie. Aan ons gezamenlijk veldwerk bewaar ik goede herinneringen. Ik dank hem verder voor alles wat hij wist te regelen. Advies inzake de kleuring van grond hebben wij gekregen van de heer L.T. Begheijn van de vakgroep Bodemkunde en Geologie. De heer B. Kroesbergen van de vakgroep Grondbewerking heeft diffusiecoëfficiënten gemeten. Jan van Kleef van het CABO hielp met het meten van spectra en Peter Stad en Lucien van Kroonenburg gaven fotografische adviezen.

Het veldwerk heb ik samen met Toon Helmink verricht op proefboerderij "De Bouwing" van het CABO. Felix de Bekke, Johan Hartholt en W. de Jager wil ik hierbij bedanken voor hun hulp en voor hun koffie. Thuis in Naarden heeft mijn

vader mij geholpen met het afdrukken van de in het veld gemaakte foto's. Met de digitalisering van de foto's ben ik geholpen door Dik Schoonderbeek van het Staringcentrum en door Fabio Maselli van het IATA-CNR in Florence.

Zonder de inspanningen van electronici en instrumentmakers is onderzoek nu eenmaal niet mogelijk. De meetopstelling voor zuurstofelektroden werd gebouwd in werkplaatsen van de Landbouwuniversiteit door Ton Erenst, Leo Herben, J. van de Goor en Evert Janssen. Allerhande losse onderdelen werden gemaakt door C.W. Holleman, instrumentmaker op het CABO. De elektroden zelf zijn kunstig geconstrueerd door Jan Beukema op de vakgroep Microbiologie in Groningen. Ik dank hem en Hans van Gemerden voor de samenwerking.

Ook bij het theoretische werk heb ik hulp gehad. Cajo ter Braak gaf mij een spoedcursus in Poisson clusters, Peter de Willigen hielp met een opnamemodel voor plantewortels en ook met wortels van Besselfunkties, Cees van Diepen stelde zijn uitgebreide bodemkundige kennis ter beschikking en beschreef voor mij in verantwoorde termen de grond op proefboerderij "De Bouwing". Naast hierboven al genoemde mensen hebben ook M.G. Huck en H. Terburg commentaar gegeven op mijn manuscripten.

Het rekenwerk zou veel moeilijker zijn geweest zonder de intensieve samenwerking met Daniël van Kraalingen op het gebied van programmatuur. Het geeft voldoening om te zien dat ook andere onderzoekers profiteren van de door ons gemaakte programma's.

Alle leden van de vakgroep TPE wil ik bedanken voor de plezierige tijd die ik daar heb doorgebracht. Met Lammert Bastiaans heb ik een kamer gedeeld, Rudy Rabbinge was voorzitter van de vakgroep en met ontelbaar veel zaken ben ik geholpen door Gon van Laar, Bert van Amersfoort, Lien Uithol, Rob Dierkx en Hennie de Ruiter. Verder wil ik Hein ten Berge, Willem Stol en Herman van Keulen van het CABO bedanken voor de samenwerking op het gebied van water en regenval en een heleboel mensen van "Born Zuid" voor de gezelligheid.

De omslag van dit boekje is gemaakt door Hans van der Linde. Tenslotte dank ik Marcel Kersten voor zijn bijdragen aan de layout en voor zijn gastvrijheid, zowel op het biologisch station "De Herdershut" op Schiermonnikoog, als in Groningen tijdens de spreekwoordelijke laatste loodjes.

Contents

1. **Introduction** 1
   - Soil structure and transport processes
   - The replica approach and the scale approach
   - The concept of an aggregated soil
   - Outline of the thesis

2. **The application of diffusion models to an aggregated soil** 7

   Introduction 7

   Method for a single aggregate 8
   - The surface-to-volume ratio
   - Soil respiration as a zero-order absorption process
   - A first-order absorption process
   - A sudden change in outer concentration
   - Discussion of results for a single aggregate

   Method for an aggregated soil 15
   - An anology
   - The distance probability density function $s(x)$
   - The function $s(x)$ as a generalized surface-to-volume ratio
   - A model soil derived from a continuous $s(x)$
   - A model soil derived from N distance probabilities
   - Example
   - Testing the method
   - Results for an aggregated soil
   - Numerical aspects

   Adaptation to wormholes and roots 27

   Conclusions 28

   Appendix 30
   - A continuous $s(x)$
   - Approximation of a continuous solution with N probabilities p_i
   - Matrix method
   - Solution for plane sheets
   - Solution for cylinders
   - Solution for spheres
   - Cylinders with a hole or root along the axis
   - A lognormal sphere radius distribution

3. **The use of cross-sectional data in diffusion models for an aggregated soil** 37

   Introduction 37

   Method 38
   - The use of spatial distances
   - The use of cross-sectional data
   - The cross section of randomly positioned spheres
   - Generation of a finite sample
   - A model of anaerobiosis

   Results 45
   - An infinite sample size

A finite sample size
Studying the sample instead of the soil
Conclusions 49
Appendix 50
The function $s^*_S(R,x)$ for a randomly intersected sphere
The function $s^*_C(R,x)$ for a randomly oriented cylinder
The calculation of cylinder volume fractions
$s^*(x)$ for a set of spheres

4. **Measuring the diffusivity of oxygen in soil on a millimeter scale** . . 55
Introduction 55
Method 57
The influence of macropores
Some experimental details
Data analysis
Testing the method
Results 66
Discussion 67

5. **A simple model of non-uniform respiration in a soil aggregate** . . . 69
Introduction 69
Model 71
The respiration rate of the aggregate
A random position of the active zone
The probability on anaerobiosis 76
Conclusions 77

6. **Anaerobiosis in a clayey soil** (with A. Th. Helmink) 79
Introduction 79
Material and methods 80
Field site and soil
Macroscopic soil respiration
Oxygen diffusion
Detection of anaerobiosis
Soil structure
Image processing
Image analysis
Results 89
The macro-scale oxygen distribution
The meso-scale oxygen distribution
Model systems
Discussion 94
Anoxic soil close to cracks
Oxic soil far from cracks
The distribution of soil activity
Some consequences of non-uniform activity

7. **Application of nutrient uptake models to non-regular distributions of roots** 99
Introduction 99
Method 102
The distance probability density function $s(x)$
Derivation of a weight function $v(R)$
Justification for the conservation of $s(x)$
The application of an uptake model
Quadratic scales
Examples
The analysis of measured distances 110
A linear distance scale
A quadratic distance scale
Application of a zero-sink uptake model 114
The model for a root in a soil cylinder
The approximate solution for a root system
Uptake calculations for three root distributions
Comparison with electrical analogue data
Comparison with Dirichlet tesselation
Comparison with data for clustered root patterns
The characteristic soil depletion time
Conclusions 123
Appendix 125
The weight functions $w(a)$ and $v(R)$
The matrix solutions
Details of the zero-sink uptake model
The weight function for Poisson clusters

8. **Worm burrows in a homogeneous clay soil** 129
Introduction 129
Description of the soil 130
A geometrical model 132
Volume and surface densities
Distance probability density functions
Generation of a spatial model system
Surface patterns
Experiments 138
Orientation and distribution of burrows
Sulfide oxydation
Discussion 142

Summary 145
Samenvatting 151
References 159
Curriculum Vitae 162

Account

Except the Introduction, the chapters of this thesis have been written in the form of journal papers. One paper has been published. The others, with minor changes in figures or text, have been submitted or will soon be submitted to various journals.

Chapter 2 Rappoldt, C. 1990. The application of diffusion models to an aggregated soil. Soil Science 150: 645-661.

Chapter 3 Rappoldt, C. 1992. The use of cross-sectional data in diffusion models for an aggregated soil. Submitted to Soil Science.

Chapter 4 Rappoldt, C. 1992. Measuring the diffusivity of oxygen on a millimeter scale. This paper will be submitted to Journal of Soil Science.

Chapter 5 Rappoldt, C. 1992. A simple model of non-uniform respiration in a soil aggregate. This paper will be submitted to Modeling of Geo-biosphere Processes.

Chapter 6 Rappoldt, C. and A. Th. Helmink. 1992. Anaerobiosis in a clayey soil. This paper will be submitted to Journal of Soil Science.

Chapter 7 Rappoldt, C. 1992. Application of nutrient uptake models to non-regular distributions of roots. Submitted to Soil Science Society of America Journal.

Chapter 8 Rappoldt, C. 1992. Diffusion near worm burrows. Submitted to Geoderma.

Chapter 1

Introduction

The presence or absence of oxygen influences biological and chemical processes in soil. An important example is denitrification, the reduction of nitrate to nitrous oxides and nitrogen gas. In agricultural soil this leads to loss of fertilizer which may cause a reduction of crop yield. Denitrification takes place when nitrate is present, organic matter is available as an energy source, and the oxygen concentration is zero or extremely low. Conditions in a soil usually vary from place to place since the microbiological processes themselves affect the conditions in the soil. Soil respiration, for instance, leads to a decrease of the local oxygen concentration. When the respiration and the resistance for oxygen transport are large enough, the oxygen concentration may locally fall to zero. Greenwood (1961) and Currie (1961) modelled this process for a homogeneous, spherical soil aggregate. When the aggregate is sufficiently large, an anoxic zone develops in its centre. Leffelaar (1987) and Arah & Smith (1989) described denitrification in such an anoxic aggregate centre. Their models combine a description of the microbiological process taking place with a description of the diffusive transport of the solutes and gases involved.

This short overview shows that anaerobiosis and denitrification are phenomena which occur at the scale of soil aggregates. For a single, homogeneous aggregate with a spherical or cylindrical shape, the transport of water and gas has been described well. For a structured soil, however, it is not clear how even the simplest calculation on anaerobiosis should be carried out. Smith (1977) and Arah & Smith (1989) use homogeneous, spherical soil aggregates with different diameters. The sphere diameters have a lognormal distribution derived from measured aggregate sizes. Real soil aggregates, however, are neither spherical nor homogeneous and the relation between the sphere model and real soil remains unclear. In other words, the existing models for anaerobiosis and denitrification in a structured soil have merely a demonstrative character. They are not operational and therefore not testable.

It seems to me that, somehow, soil physical theory should account for the complexity of real soils. This does not imply that the structure of a soil has to be known in full detail in order to calculate, for instance, an anoxic fraction. By

means of a physical analysis, those properties of the soil structure should be identified that determine diffusive transport. And only those, possibly abstract properties need to be incorporated in a model. This approach will be introduced more fully in the next two sections of this introduction. The last section gives an outline of the thesis.

Soil structure and transport processes

Describing the structure of a soil, different scale levels can be distinguished. The micro-scale is the scale of the individual particles and the pores between them. When the soil is a homogeneous porous medium, the micro-scale is the only scale on which a structure exists. The soil particles usually form aggregates, however, and the sizes of these aggregates define the meso-scale of the soil structure. Finally, the macro-scale is associated with the vertical soil profile. Different layers of a soil will usually have different properties on the micro- or meso-scale.

Transport processes can be studied on the different scale levels. The flow of water, for instance, can be described on the micro-, meso-, or macro-scale. A typical macroscopic phenomenon is bypass flow, fast downward flow of water through macropores after heavy rainfall.

Macropores play a similar role in case of oxygen transport. They remain air-filled under most circumstances and oxygen easily reaches soil layers to a depth of half a meter, for instance. Close to well aerated macropores, however, partially anoxic aggregates may occur and the study of macroscopic gradients and flows is therefore not sufficient. Anaerobiosis is essentially a meso-scale phenomenon and its description requires the quantification of processes at the aggregate level. Somehow, the detailed models of oxygen diffusion which exist for idealized soil aggregates have to be incorporated into a model for the whole soil.

This thesis forms an attempt to solve this problem. The desired model is operational and accounts for the complexity of a real soil structure. An accurate solution to this problem seems impossible, however, and the accuracy demands are necessarily moderate. A model deviating twenty or thirty percent from observed values will usually be unacceptable in theoretical physics. Describing a complex soil, such deviations might very well represent the maximum achievable accuracy.

In developing a transport model for a complex structure, two approaches can be distinguished. One may first try to make a precise geometrical model of the structure and then, essentially by simplification, find out which properties of the structure are the relevant ones in combination with a transport process. A second

and faster method is to make a motivated guess. The two methods are called the replica approach and the scale approach, respectively. They are discussed in more detail in the next section.

The replica approach and the scale approach

The visually oriented replica approach starts with a complete description of the geometry of the system. This description is kept as realistic as possible. Subsequently, differential equations describing the transport process are solved for the model system. The ideal is to solve differential equations for a mathematical replica of the studied system. This will usually require a large computational effort and the calculations have to be repeated many times in order to obtain results as function of all sorts of properties of the replica structure. The most relevant properties can be selected then as the basic ones for a simpler and operational model of the system.

The process oriented scale approach is based on a physical analysis of the system. In a structured soil, aggregates occur with different shapes and sizes. The process studied will take place, therefore, on various length and time scales simultaneously. These characteristic lengths and times need to be derived somehow from the observed structure of the system. An approximate model is then based on the derived scales only. Other properties of the system are assumed to be of minor importance and are neglected.

The scale approach is generally identified with basic insight in the system and with order of magnitude calculations, while the replica approach is identified with accuracy. For several reasons, this picture is misleading as a starting point in modelling a complex geometry.

The first reason is that the formulation of a replica model will generally be difficult and inevitably leads to simplifications. Some details of the structure have to be neglected, although the model is still meant as a geometrical replica of the system. The simplifications tend to be of a purely geometrical nature, however, and nothing guarantees that physically important properties are conserved in the model. In Chapter 7 a replica model of root systems is discussed that indeed suffers from a systematic error as a result of straightforward geometrical simplification.

The second reason is simply that a model system based on just length and time scales may already be sufficiently accurate. In this thesis, the scale approach is applied to aggregated soil (Chapters 2 and 3) and to root systems (Chapter 7). It is shown that the scale approach alone leads to operational,

quantitative models of diffusion processes. The reason behind this result is the fortunate property of diffusion processes of being only weakly influenced by the shape of the aggregates. Therefore, diffusive transports can be calculated with a sufficient precision from the prevalent length scales only.

The concept of an aggregated soil

Most chapters in this thesis consider aggregated soil. The term is not used simply as a synonym for a structured soil. In an aggregated soil a distinction can be made between a relatively uniform macropore space on the one hand and the aggregated particles on the other hand. The aggregated particles form the "soil matrix", which is surrounded and penetrated by the macropores. Concentration gradients in the macropore space will generally be smaller than the gradients in the soil matrix. Then, there is a locally uniform macropore space surrounding the soil matrix. Note that the soil particles may form complicated structures, which need not consist of neat, distinct aggregates.

Diffusion models developed for a single soil aggregate can be applied to an aggregated soil. These models are usually formulated for a spherical or cylindrical aggregate shape. Examples are the model of Greenwood (1961) and Currie (1961) for anaerobiosis in a spherical aggregate, and the detailed model of anaerobiosis and denitrification in a soil cylinder developed by Leffelaar (1987). Using the scale approach, these models can be evaluated for the whole soil.

When concentration gradients in the macropores interfere with gradients in the soil matrix, the soil structure lacks a clear aggregate level. Consequently, diffusion models for a single aggregate cannot be applied to the soil. This problem has not been solved in this thesis.

Outline of the thesis

The subject of the main part of this thesis is diffusion in aggregated soil with special attention for oxygen diffusion and anaerobiosis. In Chapter 2 the scale method is described for diffusion in aggregated systems. The characteristic length scales on which diffusion takes place are derived from a distance distribution, which can be measured for a certain soil structure. In Chapter 3 a few practical aspects of the developed method are investigated. The scale method is adapted to the use of measurements carried out in a cross section of the soil instead of in the three dimensional soil structure. Further, the consequences of a limited sample size are discussed for a model on anaerobiosis.

The parameters occurring in diffusion models for soil aggregates should be measured on the meso-scale, the scale of the aggregates themselves. In Chapter 4 the diffusivity of oxygen in soil is measured on a millimeter scale. In Chapter 5 the consequences of heterogeneity on the aggregate scale are studied. When only a part of the soil is active, respiration models become very different from models for homogeneous soil. The results of the Chapters 4 and 5 are used in Chapter 6 to interpret field data on aeration and soil structure obtained for a cracked clayey soil. The aggregates of this soil appear not to be homogeneous. The differences in local soil activity are at least a factor 100. This means that the occurrence of anaerobiosis is largely determined by the distribution of highly active parts of the soil or "hot spots". This has important consequences for the formulation of models of anaerobiosis or denitrification.

The scale approach appears to be fruitful also in another field. In Chapter 7 the method is used to calculate the effect of the root distribution on the nutrient uptake by a root system. Chapter 8 describes a brief study on worm burrows in a homogeneous clay soil. In model calculations, a system of worm burrows can be treated in the same way as a root system. The burrows studied have a profound effect on soil aeration.

Chapter 2

The application of diffusion models to an aggregated soil

Abstract. In models on diffusive transport it is necessary to make use of a simplifying description of the geometry of an aggregated soil. It is proposed to use a (hypothetical) model soil consisting of spherical, cylindrical or flat aggregates. The model aggregates have different sizes and each size class occupies a certain fraction of the total volume. These volume fractions, or weight factors, can be calculated in such a way that diffusive transports take place in approximately the same way in soil and model soil.

The method is operational. The quantity to be measured is the shortest distance from a randomly chosen point to the inter-aggregate space. The desired volume fractions can be derived from the probability distribution of this distance. The procedure does not require the existence of individual aggregates and may be applied, for instance, to a cracked clay soil.

The use of a simple model soil is based on the shape independence of diffusion processes. This shape independence has been verified by means of theoretical calculations for both a single aggregate and an aggregated soil.

INTRODUCTION

In the literature detailed studies can be found on diffusion processes in soil aggregates. Smith (1977) used a model for oxygen diffusion and soil respiration to describe anaerobiosis, and Leffelaar (1987) studied water flow and gas diffusion in relation with denitrification. In general, a diffusion model will be based on a differential equation describing the process taking place. The equation contains a term for diffusive transport and there may be source and sink terms describing chemical reactions.

The application of a model to an aggregated soil means that a differential equation is solved for the whole soil. That requires a simplifying description of the soil geometry. In this paper appropriate simplifications are studied for a single aggregate with an irregular shape and for an aggregated soil.

For a single aggregate there is an approximate method available which is

commonly used by process engineers. The real aggregate is replaced by a simpler one for which all calculations are carried out. The simple model aggregate should only have the same surface-to-volume ratio as the real aggregate. In fact, this ratio S/V is the only geometric property of the aggregate used.

An aggregated soil consists of a porous medium and of macropores. The porous medium may be present in the form of separate aggregates, but that is not necessarily the case. It may also consist of structures with a complicated shape, in which no separate aggregates can be distinguished (Fig. 2.1). These

Figure 2.1. An aggregated soil may consist of interconnected clods forming a complicated structure. The drawing shows a hypothetical cross section.

structures may have very different sizes, and their surface may be rough. The porous medium will be denoted as the intra-aggregate space and the macropores as the inter-aggregate space. A cracked clayey soil, for instance, consists of (interconnected) clods and cracks, forming the intra- and inter-aggregate space respectively.

The proposed method for applying a diffusion model to an aggregated soil is a generalization of the method for a single aggregate. This generalization is the main subject of this paper. The geometry of a soil is characterized by means of a function closely related to an S/V ratio. This function can be derived from images of the soil structure. Hence the method is operational and can be used, in principle, to combine image analysis with diffusion models.

METHOD FOR A SINGLE AGGREGATE

The surface-to-volume ratio

A single aggregate with an arbitrary shape is considered. It has an outer surface S and a volume V. It is shown in this section that the result of a

diffusion process is largely determined by the surface-to-volume ratio S/V. Aggregate shape is of minor importance and, the actual aggregate shape may be replaced by the simpler shape of an equivalent aggregate. An equivalent aggregate is a hypothetical sphere, cylinder or plane sheet with the same S/V ratio as the real aggregate.

A sphere is fully described by its radius R. Its surface-to-volume ratio is $3/R$ and the radius of the equivalent sphere belonging to a certain S/V ratio becomes $3V/S$. The cylinders considered in this paper are long, and any influence of the "top" and "bottom" surfaces is neglected. An equivalent cylinder is described by its radius, which is calculated as $2V/S$. Finally, plane sheets are large and flat ; "end" effects are neglected, and a plane sheet is fully described by its thickness. If the plane sheet radius is defined as half its thickness, the radius of an equivalent plane sheet is $1V/S$.

The use of an equivalent aggregate in model calculations is justified only when aggregate shape has a minor influence on the results. That is verified below for four diffusion models by comparing model results for a sphere, a cylinder and a plane sheet with the same S/V ratio. The four diffusion models have been taken from the literature. Therefore only a brief description of each process is given. The results are presented in the form of graphs. These graphs facilitate an assessment of the accuracy of the approximate methods without knowledge of mathematical details of the diffusion models.

Soil respiration as a zero-order absorption process

The model used originates from Greenwood (1961) and Currie (1961) and has been described also by Smith (1977) and Arah & Smith (1989). In this paper a slightly simplified version is used, not taking into account soil porosity and the solubility constant of oxygen. This simplification is motivated in the *Discussion of results for a single aggregate*.

Soil respiration is described as a zero-order absorption process, implying that in oxic parts of the soil, the respiration Q is independent of the local oxygen concentration. An anoxic zone, in which no respiration takes place, may occur. The differential equation describing the steady state for a spherical aggregate is

$$\frac{d}{dr}\left[-D\,4\pi r^2\,\frac{dc(r)}{dr}\right] = -Q\,4\pi r^2\,,\quad r_0 \le r \le R \tag{2.1}$$

with boundary conditions

$$c(r) = 0\,,\quad {dc(r)}/{dr} = 0 \quad \text{for } r = r_0 \quad \text{and} \quad c(R) = C\,.$$

Here c [mol m^{-3}] is the oxygen concentration, r [m] the distance from the centre (coordinate), r_0 [m] the unknown radius of the anoxic zone, R [m] the sphere radius, C [mol m^{-3}] the constant oxygen concentration outside the aggregate,

Q [mol m^{-3} s^{-1}] the respiration rate and D [m^2 s^{-1}] the diffusion coefficient.

The group DC/Q is a constant and plays a special role in the solution of Eq. (2.1). DC/Q has the dimension of a length squared and its square root is defined as the diffusion distance d:

$$d \equiv \sqrt{DC/Q}$$

The diffusion distance is a characteristic length belonging to the process taking place. Its definition is independent of aggregate geometry. The size of d gives an indication of the distance over which oxygen will enter into an aggregate (of arbitrary shape). When d is much smaller than aggregate size, the diffusive transport will be too small to maintain oxic conditions throughout the aggregate. That leads to a steady–state anoxic volume.

Equation (2.1) can be solved using the first two boundary conditions. The third condition is used then to find the radius of the anoxic zone r_0 and leads to

$$\begin{cases} R^2 - 3r_0^2 + \dfrac{2r_0^3}{R} = 6d^2, & d \le R/\sqrt{6} \\ r_0 = 0, & d > R/\sqrt{6} \end{cases} \tag{2.2}$$

Equation (2.2) shows that r_0 is a function of the sphere radius R and the diffusion distance d. Writing this as $r_0(R,d)$, the anoxic volume fraction becomes

$$\varphi_s(R,d) = \left(\frac{r_0(R,d)}{R}\right)^3 \tag{2.3}$$

By dividing Eq. (2.2) by R^2, it may be seen that r_0/R and, consequently, φ_s are a function of the ratio d/R only. When the sphere radius R is replaced then by $3V/S$, the anoxic volume fraction becomes a function of dS/V, the dimensionless product of the diffusion distance and the surface-to-volume ratio of the sphere. Note that the subscript "s" refers to a sphere.

For a cylinder analogous equations can be derived. The radius r_0 of the anoxic zone in a cylinder is found by solving (numerically):

$$\begin{cases} R^2 - r_0^2 + r_0^2 \ln\left(\dfrac{r_0}{R}\right)^2 = 4d^2, & d \le R/2 \\ r_0 = 0, & d > R/2 \end{cases}$$

And the anoxic volume fraction $\varphi_c(R,d)$ for a cylinder is

$$\varphi_c(R,d) = \left(\frac{r_0(R,d)}{R}\right)^2 \tag{2.4}$$

Again, replacing R by $2V/S$, the anoxic volume fraction becomes a function of dS/V.

For a plane sheet the equations are simple. For the radius r_0 of the anoxic zone holds:

$$\begin{cases} r_0 = R - \sqrt{2}\,d & , \; d \le R/\sqrt{2} \\ r_0 = 0 & , \; d > R/\sqrt{2} \end{cases}$$

The anoxic volume fraction $\varphi_p(R,d)$ of a plane sheet is equal to the ratio r_0/R. Replacing R by V/S, also φ_p becomes a function of dS/V.

For a spherical, cylindrical and flat aggregate shape, Fig. 2.2a shows graphs of the anoxic volume fraction φ as function of dS/V. This result will be discussed after descriptions of the other diffusion models are presented.

A first-order absorption process

The absorption considered in this section is proportional to the concentration at each point. A gas or solute is absorbed, for instance, as the result of a first-order reaction taking place, or the oxygen use of organisms is assumed to be proportional to the oxygen concentration. For a spherical aggregate shape the steady state of the process is described by

$$\frac{d}{dr}\left[-D\,4\pi r^2 \frac{dc(r)}{dr}\right] = -A\,4\pi r^2\,c(r), \quad 0 \le r \le R \tag{2.5}$$

with boundary conditions

$$c(R) = C \text{ and } c(0) \text{ finite.}$$

Here A [s^{-1}] is the constant ratio between absorption and concentration.

The solution of Eq. (2.5) is a concentration profile $c(r)$. At the outer surface of the sphere, for $r = R$, the concentration is equal to C. For smaller values of r the steady–state concentration is lower but always larger than zero.

The characteristic length λ appearing in the solutions for a sphere, cylinder and plane sheet is $\sqrt{D/A}$. If λ is a few times the aggregate radius, the concentration $c(r)$ approaches the outer concentration everywhere. The absorption (in mol s^{-1}) of the complete aggregate approaches then the maximum value AVC. The actual absorption divided by this maximum is defined as the effectiveness factor η.

For spheres, cylinders and plane sheets η is known as a function of the radius R and the length λ. For spheres Bird *et al.* (1960, section 17.6) give a complete derivation of:

$$\eta_s(R,\lambda) = 3\left(\frac{\lambda}{R}\right)^2 \left[(R/\lambda)\coth(R/\lambda) - 1 \right] \tag{2.6}$$

For cylinders the solution is (Bird *et al.*,1960,problem 17.M)

$$\eta_c(R,\lambda) = 2\left(\frac{\lambda}{R}\right) \frac{I_1(R/\lambda)}{I_0(R/\lambda)} \tag{2.7}$$

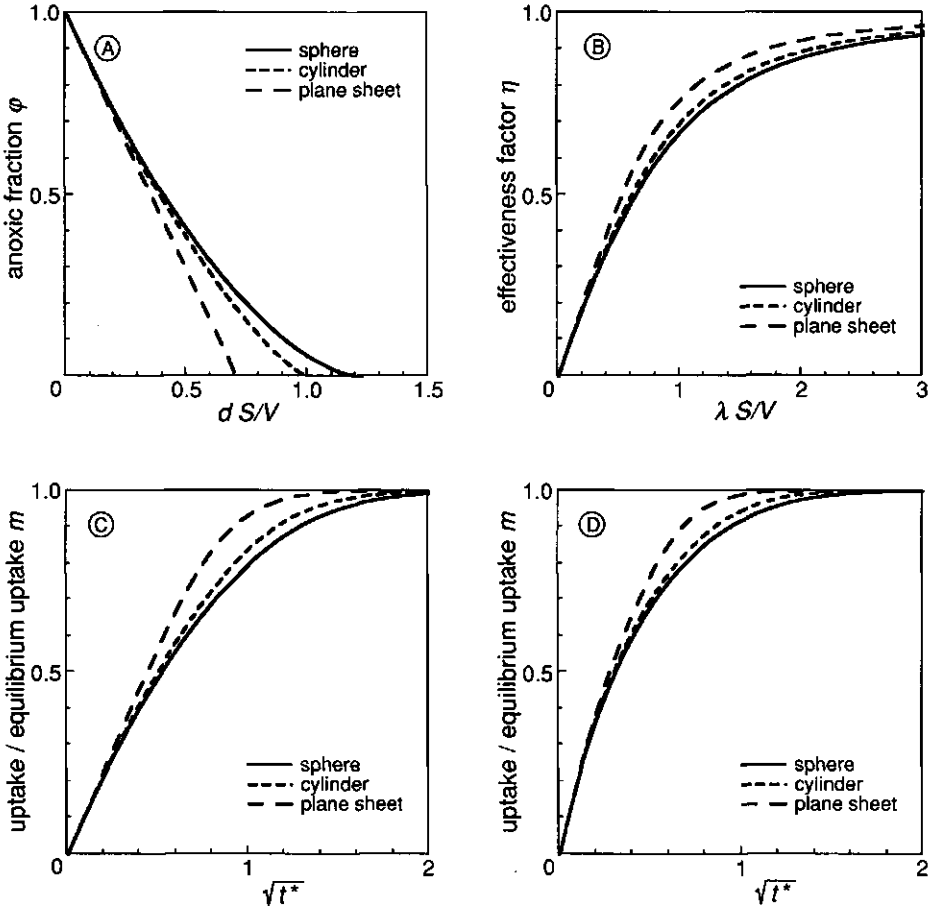

Figure 2.2. Comparison of results of diffusion models applied to a sphere, a cylinder and a plane sheet. Shape is of minor importance, provided aggregate size is expressed as a surface-to-volume ratio S/V. Different diffusion models have been used: (A) The steady state of oxygen diffusion with a zero–order respiration process ; the diffusion distance d is defined as $\sqrt{DC/Q}$ (cf. Eq. (2.1)) ; (B) The steady state of a first–order (oxygen) absorption process ; η is the aggregate absorption expressed as a fraction of the absorption for infinite D ; the diffusion distance λ is defined as $\sqrt{D/A}$ (cf. Eq. (2.5)) ; (C) Gas or solute uptake after a sudden increase in outer concentration ; after the increase at $t = 0$, the outer concentration does not change ; the dimensionless time t^* is defined in Eq. (2.10) ; (D) After a sudden increase, the outer concentration slowly decreases due to the uptake of gas or solute by the aggregate ; outer volume and aggregate volume have equal size.

Here I_0 and I_1 are modified Bessel functions of the first kind. For a plane sheet the effectiveness factor is (Bird *et al.*,1960, problem 17.I)

$$\eta_p(R,\lambda) = \left(\frac{\lambda}{R}\right)\tanh(R/\lambda) \tag{2.8}$$

Again, these equations can be rewritten using the surface-to-volume ratio of sphere, cylinder or plane sheet instead of their radii. In Fig. 2.2b three graphs give the effectiveness factor as a function of $\lambda S/V$.

A sudden change in outer concentration

When the concentration of a gas in the space around an aggregate suddenly changes, the concentration inside the aggregate will follow relatively slowly. It requires some time before a new equilibrium concentration is reached everywhere. For simplicity the description below refers to a sudden concentration rise from 0 to C. The results, however, are valid for a sudden change in general.

Two cases are distinguished. In the first case the outer concentration is supposed to rise suddenly at $t=0$ and remains constant after the change. It is not affected by the diffusive transport into the aggregate.

In the second case the outer concentration also rises suddenly at $t=0$, but decreases as a result of the subsequent flow of gas into the aggregate. The decrease depends on the surrounding volume. This volume is assumed to be α times as large as the aggregate volume V. For $\alpha=1$, for instance, aggregate volume and surrounding volume are equal, and the outer concentration will decrease until the new equilibrium concentration $C/2$ is reached everywhere. For $\alpha=\infty$ the outer concentration does not decrease. Hence, the case of a constant outer concentration is a limiting case of the diffusion problem for a finite outer volume.

Crank (1956) refers to this problem as diffusion from a well–stirred solution of limited volume. It is thus assumed that no concentration gradient occurs outside the aggregate and that the initial rise in outer concentration is instantaneous. The differential equation for a sphere is

$$4\pi r^2\frac{\partial c}{\partial t} = \frac{\partial}{\partial r}\left(D\,4\pi r^2\frac{\partial c}{\partial r}\right) \tag{2.9}$$

with the initial condition

$$c(r,t)=0 \quad \text{for } r<R,\ t=0$$

and with boundary condition

$$\frac{\partial c}{\partial t} = -\frac{3}{\alpha R}D\frac{\partial c}{\partial r} \quad \text{for } r=R,\ t>0$$

Crank (1956) gives an expression for the gas uptake $m_s(R,t)$ of the sphere. The

uptake is expressed as a fraction of the uptake after infinite time (the equilibrium uptake). Expressions for the uptake $m_c(R,t)$ of a cylinder and $m_p(R,t)$ of a plane sheet can also be found in Crank (1956). Sphere, cylinder and plane sheet radius can be replaced again by $3V/S$, $2V/S$ and V/S respectively. Then, in all three cases, the uptake becomes a function of a dimensionless time t^* defined as

$$t^* = tD\left(S/V\right)^2 \tag{2.10}$$

In Fig. 2.2c graphs are given for a constant outer concentration ($\alpha=\infty$) and in Fig. 2.2d for equal aggregate and outer volume ($\alpha=1$).

Discussion of results for a single aggregate

The curves in Fig. 2.2 for a sphere, a cylinder and a plane sheet are close together. The result for an aggregate with another shape is likely to be somewhere in between. Therefore, for a real aggregate with an irregular shape, calculations need not to be carried out. In a diffusion model the real aggregate can be represented by an equivalent sphere, cylinder or plane sheet.

The use of an equivalent aggregate leads to approximate results. The differences in Fig. 2.2 between curves for a sphere, cylinder and plane sheet give an impression of the size of the errors. For calculations on soil aggregates there seems to be no reason to require a higher accuracy. Other sources of error are likely to be at least as important.

Practical calculations require the use of a solubility and a soil porosity in the differential equation describing a process (e.g. Arah & Smith, 1989). The addition of these constants leads to a somewhat more complicated definition of the dimensionless groups used as x-coordinate in the graphs of Fig. 2.2. The graphs themselves remain unchanged, however, as does the conclusion with respect to the use of an S/V ratio. Therefore, in this paper, the differential equations have been used in their simplest form.

The surface-to-volume ratio S/V of an aggregate may be regarded as a measure of its (inverse) size. For a constant aggregate shape, S/V decreases with increasing aggregate size. Results of a diffusion model tend to depend on the size of an aggregate only, provided it is expressed as S/V. This formulation points towards the limitations of the S/V method. Only a single number is used to measure aggregate size. When several length scales are involved, the method is likely to fail. In case of a rough or bumpy aggregate surface, for instance, there is a second length scale associated with the surface roughness. This problem can be solved by using the method for an aggregated soil described below. That method takes into account the presence of several length scales.

METHOD FOR AN AGGREGATED SOIL

An analogy

An approximate method is described for the application of a diffusion model to an aggregated soil. The method is necessarily more complicated than the method for a single aggregate discussed above. There is a close analogy, however, which is expressed by the scheme in Fig. 2.3.

The left side of Fig. 2.3 recapitulates the method for a single aggregate. The geometry is characterized by a single number, the surface-to-volume ratio S/V. This number is used to calculate the size of an equivalent sphere, cylinder or plane sheet (with equal S/V ratio). In a diffusion model the real aggregate is represented by one of these equivalent aggregates. The method is tested by comparing diffusion model results for a sphere, a cylinder and a plane sheet with equal S/V ratios.

The right side of Fig. 2.3 shows a scheme of the method for an aggregated soil. Soil geometry is characterized by a distance probability density function $s(x)$, which is defined below. The function $s(x)$ plays the same role as the ratio S/V in the method for a single aggregate. In case of a single aggregate S/V is used

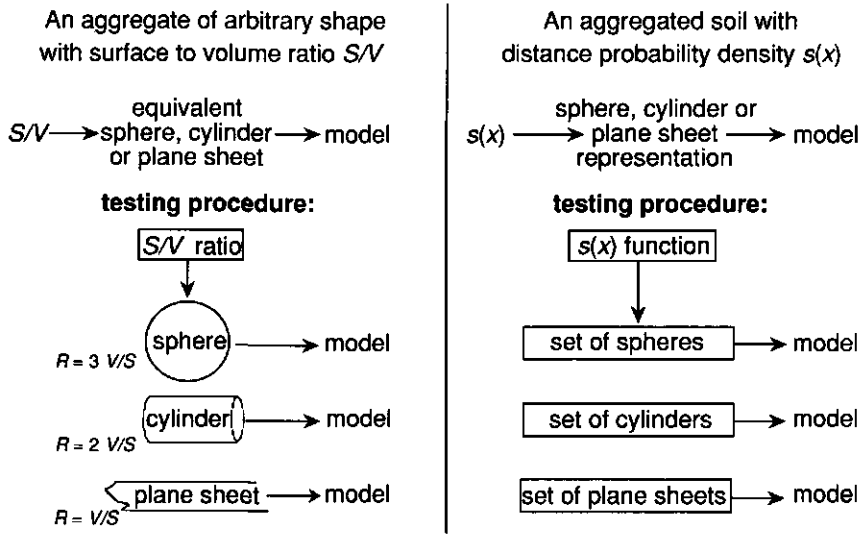

Figure 2.3. The method for an aggregated soil is analogous to the use of an equivalent sphere, cylinder or plane sheet for a single aggregate. Instead of the surface volume ratio S/V the distance probability density function $s(x)$ is used as the conserved property. The two methods have been tested for several diffusion models (results in Figs. 2.2 and 2.8).

to define an equivalent aggregate. Similarly, a function $s(x)$ can be used to define a (hypothetical) model soil. A model soil is a set of spheres, cylinders or plane sheets, which is characterized by a certain size distribution. This size distribution is chosen in such a way that model soil and real soil have equal functions $s(x)$. The model soil can be used then to represent the real soil in calculations on diffusion processes. The three types of model soil are therefore called the sphere, cylinder and plane sheet representation of the real soil (see Fig. 2.3).

The use of a model soil in diffusion models is justified only when the result of a diffusion process is largely determined by the distance probability density function of the soil. Again, the influence of "shape" should be small. That has been verified by comparing results of diffusion models applied to a set of spheres, a set of cylinders and a set of plane sheets with the same function $s(x)$.

In the first two sections below the distance probability density function $s(x)$ is introduced. Then the problem of finding a model soil with a given (i.e., measured) $s(x)$ is solved. Finally, the method is tested by examining the influence of shape.

The distance probability density function $s(x)$

Each point of the intra–aggregate space has a shortest distance x to the inter-aggregate space. The distance x belonging to a randomly chosen point can be considered as a stochastic variable. The function $s(x)$ is defined then as the probability density of x.

The definition of $s(x)$ as a distance probability density function is operational, i.e. it implies a way to measure $s(x)$: for a large number of test points the shortest distance to the inter-aggregate space is measured. The test points may be either randomly chosen or may form a dense grid. N distance intervals are chosen and the fraction of distances in each interval is calculated. The result is a series of N distance probabilities p_i. When accurate distance probabilities are available for a large number of intervals, one might consider the estimation of a continuous $s(x)$ by means of a smoothing and interpolation technique.

Both a continuous function $s(x)$ and a series of distance probabilities can be used to derive a sphere, cylinder or plane sheet representation of the real soil.

The function $s(x)$ as a generalized surface-to-volume ratio

Before considering in detail the calculation of a model soil, the function $s(x)$ needs to be derived for an individual sphere, cylinder and plane sheet. The definition of $s(x)$ as a distance probability density function can be directly applied. The distance x simply is the distance from a randomly chosen point to the outer surface of the aggregate.

It is interesting, however, to consider an alternative definition of $s(x)$, which directly refers to the surfaces through which diffusive transports take place. The derivation below shows, for a cylinder, that the two definitions of $s(x)$ are equivalent.

For a long cylinder with radius R and length H the (inner) surface function $S(x)$ is defined as

$$S(x) = 2\pi(R-x)H\ ,\ 0 \le x \le R$$

It is the size of the surface at a distance $R-x$ from the centre and at a distance x from the outer surface. The integral of $S(x)$ over the interval $[0,R]$ is the total volume πHR^2 of the cylinder. Dividing $S(x)$ by this volume gives $s(x)$, the inner surface per unit volume:

$$s(x) = \frac{2}{R}\left(1-\frac{x}{R}\right)\ ,\ 0 \le x \le R$$

For $x = 0$, $s(x)$ is equal to the ratio S/V between outer surface and volume. The function $s(x)$ may thus be regarded as a generalized surface-to-volume ratio.

The integral of $s(x)$ over a distance interval $[x_1,x_2]$ is a volume fraction. It is the fraction of the aggregate volume between the inner surfaces at distances x_1 and x_2 from the outer surface. For a cylinder this is

$$\int_{x_1}^{x_2} s(x)\,dx = \left(1-\frac{x_1}{R}\right)^2 - \left(1-\frac{x_2}{R}\right)^2$$

In general, a volume fraction can be treated as a probability. It is identical to the probability that a randomly chosen point is part of it. Hence, the above volume

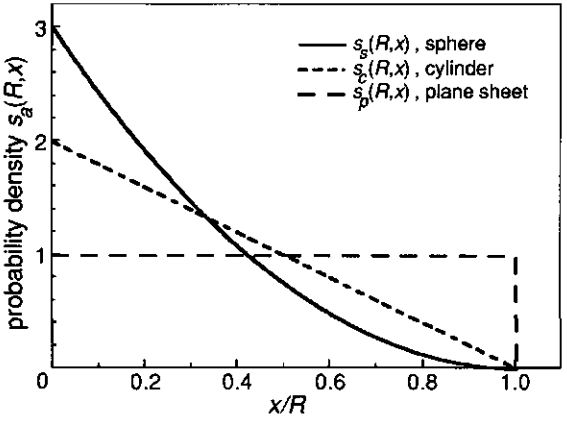

Figure 2.4. The distance probability density function for a sphere, a cylinder and a plane sheet (Eq. (2.12)).

fraction is equal to the probability that the distance x, belonging to a randomly chosen point, lies in the interval $[x_1,x_2]$:

$$\Pr(x_1 < x < x_2) = \int_{x_1}^{x_2} s(x)\,dx \tag{2.11}$$

This implies that $s(x)$, being an inner surface per unit volume, is also a distance probability density function. The two definitions are equivalent.

For a plane sheet, cylinder and sphere, the desired function is most easily found as an inner surface per unit volume. The three functions are written as $s_p(R,x)$, $s_c(R,x)$ and $s_s(R,x)$, respectively:

$$\begin{cases} s_p(R,x) = \frac{1}{R} & ,\ 0 \le x \le R \\ s_p(R,x) = 0 & ,\ x > R \end{cases} \tag{2.12a}$$

$$\begin{cases} s_c(R,x) = \frac{2}{R}\left(1-\frac{x}{R}\right) & ,\ 0 \le x \le R \\ s_c(R,x) = 0 & ,\ x > R \end{cases} \tag{2.12b}$$

$$\begin{cases} s_c(R,x) = \frac{3}{R}\left(1-\frac{x}{R}\right)^2 & ,\ 0 \le x \le R \\ s_c(R,x) = 0 & ,\ x > R \end{cases} \tag{2.12c}$$

In Fig. 2.4 graphs have been drawn.

A model soil derived from a continuous $s(x)$

At first an expression for the function $s(x)$ of a model soil is derived making use of Eq. (2.12). Then the reverse problem of finding a model soil with a prescribed $s(x)$ can be solved.

A model soil is a set of flat, cylindrical or spherical aggregates. The plane sheets, cylinders or spheres do not possess a spatial position or an orientation. They are imaginary model aggregates and their radius is their only property. The model aggregates with a radius in some interval $[R_1,R_2]$ occupy a fraction Δv of the total model soil volume. This volume fraction Δv is written as

$$\Delta v = \int_{R_1}^{R_2} v_a(R)\,dR$$

The continuous function $v_a(R)$ is the, yet unknown, volume fraction density of the model soil (the subscript "a" refers to "aggregate" which may be either "sphere", "cylinder" or "plane sheet", cf. Eqs. (2.6), (2.7), (2.8) and (2.12)).

$v_a(R)\,dR$ is the probability that a randomly chosen point belongs to a model aggregate with radius between R and $R+dR$. Then, the $s(x)$ function of the model soil can be written as an integral over aggregate radius:

$$s(x) = \int_x^\infty s_a(R,x)\, v_a(R)\, dR \tag{2.13}$$

Here $s_a(R,x)$ is the distance probability density function of a model aggregate with radius R (Eq. (2.12)). Eq. (2.13) shows how the $s(x)$ function of the model soil is "build up" from the distance probability density functions of spheres, cylinders or plane sheets.

It is assumed now that a function $s(x)$ is known. This may be a theoretically calculated function or a measured function for a real soil. The distance probability density function of the model soil is set equal to this calculated or measured one. Then Eq. (2.13) becomes an equation with unknown $v_a(R)$. By solving this equation a plane sheet, a cylinder or a sphere model soil is found. In the Appendix it is shown that, for a plane sheet model soil,

$$v_p(R) = -x \frac{ds(x)}{dx} \Big/_{x=R}, \tag{2.14a}$$

for a cylinder model soil

$$v_c(R) = \frac{1}{2} x^2 \frac{d^2 s(x)}{dx^2} \Big/_{x=R} \tag{2.14b}$$

and for a sphere model soil

$$v_s(R) = -\frac{1}{6} x^3 \frac{d^3 s(x)}{dx^3} \Big/_{x=R} \tag{2.14c}$$

Note that depending on the type of model soil, the calculation of $v_a(R)$ requires the existence of a first, second or even third order derivative of $s(x)$.

As an example, the cylinder representation of a single sphere with radius R_s is calculated. The distance probability density function for a sphere was given in Eq. (2.12b). After writing R_s for the sphere radius, Eq. (2.14b) is applied. The volume fraction density as function of the (cylinder) radius R becomes:

$$v_c(R) = \frac{3R^2}{R_s^3}, \quad 0 \le R \le R_s \tag{2.15}$$

A model soil derived from *N* distance probabilities

Instead of a continuous distance variable x, N distance intervals are used. To each interval i ($i=1,...,N$) belongs a distance probability p_i. That is the probability that the shortest distance x from a randomly chosen point to the

inter–aggregate space falls in the i–th interval.

The i–th distance interval is written as $[x_{i-1}, x_i]$. The distance x_i is the upper bound of the i–th interval and x_0 is defined to be zero. The probabilities p_i can be measured by determining the distance x for a large number of test points. Distance intervals are chosen and p_i is estimated as the fraction of measured distances falling in interval i.

The N distance probabilities p_i can be used to define a (hypothetical) model soil. The model soil consists of plane sheets, cylinders or spheres with N different sizes. The N aggregate radii are set equal to the upper bounds of the distance intervals. Hence

$$R_i = x_i\,,\quad i=1,...,N \tag{2.16}$$

The aggregates with radius R_i occupy a fraction v_i of the model soil volume. The model soil is fully described by the N fractions v_i, since its aggregates do not possess a spatial position or orientation. The N volume fractions v_i need to be derived from the N (measured) distance probabilities p_i. Two methods are given.

The first method requires that all distance intervals have equal width. The probabilities p_i will form a decreasing series (large distances are rare). If the p_i are accurate numbers, one may estimate the derivatives in Eq. (2.14) from differences in successive p_i values. For a plane sheet representation that leads to

$$\begin{cases} v_i = i(p_i - p_{i+1})\,, & i \le N-1 \\ v_N = N p_N \end{cases} \tag{2.17a}$$

for a cylinder representation

$$\begin{cases} v_i = \frac{1}{2} i^2 (p_i - 2p_{i+1} + p_{i+2})\,, & i \le N-2 \\ v_N = 0 \qquad\qquad\qquad\qquad\quad , & i = N-1, N \end{cases} \tag{2.17b}$$

and for a sphere representation

$$\begin{cases} v_i = \frac{1}{6} i^3 (p_i - 3p_{i+1} + 3p_{i+2} - p_{i+3})\,, & i \le N-3 \\ v_N = 0 \qquad\qquad\qquad\qquad\quad , & i = N-2, N-1, N \end{cases} \tag{2.17c}$$

In the Appendix it is shown that, for $N \to \infty$, these expressions correspond to Eq. (2.14) for a continuous $s(x)$ function. In fact, Eq. (2.17) is an attempt to approach a continuous solution without calculating a continuous $s(x)$. Satisfactory results require accurate probabilities p_i and at least some tens of distance intervals.

The second method will be referred to as the matrix method. Volume

fractions are calculated from the requirement that the model soil exactly reproduces the measured distance probabilities p_i. That requirement leads to a set of N linear equations with N unknown volume fractions:

$$p_i = \sum_{j=1}^{N} P_{ij} v_j \quad , \; i = 1...N \tag{2.18}$$

The left side of each equation is a measured probability p_i. The right side is a distance probability calculated for the, yet unknown, model soil. The volume fraction v_j is equal to the probability that a randomly chosen point lies within an aggregate with radius R_j. And P_{ij} is defined as the probability that, given a point in an aggregate with radius Rj, the distance to the outer surface falls in the i-th distance interval. The probabilities (matrix elements) P_{ij} are calculated from the distance probability density function for a plane sheet, cylinder or sphere (see Eqs. (2.11) and (2.12)):

$$P_{ij} = \int_{x_{i-1}}^{x_i} s_a(R_j, x)\, dx \tag{2.19}$$

The model soil volume fractions are found then by solving Eq. (2.18).

In principle, volume fractions can be calculated for an arbitrary number of distance intervals N. Different choices of N lead to different model soils to which a diffusion model may be applied. In general, for a sufficiently large N, the result of a diffusion model becomes stable. A further increase of N does not influence the result, which implies that the diffusion model converges. The choice of N should be determined from that convergence. In the next section an example is given.

When all distance intervals have equal width, an expression can be derived for the matrix elements P_{ij} and Eq. (2.18) can be solved analytically. Details are given in the Appendix. Here, the main results are described.

For plane sheets the solution of Eq. (2.18) again leads to Eq. (2.17a). Hence, in case of plane sheet volume fractions, the two methods coincide. Cylinder volume fractions derived with Eq. (2.18) tend to form an "oscillating" series. In a graph, the odd and even volume fractions would lie at opposite sides of a neat curve. In spite of oscillating volume fractions, however, the result of a diffusion model generally converges (see the next section for an example). The convergence even tends to be relatively fast, i.e. the matrix method requires less distance intervals than the use of Eq. (2.17b). That is an important advantage.

A sphere representation cannot be derived with the matrix method. Equation (2.18) leads to strongly oscillating sphere volume fractions and results of diffusion models diverge for increasing N.

Example

Two cylinder representations of a single sphere with radius 1 have been calculated using different methods. To both cylinder representations a diffusion model describing local anaerobiosis has been applied. The two approximate results are compared with each other and with the exact result for the sphere.

The first cylinder representation considered is based on 20 distance probabilities p_i ($i = 1,...,20$). The p_i have been calculated by integrating the distance probability density function of the sphere (Eq. (2.12c)) over 20 distance intervals of equal width $\delta (= 0.05)$. The matrix method has been used then to find the 20 cylinder volume fractions v_i (Eq. (2.A3)). The volume fraction densities v_i/δ are given as a histogram in Fig. 2.5. Despite the fact that the used p_i values are exact, the volume fractions oscillate strongly. These oscillations, however, do not lead to problems in calculating anoxic volume fractions for the cylinder representation.

The anoxic volume fraction is calculated for the cylinder representation by

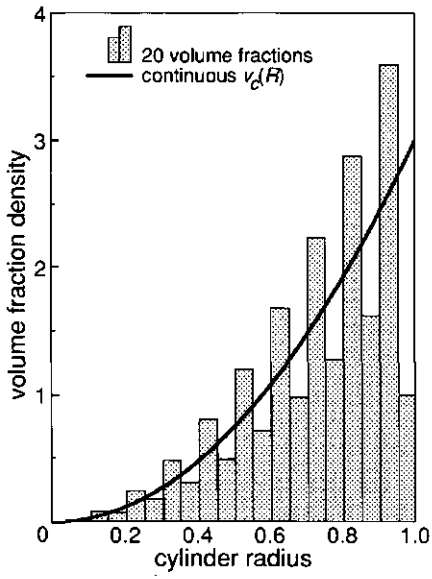

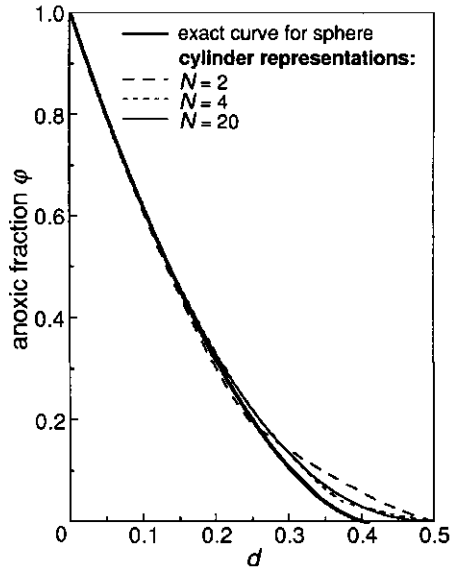

Figure 2.5. (left) Cylinder representations of a single sphere with $R_S = 1$. The thick line is the continuous volume fraction density derived as Eq. (2.15). The histogram consists of 20 volume fractions calculated with the matrix method (Eq. (2.A3) with $N = 20$). The volume fractions have been divided by the class size 0.05 to get volume fraction densities.

Figure 2.6. (right) The anoxic volume fraction of a sphere with radius 1 (thick line). The other lines are obtained for cylinder representations derived with the matrix method. The result of the diffusion model converges for increasing N. The continuous cylinder representation in Fig. 2.5 also leads to the line for $N = 20$.

applying the diffusion model to all cylinder size classes separately. Equation (2.4) describes the anoxic fraction $\varphi_c(R,d)$ of a cylinder with radius R. For each cylinder radius R_j ($j=1,...,20$) this function is calculated and the results for the 20 cylinder size classes are added using the volume fractions v_j as weights:

$$\varphi(d) = \sum_{j=1}^{N} v_j \, \varphi_c(R_j,d) \qquad (2.20)$$

In Fig. 2.6 a graph of this function has been drawn. It is close to the exact curve for the sphere, which has been calculated with Eqs. (2.2) and (2.3).

It should be verified that the result for $N=20$ is insensitive to a change in the number of distance intervals N. Therefore the calculations have been repeated for $N=2$ and $N=4$ and the results have been drawn as dashed lines in Fig. 2.6. The line for $N=4$ is already very close to the line for $N=20$. Hence, the result of the diffusion model indeed converges and the limiting function is practically reached for $N=20$.

The second cylinder representation is directly based on the continuous distance probability density function of the sphere and was already derived above (Eq. (2.15)). A graph of $v_c(R)$ has been drawn in Fig. 2.5. For this cylinder representation the anoxic volume fraction can be calculated by integrating $\varphi_c(R,d)$ over the cylinder volume distribution (instead of calculating a sum over N size classes as in Eq. (2.20)). The result coincides with the line for $N=20$ in Fig. 2.6, which implies that the two cylinder representations in Fig. 2.5 lead to the same diffusion model result.

Testing the method

The method for an aggregated soil can be tested by applying a diffusion model to a set of spheres, a set of cylinders and a set of plane sheets with equal functions $s(x)$ (cf. Fig. 2.3). When the results for the three model soils are close together, the behavior of a real soil (with the same $s(x)$) is likely to be somewhere in between.

First functions $s(x)$ have to be chosen from which model soils can be derived. The used functions have been calculated for a "sphere soil" consisting of spheres with a lognormal radius distribution. Lognormal aggregate size distributions have been observed in the field (Allmaras *et al.*,1965 ; Gardner,1956) and the large size ranges involved enable a thorough test of the method. Different values for the parameters of the lognormal distribution lead to different functions $s(x)$.

A lognormal radius distribution is characterized by a geometric mean radius R_g and a factor F expressing size variability. The radius interval of one standard deviation above and below the geometric mean is $[R_g/F, R_g F]$. When $F=2$, for

instance, 68% of the spheres has a radius between $R_g/2$ and $2R_g$. In the special case of $F=1$ there is no size variability. Details can be found in the Appendix.

A certain choice of R_g and F corresponds to a certain volume fraction density function $v_s(R)$ of the sphere soil (see Appendix). The function $s(x)$ of the sphere soil is then found as (cf. Eq. (2.13))

$$s(x) = \int_x^\infty s_s(R,x)\, v_s(R)\, \mathrm{d}R \tag{2.21}$$

Since discrete probabilities are somewhat easier to handle than a continuous $s(x)$ function, distance probabilities p_i have been calculated by integrating $s(x)$ over 50 distance intervals of equal width. Then Eq. (2.17) has been used to derive a set of spheres, a set of cylinders and a set of plane sheets. Each of the three sets consists of 50 radius values with an associated volume fraction v_i.

As an example, graphs have been drawn in Fig. 2.7. The thick line is the continuous volume fraction density function $v_s(R)$ for the sphere soil with a lognormal radius distribution with parameters $R_g=2$ and $F=2$. From $s(x)$, calculated according to Eq. (2.21), three sets of volume fractions have been derived. As expected, the sphere representation (the non-connected dots in Fig. 2.7) closely resembles the original sphere soil. The deviations result from the use of distinct size classes and from small numerical errors (cf. the remark following Eq. (2.17)). The cylinder and plane sheet representation clearly have different volume fraction distributions.

A diffusion model is applied to a set of spheres, cylinders, or plane sheets by adding the results for the different radius values, using the volume fractions v_i as weights. For a first-order absorption process this is expressed by:

$$\eta(\lambda) = \sum_{i=1}^{N} v_i\, \eta_a(R_i,\lambda) \tag{2.22}$$

$\eta_a(R,\lambda)$ is the effectiveness factor for a model aggregate (see Eqs. (2.6), (2.7) and (2.8)). The weighted sum $\eta(\lambda)$ is the effectiveness factor for the model soil. Other diffusion models can be applied by using similar expressions (cf. Eq. (2.20)).

Results for an aggregated soil

The method for an aggregated soil has been tested for the same diffusion models that have been used to test the method for a single aggregate (cf. Fig. 2.2). Anoxic volume fractions have been calculated for three model soils with the same function $s(x)$. The calculations have been repeated for three different functions $s(x)$ belonging to three values of F (see previous section). Fig. 2.8a shows the results. Indeed, for each choice of F, the curves for the three model

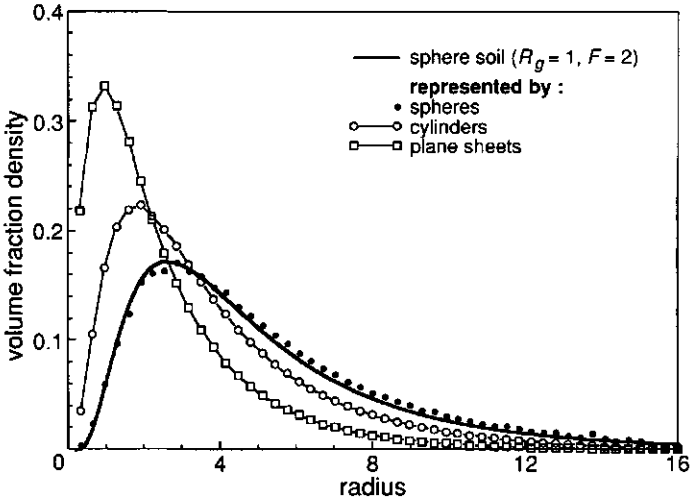

Figure 2.7. Volume fraction density function for a "sphere soil" with a log-normal distribution of sphere radius (thick line). The points are volume fraction densities for a set of spheres, a set of cylinders and a set of plane sheets representing the sphere soil (Eq. (2.17) with $N = 50$). For clarity, cylinder and plane sheet volume fraction densities have been connected with a thin line.

soils are close together. Note that different choices of R_g lead to the same graphs when d/R_g is used as independent variable.

In Fig. 2.8b similar results are given for diffusion with a first order absorption process.

In Fig. 2.8c graphs have been drawn of gas or solute uptake from the inter–aggregate space after a sudden rise in concentration at $t=0$. After the sudden rise, the concentration in the inter-aggregate space is constant ($\alpha=\infty$). The uptake of a model soil can be calculated then as a sum of analytic solutions $m_a(R_i,t)$ with the volume fractions v_i used as weights (see Eq. (2.22) and the explanation following Eq. (2.9)). The result is conveniently expressed as function of a dimensionless time t^{**} defined as

$$t^{**} = {}^{t D}/_{R_g^2} \tag{2.23}$$

When the concentration in the inter-aggregate space decreases as a result of the uptake by the soil, the processes in small and large aggregates will influence each other. Small aggregates quickly approach equilibrium with the surrounding concentration. Then, due to the absorption by the larger aggregates, the inter–aggregate concentration decreases and the gas or solute content of the smaller aggregates may even start to decrease. Clearly this cannot be described by making use of analytic solutions for a single aggregate. The total uptake has to be found by numerical simulation of the uptake for all aggregate size classes.

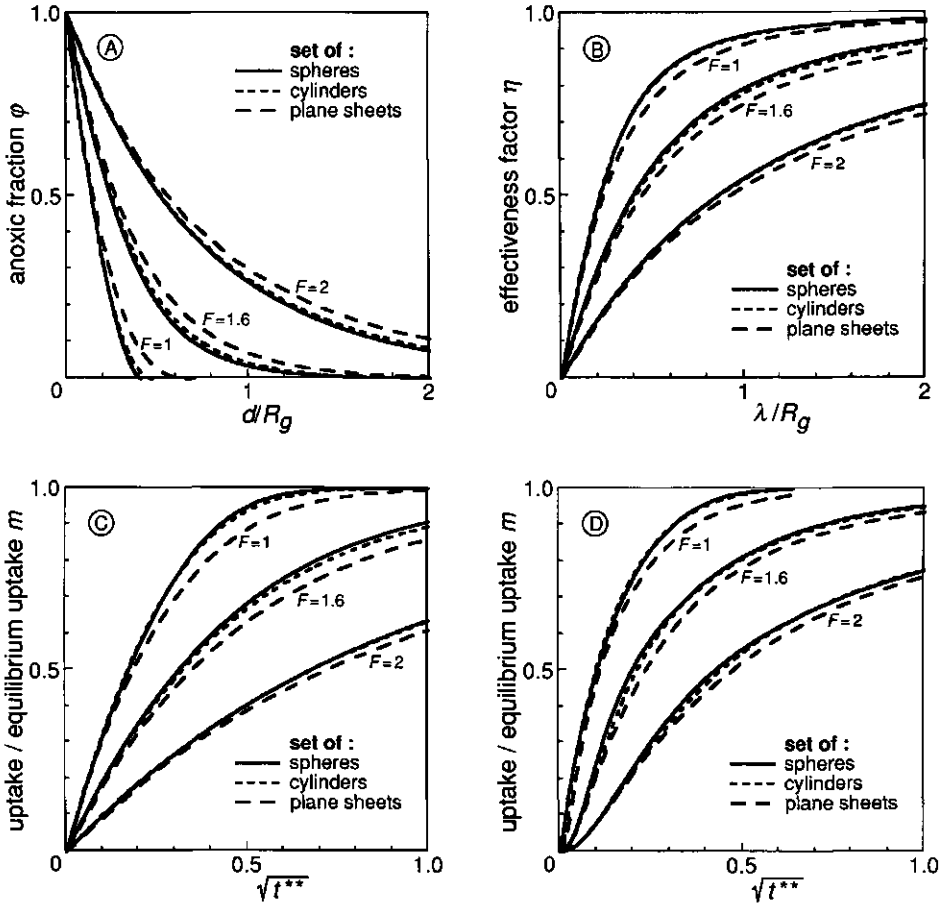

Figure 2.8. Comparison of results of diffusion models applied to a set of spheres, a set of cylinders, and a set plane sheets with equal $s(x)$ functions (cf. Fig. 2.2). Each set of three lines corresponds to a different choice for $s(x)$ (see Eq. (2.21) and Appendix). The same four models have been used as in Fig. 2.2. The dimensionless time t^{**} used in (c) and (d) is defined in Eq. (2.23).

Fig. 2.8d shows the results. The volume of the inter-aggregate space was set equal to the total aggregate volume ($\alpha = 1$). Again the curves for spheres, cylinders and plane sheets are close together. (For small times, numerical errors cause the calculated uptakes to be somewhat too small ; initial uptake should be proportional to the square root of time.)

Numerical aspects

The calculations discussed in this paper have been carried out by means of about 70 commented (sub)programs written in standard FORTRAN-77. They are available on request.

The distance probability density functions $s_a(R,x)$ and the solutions of the used diffusion models $\varphi_a(R,d)$, $\eta_a(R,\lambda)$ and $m_a(R,t)$ have been written as (FORTRAN) functions. That considerably simplifies the subsequent calculation of integrals or weighted sums over aggregate radius (cf. Eqs. (2.20), (2.21) and (2.22)). Integrals have been calculated by means of the Gauss-Legendre method or by using Simpson rule in a form enabling accuracy control (Press *et al.*,1986). The results in Fig. 2.8d have been calculated by simulating concentrations using a fourth order Runge Kutta algorithm with stepsize control (Press *et al.*, 1986).

ADAPTATION TO WORM BURROWS AND ROOTS

When diffusive transports are considered to or from (worm)burrows, the above described method requires some adaptation. All burrows together form the inter-aggregate space and the distance x belonging to a point of the soil is defined as the distance to the centre of the nearest burrow. The distance probability density function $s(x)$ will increase for low distances according to the size of concentric surfaces around the burrows. For large distances, $s(x)$ decreases and eventually reaches zero. A model soil can be derived from such a function.

Cylinders with a burrow along their axis are used as model "aggregates". Diffusive transports in the model soil only take place through the surface of the burrow. The outer cylinder surface is subject to a zero flow condition. In this way the shape of the model soil is somewhat adapted to the system to be described. Again, the cylinder radius values are set equal to the upper bounds of N distance intervals. In the Appendix it is shown that the cylinder volume fractions are then given by

$$\begin{cases} v_i = i^2\left(\dfrac{p_i}{2i-1} - \dfrac{p_{i+1}}{2i+1}\right), & i<N \\ v_N = \dfrac{N^2}{2N-1}p_N \end{cases} \qquad (2.24)$$

The cylinder volume fractions are independent of the burrow diameters since x is defined as the distance to the centre of the nearest burrow. In model calculations the diameter of the burrows along the cylinder axes may be chosen according to a measured or assumed size distribution.

This method may also be used for the calculation of nutrient uptake by a root system. The model soil consists then of cylinders with a root along their axes. The different cylinder size classes correctly represent the soil volume fractions at different distances from the root system. In Chapter 7 the method for root systems is further elaborated. For different root distributions model systems are derived to which an uptake model is applied. Results are compared with electrical analogue data from the literature.

CONCLUSIONS

For a single aggregate and for an aggregated soil, shape has a minor influence on results of diffusion models (Figs. 2.2 and 2.8). That provides the use of a simple model soil with a physical basis. The use of a model soil is not restricted to demonstrative, theoretical calculations. Despite its geometrical simplicity, a model soil can be used in quantitative calculations on diffusion processes. Moreover, a complicated and realistic description of the geometry of an aggregated soil would probably lead to marginal improvements only, at the expense of computational and conceptual simplicity.

Different types of transport models may make use of a model soil. The only requirement is that model results are relatively independent of shape. Models on gas diffusion and diffusion of solutes in water are the most obvious examples. For heat transport the method will also work, since diffusion and heat transport are very similar processes. Also gravity–free flow of water in soil aggregates can be formulated as diffusion. In case of doubt one may test the shape dependence of a transport model by applying it to (sets of) spheres, cylinders, and plates.

Soil aggregates share their "outer world", the inter-aggregate space. If the condition of the inter-aggregate space is influenced by diffusive flows into or from aggregates, the aggregates of a model soil cannot be considered as independent objects. As a consequence, the application of a diffusion model requires numerical simulation of concentrations, even if the diffusion model is a simple one (e.g. Fig. 2.8d). An elaborate example would be the simulation of water vapor pressure in cracks, influenced by exchange with the atmosphere and by transport of water and water vapor in a cylinder model soil.

The sphere, cylinder or plane sheet volume fractions of a model soil are calculated from distance probabilities. Sphere volume fractions are very sensitive to errors and can only be calculated when at least some tens of accurate distance probabilities are available. Most appropriate in many situations will be the calculation of cylinder volume fractions with the matrix method. One should try a few values N, the number of distance intervals, in order to verify the

convergence of diffusion model results. Note that distance intervals need not to have equal widths (see Appendix). Plane sheet volume fractions are easy to calculate and may be used if also cylinder volume fractions cannot be obtained.

Distance probabilities can be derived from measured distances. In principle, spatial distances are needed, measured in a three dimensional image of the soil. In a few cases simplifications are possible. When cracks are vertical, for instance, spatial distances can be determined in a horizontal intersection. Also in case of an isotropic soil structure one may use distances measured in the plane of an intersection. That requires an adaptation of the method for calculating model soil volume fractions. In a subsequent paper this will be discussed into detail.

The method developed in this paper requires the existence of a distinction between a relatively uniform porous medium and an inter-aggregate space around it. Such a distinction cannot be made, if there is a continuous size distribution of macropores and micropores. The soil cannot be regarded then as an aggregated system and the method described in this paper will fail.

A distance probability distribution may be useful, also independent of physical transport models. When studying displacements of animals or bacteria, for instance, one may wish to calculate the soil volume fraction at a given distance from the inter-aggregate space. A distance probability density function is exactly what is needed.

APPENDIX

A continuous $s(x)$

The problem of finding a model soil volume fraction density $v_a(R)$ from a function $s(x)$ was formulated in Eq. (2.13) as

$$s(x) = \int_x^\infty s_a(R,x)\, v_a(R)\, dR \tag{2.A1}$$

Here $s(x)$ is a prescribed distance probability density function (p.d.f.) and $s_a(R,x)$ is the distance p.d.f. of a sphere, cylinder or plane sheet. The lower bound of the integration interval can be set to x, since the functions $s_a(R,x)$ are zero for $R<x$ (see Eq. (2.12)). Differentiating both sides of Eq. (2.A1) leads to

$$\frac{ds(x)}{dx} = -s_a(R,x)\, v_a(R)\big|_{R=x} + \int_x^\infty \frac{ds_a(R,x)}{dx}\, v_a(R)\, dR$$

For a plane sheet the integrand in this expression is zero. Hence, for a plane sheet model soil

$$\frac{ds(x)}{dx} = -\frac{1}{x} v_p(x)$$

which is equivalent to Eq. (2.14a). The solutions for a cylinder and sphere representation are found by differentiating Eq. (2.A1) two and three times respectively.

Approximation of a continuous solution with N probabilities p_i

Instead of a continuous distance p.d.f. $s(x)$, only N distance probabilities p_i are known for N intervals $[x_{i-1}, x_i]$ with $x_0 = 0$ and x_N the largest distance found. The p_i are related to an underlying $s(x)$ function according to

$$p_i = \int_{x_{i-1}}^{x_i} s(x)\, dx$$

If all distance intervals have equal width δ, differences between successive p_i values reflect differences in the value of $s(x)$. The forward difference operator Δ is used for a short notation:

$$\Delta p_i = p_{i+1} - p_i$$

$$\Delta^2 p_i = p_{i+2} - 2p_{i+1} + p_i$$

$$\Delta^3 p_i = p_{i+3} - 3p_{i+2} + 3p_{i+1} - p_i$$

The N aggregate size classes of the model soil are chosen according to

Eq. (2.16). The associated volume fractions v_i have to be found from the distance probabilities p_i. Using the notation above, the finite difference version of Eq. (2.14) becomes (cf. Eq. (2.17)):

$$\text{for plane sheets:} \quad v_i = -i\Delta p_i \tag{2.A2a}$$

$$\text{for cylinders:} \quad v_i = +\frac{1}{2} i^2\Delta^2 p_i \tag{2.A2b}$$

$$\text{for spheres:} \quad v_i = -\frac{1}{6} i^3\Delta^3 p_i \tag{2.A2c}$$

To proof these relations it has to be shown that, for a fixed x, the volume fraction density v_i/δ approaches the continuous $v(x)$ derived above. The proof makes use of Taylor expansions of $s(x)$. In case of plane sheets the definition of the first order derivative is equivalent to

$$s(x+\delta) - s(x) = \delta \frac{ds(x)}{dx} \quad , (\delta \downarrow 0)$$

Multiplying this by δ gives

$$p_{i+1} - p_i = \delta^2 \frac{ds(x)}{dx} \, , (\delta \downarrow 0)$$

And, using $i = x/\delta$ for a fixed value of x,

$$\lim_{\delta \downarrow 0} \left(v_i/\delta\right) = \lim_{\delta \downarrow 0} \left(-i\Delta p_i/\delta\right) = -x \frac{ds(x)}{dx}$$

With higher order Taylor expansions, the other expressions in Eq. (2.A2) can be proven in the same way. The choice of v_N in Eq. (2.17a) is motivated by the result of the matrix method for plane sheets, but may well be understood by assuming $p_{N+1} = 0$.

Matrix method

The N distance intervals need not to have equal width. The aggregate size classes of the model soil are defined again by Eq. (2.16). The corresponding volume fractions are found from the requirement that distance probabilities in soil and model soil are precisely equal. That leads to a set of N equations with N unknown volume fractions v_j (Eq. (2.18)). The matrix elements P_{ij} are calculated with Eq. (2.19). The volume fractions are found then by inverting the matrix P after calculating all its elements. Note that the distance probability density function $s_a(R_j,x)$ in Eq. (2.19) is in principle an arbitrary function. A model soil does not necessarily consist of plane sheets, cylinders or spheres.

For N distance intervals of equal width, analytic solutions for a plane sheet, cylinder and sphere model soil are given below.

Solution for plane sheets

Matrix elements $P_{ij}\,(i,j=1,...,N)$ are calculated with Eqs. (2.12a) and (2.19):

$$\begin{cases} P_{ij} = \dfrac{1}{j}, & i \le j \\ P_{ij} = 0, & i > j \end{cases}$$

The inverse of the matrix P is given by

$$\begin{cases} P_{ij}^{-1} = +i & , \; j = i \\ P_{ij}^{-1} = -i & , \; j = i+1 \\ P_{ij}^{-1} = 0 & , \; j < i \text{ or } j > i+1 \end{cases}$$

This can be shown by calculating $P^{-1}P$. The plane sheet volume fractions following from this inverse matrix are exactly the ones given in Eq. (2.17a).

Solution for cylinders

Matrix elements $P_{ij}\,(i,j=1,...,N)$ are calculated with Eqs. (2.12b) and (2.19). In case of N equal distance intervals

$$\begin{cases} P_{ij} = \dfrac{2(j-i)+1}{j^2} & , \; i \le j \\ P_{ij} = 0 & , \; i > j \end{cases}$$

The inverse P^{-1} is given by

$$\begin{cases} P_{ij}^{-1} = 0 & , \; j < i \\ P_{ij}^{-1} = +i^2 & , \; j = i \\ P_{ij}^{-1} = -3i^2 & , \; j = i+1 \\ P_{ij}^{-1} = (-1)^{j-i}\,4i^2 & , \; j \ge i+2 \end{cases}$$

Again this can be proven by carefully calculating the elements of $P^{-1}P$. The volume fractions following from P^{-1} are

$$\begin{cases} v_i = i^2\left[p_i - 3p_{i+1} + 4\sum_{j=i+2}^{N}(-1)^{j-i}p_j\right] & , \; i \le N-2 \\ v_i = i^2(p_i - 3p_{i+1}) & , \; i = N-1 \\ v_N = N^2 p_N \end{cases} \qquad (2.A3)$$

The expression for $i \leq N-2$ is not equal to Eq. (2.A2b). The volume fraction densities v_i/δ do not necessarily converge to the continuous $v(R)$ for large N. From Eq. (2.A3) however, it follows that

$$\frac{1}{2}\left[\frac{v_i}{i^2} + \frac{v_{i+1}}{(i+1)^2}\right] = \frac{1}{2}\Delta^2 p_i \quad , \; i \leq N-2$$

This implies that the average of two successive volume fractions approaches the desired limit for $N \rightarrow \infty$. Individual volume fractions, however, may "oscillate": odd and even elements of the series v_i/δ lie at opposite sides of a continuous $v(R)$. Such instabilities can be easily produced by errors in the probabilities p_i (the sign of a certain p_i in Eq. (2.A3) is different in v_i and v_{i+1}). Oscillations may also have a purely mathematical background, for instance, in case of the cylinder representation of a single sphere (Fig. 2.5).

Oscillations between successive volume fractions only lead to unstable diffusion model results if they are severe. If the solution of the applied diffusion model is continuous in the cylinder radius, the oscillations will (partly) outweigh each other. The matrix method has the advantage over Eq. (2.17b) that the model soil exactly reproduces the distance probabilities p_i. This probably causes diffusion model results to converge for relatively low values of N. The lines in Fig. 2.8 for cylinders were calculated using Eq. (2.17b) with $N=50$. Using the matrix method, 20 size classes are sufficient (see also the convergence of the lines in Fig. 2.6 for increasing N).

Note that Eq. (2.A3) may lead to negative volume fractions. That will be the case when the p_i values form a slowly decreasing or even increasing series. Negative volume fractions are not a problem in principle. As long as the applied diffusion model converges for increasing N, the method works. Increasing distance probabilities, however, imply that the intra–aggregate space (partly) consists of holes. Another type of model soil might lead then to better results (see Adaptation to worm burrows and roots).

Solution for spheres

Matrix elements P_{ij} $(i,j = 1,...,N)$ are calculated with Eqs. (2.12c) and (2.19). In case of N equal distance intervals

$$\begin{cases} P_{ij} = \dfrac{3(j-i)^2 + 3(j-i) + 1}{j^3}, & i \leq j \\ P_{ij} = 0 \qquad\qquad\qquad\qquad , & i > j \end{cases}$$

The inverse for $N=6$ is

$$\begin{pmatrix} 1 & -7 & 30 & -114 & 426 & -1590 \\ 0 & 8 & -56 & 240 & -912 & 3408 \\ 0 & 0 & 27 & -189 & 810 & -3078 \\ 0 & 0 & 0 & 64 & -448 & 1920 \\ 0 & 0 & 0 & 0 & 125 & -875 \\ 0 & 0 & 0 & 0 & 0 & 216 \end{pmatrix}$$

Sphere volume fractions calculated from this inverse matrix will generally oscillate between large negative and positive values. For increasing N, the oscillations increase. That leads to diverging results, when a diffusion model is applied to a sphere representation. Hence, sphere volume fractions should not be calculated with the matrix method.

Cylinders with a hole or root along the axis

When the inter–aggregate space is consists of worm burrows or in case of a root system, the geometry of the model soil may be adapted in order to prevent errors to become too large. Again a model soil may be derived consisting of cylinders with various sizes. The inter–aggregate space is situated now along the axes of the cylinders in the form of a burrow or root. The outer cylinder surface is subject to a zero flow condition. The burrow or root diameters can be taken equal to measured ones. Cylinder volume fractions are calculated again from a distance probability density function $s(x)$. For each point, x is defined as the distance from that point to the centre of the nearest burrow (or root). Hence, the distance p.d.f. of the soil is independent of the size of the burrows. The calculation of cylinder volume fractions is based on the distance p.d.f. $s(R,x)$ for a single cylinder:

$$\begin{cases} s(R,x) = \dfrac{2x}{R^2}, & 0 \le x \le R \\ s(R,x) = 0 \quad , & x > R \end{cases}$$

Again, N distance intervals are chosen with upper bounds x_i ($i = 1,...,N$). For equal interval widths Eqs. (2.16) and (2.19) lead to

$$\begin{cases} P_{ij} = \dfrac{2i-1}{j^2} \quad , & i \le j \\ P_{ij} = 0 \qquad , & i > j \end{cases}$$

with inverse

$$\begin{cases} P_{ij}^{-1} = \dfrac{+f^2}{2i-1} & , \; j = i \\ P_{ij}^{-1} = \dfrac{-f^2}{2i+1} & , \; j = i+1 \\ P_{ij}^{-1} = 0 & , \; j < i \text{ or } j > i+1 \end{cases}$$

From this expression directly follows Eq. (2.24) for the cylinder volume fractions.

A lognormal sphere radius distribution

The $s(x)$ functions used for testing the method for an aggregated soil were calculated for a "sphere soil" with a lognormal radius distribution. The probability density function $p(R)$ is

$$p(R) = \frac{1}{R} \frac{1}{\sigma\sqrt{2\pi}} \exp\left\{-\frac{(\ln R - \mu)^2}{2\sigma^2}\right\}$$

Here μ and σ are the mean and standard deviation of the normal distribution (of ln R). The geometric mean radius R_g and the variability factor F are defined as

$$R_g = e^{\mu} \quad \text{and} \quad F = e^{\sigma}$$

Using these relations, $p(R)$ may be calculated for any choice of R_g and F. The average sphere volume $\overline{V}$ is found as

$$\overline{V} = \int_0^{\infty} \frac{4}{3}\pi R^3 p(R)\, dR$$

The volume fraction density $v_s(R)$ is then given by

$$v_s(R) = \frac{1}{\overline{V}} \frac{4}{3}\pi R^3 p(R)$$

The $s(x)$ function belonging to a certain choice of R_g and F is calculated according to Eq. (2.21). Note that, in case of a lognormal radius distribution, also aggregate volume is lognormally distributed. The variability factor belonging to that distribution is equal to F^3.

Chapter 3

The use of cross-sectional data in diffusion models for aggregated soil

Abstract. A method is described for the derivation of a model soil from distance measurements in a cross section of an isotropic soil. The model soil consists of cylinders with different radii, each representing a length scale present in the soil structure. The model soil can be used in calculations on diffusion processes in the soil aggregates.

A cross section containing a few aggregates only leads to a large statistical uncertainty in model results, when these are meant as predictions for the average soil behavior. An example on oxygen diffusion shows that the prediction of small anoxic fractions requires a relatively large sample size. Testing the diffusion model against a measured anoxic fraction is less demanding. When the soil geometry and the anoxic fraction are derived from the same soil sample, the sample is studied as an isolated system. If the diffusion process studied is well described, the results obtained with a model soil will be valid for the sample, but will have a limited predictive value for the soil.

In case of anisotropy, distance measurements in three dimensions are required. Spatial distances cannot compensate, however, for a small sample size.

INTRODUCTION

In Chapter 2 it has been shown that the structure of an aggregated soil can be characterized by means of distance measurements. For a large number of test points the distance to the nearest macropore or crack needs to be determined. From the frequency distribution of the measured distances a model soil can be derived, which consists of spheres, or cylinders, or plane sheets with different sizes. Each size represents a length scale occurring in the soil structure. The model soil is meant to replace the real soil in calculations on diffusion processes in soil aggregates.

In this paper two practical aspects of measuring distances in the soil are discussed. True spatial distances, measured in three dimensional soil samples,

are difficult to obtain. Much easier are measurements on (digitized) photographs of cross sections. Distances measured in a cross section, however, will generally differ from spatial distances. For an isotropic soil structure this problem can be solved relatively easily. In this chapter a method is described for deriving a cylinder model soil from distances measured in the plane of a cross section.

A second problem arises from the finite size of soil samples. A distance distribution measured for a small sample is not representative for the soil structure on the field scale. Hence, a model soil derived from such a distance distribution will not correctly represent the whole soil and the results of a diffusion model applied to the model soil will not be realistic. This is demonstrated by simulating measurements for a soil consisting of spherical aggregates.

METHOD

The derivation of a model soil from three dimensional distances has been discussed extensively in Chapter 2. A model soil is derived in such a way that it has the same distance distribution as the real soil. Although a model soil may consist of spheres, or cylinders, or plane sheets, the use of cylinders has a few advantages. A cylinder model soil is more easily derived from measured distances than a sphere model soil, and results of diffusion models take an intermediate position between results for spheres and plane sheets. In this chapter, it is shown that a cylinder model soil can be also derived from cross-sectional distances. This is more difficult for model soils consisting of spheres or plane sheets.

Below, the method for deriving a cylinder model soil from three dimensional distances is briefly described. The method is then adapted to the use of two dimensional distances, measured in a cross section of an isotropic soil. The idea of this adaptation is simple. Instead of conserving the distribution of spatial distances, the distribution of cross-sectional distances is conserved. The method is tested by applying a soil respiration model to a set of spheres with a lognormal radius distribution and to a cylinder model soil based on a cross section of the spheres. The result demonstrates that the loss of information by using cross-sectional data is negligible.

The comparison between results for the real "sphere soil" and a cylinder model soil is made in two ways. At first, a cylinder model soil is derived from the distance distribution of an infinitely large cross section of the sphere soil. Then, a cylinder model soil is obtained from the cross section of a finite number of spheres. A finite sample size leads to statistical variability in the measured distance distribution, which in turn leads to a statistical uncertainty in the results

of a diffusion model. For the anoxic fraction predicted by a soil respiration model, this uncertainty is calculated by simulating the sampling process.

The use of spatial distances

For a large number of points the distance x to the nearest macropore or crack is measured. The distance range is divided into N distance intervals $[x_0, x_1], [x_1, x_2], [x_2, x_3], \ldots, [x_{N-1}, x_N]$. The lower bound x_0 of the first interval is set at zero and x_N is set equal to the largest distance found. The fraction of distances in class i is written as p_i, which is the probability that the distance x falls in the interval $[x_{i-1}, x_i]$. The model consisting of cylinders should have the same set of distance probabilities p_i ($i = 1,...,N$). That can be realized by means of cylinders with N discrete radii, which are set equal to the upper bounds of the distance classes. Hence,

$$R_i = x_i, \quad i = 1,...,N$$

The cylinders with radius R_j ($j = 1,...,N$) occupy a yet unknown fraction v_j of the model soil volume. The distance probabilities p_i for the model soil are calculated as

$$p_i = \sum_{j=1}^{N} P_{ij} v_j, \quad i = 1,...,N \tag{3.1}$$

This equation may be understood in the following way. The volume fraction v_j is the probability that a randomly chosen point lies in a cylinder with radius R_j. Further, P_{ij} is the probability for a cylinder with radius R_j to "produce" a distance in class i. The overall probability of finding a distance in class i becomes then the product $P_{ij} v_j$, summed over all radius classes.

The matrix elements P_{ij} are calculated as

$$P_{ij} = \int_{x_{i-1}}^{x_i} s_c(R_j, x)\, dx$$

in which $s_c(R_j, x)$ is the distance probability density function of a cylinder with radius R_j:

$$\begin{cases} s_c(R_j, x) = \dfrac{2}{R_j}\left(1 - \dfrac{x}{R_j}\right), & 0 \le x \le R_j \\ s_c(R_j, x) = 0, & x > R_j \end{cases}$$

In Fig. 3.1 a graph of $s_c(R_j, x)$ has been drawn for $R_j = 1$.

The distance probabilities of the model soil are set equal to the measured ones. Equation (3.1) becomes then a set on N linear equations with N unknown volume fractions v_j. In case of distance intervals with equal widths, the linear set

can be solved analytically. That leads to cylinder volume fractions which are directly expressed as function of (measured) distance probabilities (see Chapter 2).

The use of cross-sectional data

Instead of measuring true spatial distances from test points to the nearest macropore or crack, distances are measured in a cross section of the soil. Test points are chosen in the plane and distances to the nearest macropore or crack intersection are determined. The frequency distribution of these distances differs from the distribution of true spatial distances. The distance probability density function for the cross section of an isotropic soil is written as $s^*(x)$. Finite probabilities, measured or calculated for distance intervals, are written as p_i^*.

The true spatial distance belonging to a certain test point, is the distance to the nearest point of the inter-aggregate space. That nearest point will usually lie outside the plane of the cross section. Hence, each distance x measured in the plane will be equal to, or larger than the spatial distance belonging to the test point. On the average, distances measured in an intersecting plane will be larger and the distance probability density function $s^*(x)$ will show a shift to larger distances compared to $s(x)$.

The use of distance probabilities p_i^* in Eq. (3.1) would lead to biased weights v_j. The problem can be solved by cross-sectioning the model soil as well: instead of deriving a model soil with the distance probabilities p_i of the real soil, the profile probabilities p_i^* are conserved. The derivation proceeds along the same lines. Again, N cylinder radii are set equal to the upper bounds of the distance intervals and to each radius R_j belongs a volume fraction (or weight) v_j.

At first the probabilities p_i^* need to be calculated for a cylinder model soil with, yet unknown, volume fractions v_j. The model soil is made isotropic by giving the cylinders a random orientation in space. One may imagine a large number of randomly oriented cylinders with different sizes. How the cylinders are actually positioned relative to each other is irrelevant. The volume fractions belonging to the N radii are still the only parameters of the model system. As the contribution of cylinders with radius R_j to the total area of a cross section is proportional to the occupied volume fraction v_j, the probability p_i^* of measuring a distance in the i-th interval becomes, analogous to Eq. (3.1),

$$p_i^* = \sum_{j=1}^{N} P_{ij}^* v_j , \quad i=1,...,N \tag{3.2}$$

The matrix element P_{ij}^* is the probability that randomly oriented cylinders with radius R_j produce a distance in the i-th interval. This probability is calculated as

$$P_{ij}^{*} = \int_{x_{i-1}}^{x_i} s_C^{*}(R_j,x)\,\mathrm{d}x$$

in which $s_C^{*}(R_j,x)$ is the distance probability density function for the cross section of randomly oriented cylinders with radius R_j. This function has to be calculated numerically.

The cross section of a single cylinder is an ellipse for which the distance probability density function is calculated numerically. The overall probability density $s_C^{*}(R,x)$ is obtained then as an integral over the cylinder orientations, accounting for the fact that the contribution of each ellipse is proportional to the area of its cross section. Details of the numerical procedure can be found in the Appendix. In Fig. 3.1 a graph of $s_C^{*}(R,x)$ has been drawn for $R=1$. The curve shows the expected shift to larger distances compared with the graph of $s_C(R,x)$ for the same cylinder.

Now, the distance probabilities in Eq. (3.2) can be set equal to measured probabilities p_i^{*}. Again, the result is a set of N linear equations with N unknown volume fractions v_j. The solution has to be found numerically. In case of equal distance intervals, the matrix P_{ij}^{*} depends on N only and not on the distances and radii. Then, for certain values of N, inverse matrices may be calculated. With help of these inverse matrices, cylinder volume fractions follow immediately from measured probabilities p_i^{*}. The inverse matrix for $N=8$ is given in the Appendix.

For increasing N, the cylinder volume fractions approach a continuous weight function. There are no instabilities resulting from the use of discrete cylinder

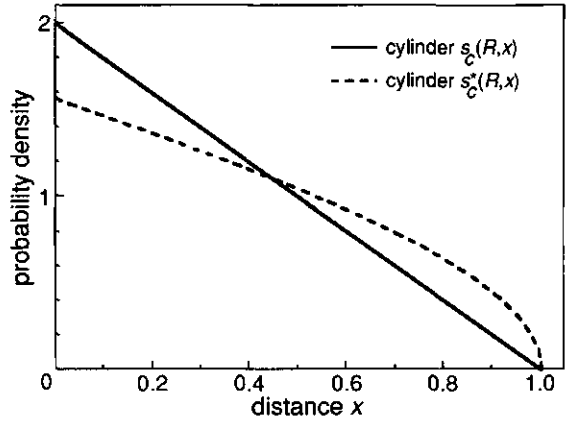

Figure 3.1. The distance probability density functions $s_C(R,x)$ for a cylinder with $R=1$ and $s_C^{*}(R,x)$ for the cross section of randomly oriented cylinders with radii $R=1$ (see Eq.(3.A2)).

sizes. With respect to this point, two-dimensional distances are easier to handle than spatial distances.

The derivation of sphere volume fractions from cross-sectional distances suffers from the same problem as the derivation of these volume fractions from spatial distances (cf. Chapter 2). Plane sheet volume fractions cannot be obtained from cross-sectional data with the method developed in this paper. The difficulties with spheres and plane sheets are briefly discussed in the Appendix.

The cross section of randomly positioned spheres.

The method is tested by applying a model of oxygen diffusion to a "soil" consisting of spheres with a lognormal radius distribution. The diffusion model is applied directly to the spheres, and to a model soil derived from a cross section of the sphere soil. The anoxic fraction of the model soil can be compared then with the true anoxic fraction of the sphere soil. Distance probabilities p_i^* are obtained in two ways. At first they are calculated for an infinitely large cross-sectional surface. Then, in the next section, the process of cross-sectioning the sphere soil is simulated numerically, which leads to distance probabilities for a finite part of the sphere soil.

The distance probability density function of a single sphere with radius R is (cf. Chapter 2)

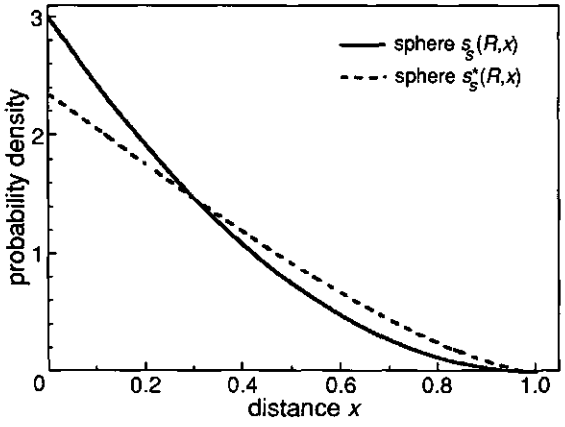

Figure 3.2. The distance probability density functions $s_S(R,x)$ for a sphere with $R=1$ and $s_S^*(R,x)$ for the cross section of randomly oriented spheres with radii $R=1$ (Eq.(3.3)).

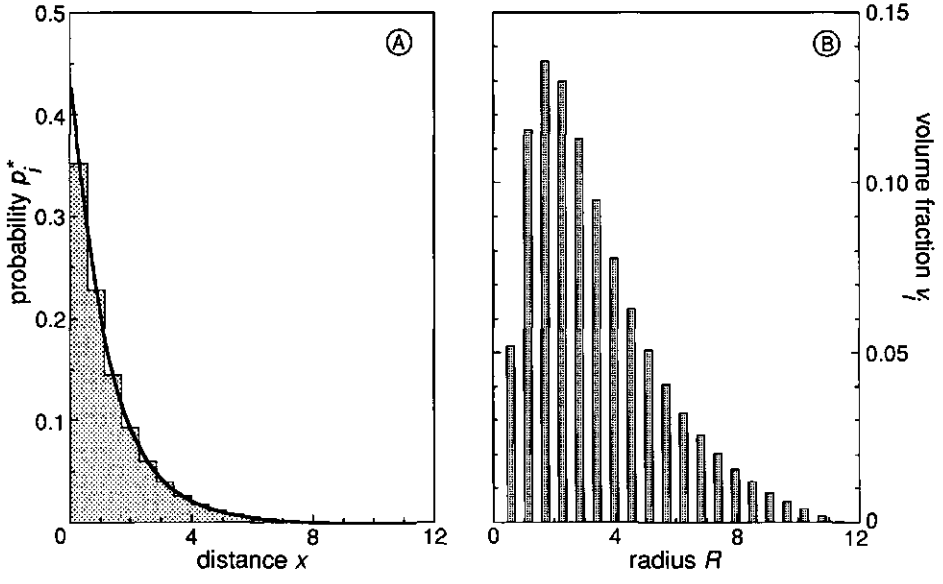

Figure 3.3. (A) The function $s^*(x)$ for an intersection of a sphere soil with geometric mean radius $R_g = 1$ and variability factor $F = 2$ with 20 distance probabilities p_i^* derived from it by integration. The continuous function $s^*(x)$ has been multiplied by the interval width in to get equal vertical scales. (B) Volume fractions or weights derived for a cylinder model soil with the same distance probabilities p_i^* as the sphere soil.

$$\begin{cases} s_s(R,x) = \dfrac{3}{R}\left(1-\dfrac{x}{R}\right)^2, & 0 \le x \le R \\ s_s(R,x) = 0 & , \; x > R \end{cases}$$

The cross section of this sphere is a circle of which the size depends on the position of the intersecting plane relative to the centre of the sphere. In the Appendix it is shown that for a cross section at random "height" the distance probability density function is

$$\begin{cases} s_s^*(R,x) = \dfrac{3}{R}\left\{\dfrac{\pi}{4} - \dfrac{x}{2R}\sqrt{1-\left(\dfrac{x}{R}\right)^2} - \dfrac{1}{2}\arcsin\left(\dfrac{x}{R}\right)\right\}, & 0 \le x \le R \\ s_s^*(R,x) = 0 & , \; x > R \end{cases} \tag{3.3}$$

In Fig. 3.2 graphs have been drawn of the functions $s_s(R,x)$ and $s_s^*(R,x)$ for a sphere with $R = 1$. Again, the graphs demonstrate a shift to larger values when distances are determined in the plane of a cross section.

The lognormal radius distribution of the sphere soil is characterized by a geometric mean radius R_g and a factor F expressing the size variability. The radius interval of one standard deviation around the geometric mean is

$[R_g/F, R_g F]$. The spheres occupy random positions in space, which implies that, for each sphere size separately, Eq. (3.3) can be used. The function $s^*(x)$ for the sphere soil is found then as an integral of Eq. (3.3) over the distance distribution, accounting for the fact that spheres contribute to the overall probability density in proportion to their volume (see Appendix). Figure 3.3a shows a graph of $s^*(x)$ for $R_g = 1$ and $F = 2$. The same figure shows 20 distance probabilities p_i^* derived from the continuous function $s^*(x)$.

The 20 distance probabilities have been used to calculate the volume fractions for a cylinder model soil by solving Eq. (3.2). Figure 3.3b shows the result. Note that no information has been used on the nature of the underlying sphere size distribution. The cylinder volume fractions have been derived from the probabilities p_i^* only.

Generation of a finite sample

Distance probabilities p_i^* calculated in the above described way, refer to an infinitely large cross section. In the statistical sense, the values of p_i^* in Fig. 3.3a are expectation values. If the cross section contains a finite number of aggregates only, the probabilities p_i^* will vary among different samples. That leads to variability in the derived model soil and in the result of a diffusion model applied to it.

From the above described sphere soil a sample may be taken consisting of a prescribed number of circles. The sample generation proceeds as follows. A sphere radius is randomly chosen from a lognormal distribution. Then an intersection height is randomly chosen between zero and a fixed, large value. When the intersection height is smaller than the sphere radius, the sphere has been hit and the resulting circle is included in the sample. The process is repeated until the required number of circles is found. This procedure accounts for the fact that the probability of being included in a cross section is proportional to the sphere radius.

For a generated sample of circles, distance probabilities p_i^* are easily calculated. The number of distance classes N was set at 20, since a further increase of N did not influence the final results. Equation (3.2) is solved then to obtain the 20 cylinder volume fractions of the model soil belonging to the generated sample.

A model of anaerobiosis

A diffusion model is applied to a model soil by evaluating the model for each cylinder size separately and by calculating then a weighted sum of results, using

the volume fractions v_j as weights. Calculations have been done for a model of soil respiration and anaerobiosis. The results are compared with exact results obtained directly for the sphere soil by integrating the anoxic volume over the radius distribution.

The respiration model originates from Greenwood (1961) and Currie (1961). A slightly simplified version has been used, which has been described in Chapter 2. The anoxic fraction of a spherical or cylindrical aggregate depends on the diffusion distance d defined by

$$d \equiv \sqrt{DC/Q} \tag{3.4}$$

in which D is the diffusion coefficient, C the oxygen concentration at the aggregate surface and Q the specific respiration rate.

The diffusion distance d has the dimension of a length. It is a process parameter and does not depend on geometrical properties of the soil aggregate. When d is much less than aggregate size, oxygen will only be present in a thin layer near the surface. When d is above a certain threshold value, the aggregate is completely oxic. The precise relation between d and the anoxic fraction depends on the geometry of the aggregate. The solutions for a spherical and cylindrical geometry were both given in Chapter 2.

RESULTS

An infinite sample size

For a sphere soil characterized by values of R_g and F, a cylinder model soil is derived as shown in Fig. 3.3. For both the sphere soil and its cylinder representation, the relation between the diffusion distance d and the anoxic volume fraction φ is calculated. Figure 3.4 shows the result for three values of F. By giving the anoxic volume as a function of d/R_g, the curves depend only on F and become independent of the value of R_g.

For each value of F the curves for the spheres and the cylinders are close. Hence, in case of isotropy the conservation of $s^*(x)$ works as well as the conservation of spatial distances.

A finite sample size

Samples of 20 circles have been generated for a sphere soil with $F = 2$. For each sample, distance probabilities p_i^* and a cylinder model soil have been calculated. Then, after choosing a value for d, an anoxic volume fraction can be found for both the whole sphere soil and the model system derived from the

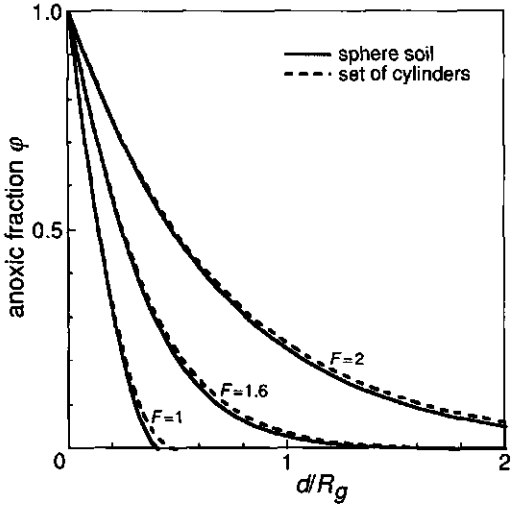

Figure 3.4. The anoxic volume fraction of a sphere soil and a cylinder model soil as function of the d/R_g in which the diffusion distance d is defined as $\sqrt{DC/Q}$ (Eq. (3.4)). The cylinder model soil is derived with Eq. (3.2) from the distance probabilities shown in Fig. 3.3a.

20 circles. The fraction of the sphere soil is the true anoxic fraction of the system and the result for the model soil varies as a result of the small sample size. In Fig. 3.5a this is demonstrated for 5000 samples of 20 circles.

For each point in Fig. 3.5a, the same value of d was applied to sphere soil and model soil. This means that no uncertainty has been simulated in the parameters of the diffusion process. The large variability in Fig. 3.5a results entirely from the sampling procedure. Especially small anoxic fractions are hard to predict. The reason is that the contribution of rare, large aggregates to the samples varies strongly.

In Fig. 3.5 also graphs are given for a sample size of 40, 80 and 160 circles. As usual, a four times larger sample size leads to a two times smaller variability in the result. Even when a sample of 160 circles (aggregates) is analysed, an anoxic fraction of 10 % is only roughly predicted and an anoxic fraction of 5% cannot be safely predicted (see Fig. 3.5d). In the limit for an infinite sample size, all points lie on a line corresponding to the difference between the two curves for $F = 2$ in Fig. 3.4.

The results in Fig. 3.5 are valid for $F = 2$ only. This value for the size variability is not extremely large, however. The model soil in Fig. 3.3b gives an impression of the aggregate size variability corresponding to this choice. Larger values of F result into a still larger uncertainty in model prediction.

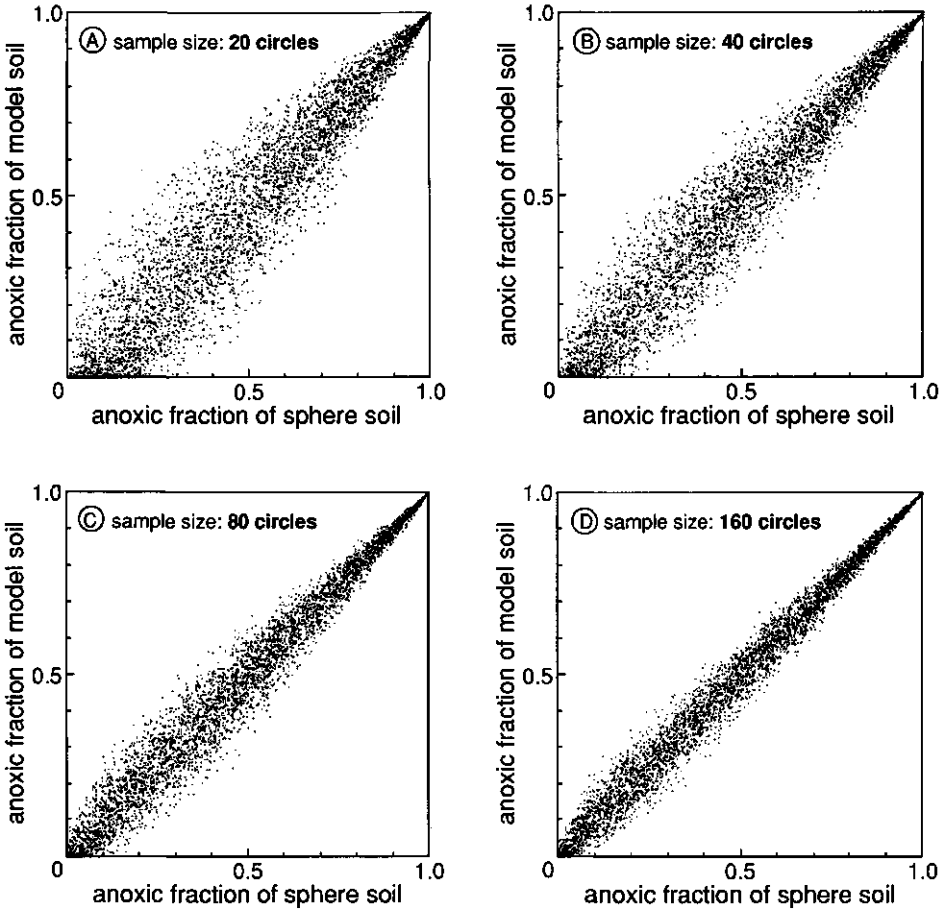

Figure 3.5. Comparison between the anoxic fraction of a sphere soil with $R_g = 1$ and $F = 2$ and the anoxic fraction of the model soil derived from a cross section of the sphere soil. In each graph, the result of 5000 cross sections is given. A cross section contains 20, 40, 80 or 160 circles.

Studying the sample instead of the soil

The above results demonstrate that it will be difficult to use a diffusion model for an aggregated soil for prediction. Even if aggregate size is the only varying factor, large samples are required for a description of the soil geometry which is suitable for model prediction. The reason is simply that soil samples need to be *representative. Testing a diffusion model, however, a relatively small sample may* be studied as an isolated aggregated system. The model requires distance

probabilities derived from the sample as input data. And the result of the diffusion model is compared with a property of the same sample for which the distance probabilities were measured.

The use of small samples for model testing has been simulated for the sphere soil defined above. For the samples used to construct Fig. 3.5b, also the anoxic surface fraction has been calculated. That is a property of the sample and its statistical expectation is equal to the anoxic volume fraction for the whole sphere soil (Delesse, 1847 referred to by Weibel, 1979). Hence, the result for a cylinder model soil can be regarded as a prediction of the anoxic surface fraction. In Fig. 3.6 the two quantities are compared for 5000 samples of 40 circles. The variability is much less than in Fig. 3.5b, although sample size is equal. The reason is that the geometry of the sample and its anoxic surface fraction are correlated properties. A large circle, for instance, has a relatively large anoxic part and leads to the presence of large cylinders in the model soil. Hence, the cylinder model soil forms a description of the sample and not of the soil.

The remaining variability in Fig. 3.6 is due to the fact that 40 circles are used instead of 40 whole spheres. For a sample of 40 whole spheres, a cylinder representation leads to an almost exact anoxic fraction. The use of a cross section of 40 spheres, however, leads to some statistical variability.

The large variability in Fig. 3.5b is caused by both a small sample size and by the use of cross-sectional distances. The variability resulting from the use of a cross section instead of full spheres, however, is small (Fig. 3.6). Hence, the major part of the variability in Fig. 3.5 is caused by a finite sample size. This

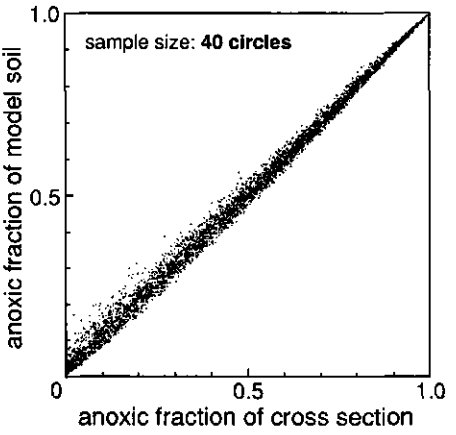

Figure 3.6. Comparison between the anoxic fraction of a cross-sectional surface with the anoxic fraction calculated for a cylinder model soil derived from the same cross section. Results are shown for 5000 cross sections (samples) consisting of 40 circles, generated for a sphere soil with $R_g = 1$ and $F = 2$.

implies that problems resulting from a too small sample size cannot be solved by the use of three dimensional distances. Clearly, in case of anisotropy, three dimensional distances are needed for a correct description of the soil structure. They do not reduce sample size requirements, however.

CONCLUSIONS

When a three dimensional picture of the soil structure is available, a cylinder model soil can be derived from the distribution of the three dimensional distance from a random point in the soil to the nearest crack or macropore. The volume fractions, or weights, of the model soil are calculated in such a way that the model soil has the same distance distribution as the real soil. The distance distribution is thus used as a conserved property in deriving the model soil.

When the soil structure is isotropic, the method of obtaining a model soil can be adapted to the use of distances measured in the plane of a cross section. Instead of conserving the distribution of the true, spatial distance, the distance distribution belonging to a cross section is conserved. The model soil is made isotropic by assigning a random orientation to all cylinders. Then, distance probabilities for a cross section of the model system can be found and can be set equal to measured probabilities. In case of an isotropic soil structure, the loss of information by using cross-sectional data is negligible.

An alternative approach is to correct two dimensional distances for the fact that they are somewhat too large. After such a correction the distances can be handled as true spatial distances. An accurate correction depends on aggregate shape, however, and the analysis of aggregate shape in order to correct measured distances would deprive the whole method of its simplicity. Therefore, uncertainties in the correction have to be accepted. One might use a fixed aggregate shape, for instance, to calculate corrected distance probabilities. Such an explicit correction has not been developed in this paper. Instead, the problem is solved by cross-sectioning the model soil as well. This may be regarded as an implicit correction, assuming a cylindrical aggregate shape. Corrected distance probabilities have not to be calculated explicitly, although that can be done afterwards by calculating $s(x)$ for the obtained model soil.

In practice, the sample used to characterize the soil structure necessarily has a finite size. A small sample size leads to a large statistical uncertainty in model results when these are meant as predictions for the soil as a whole. Model testing is less demanding. A model may be tested by studying a soil sample as an isolated system. In that case, the sample needs not to be representative, but model results obtained for the sample do have little predictive value for the soil.

In case of isotropy, the error due to the use of cross-sectional distances will usually be much smaller than the statistical variability resulting from the finite number of (intersected) aggregates in a sample. It should be emphasized that the use of three dimensional pictures cannot compensate for a small sample size.

APPENDIX

The value of x belonging to a point inside a three dimensional aggregate is defined as the distance between that point and the nearest point of the outer surface. The function $s(x)$ is defined as the probability density function belonging to the distribution of the distance x for a randomly chosen point.

The points at a distance x from the outer surface form an "inner surface". The distance probability density function may be defined as the size of this inner surface divided by the object volume (Chapter 2). For $x=0$, the function $s(x)$ is equal to the ratio of outer surface and volume of the aggregate. For other values of x, $s(x)$ equals the ratio between an "inner surface" and the total volume. For symmetrical objects this definition of $s(x)$ provides a simple way to find an expression for $s(x)$. For a long cylinder with radius R, for instance, the distance p.d.f. is

$$\begin{cases} s(x) = \frac{2}{R}\left(1-\frac{x}{R}\right) & , \ 0 \le x \le R \\ s(x) = 0 & , \ x > R \end{cases}$$

For a two dimensional object, there is an analogous method. All points at a distance x from the edge form an "inner perimeter" with length $L(x)$. The distance p.d.f. $s(x)$ is the inner perimeter length divided by the total area S of the two-dimensional object.

To calculate the $s^*(x)$ function of a three dimensional object one should imagine a plane containing all possible cross sections of the object. The distance p.d.f. $s^*(x)$ is defined then for all cross sections together. The total (or average) length $L(x)$ is divided by a total (or average) area S. Alternatively one may use the distance p.d.f. $s_i(x)$ of the individual cross sections, for which holds

$$s_i(x) = \frac{L_i(x)}{S_i}$$

Then

$$s^*(x) \equiv \frac{\sum L_i(x)}{\sum S_i} = \frac{\sum S_i s_i(x)}{\sum S_i} = \sum \left(\frac{S_i}{\sum S_i}\right) s_i(x) \qquad (3.A1)$$

Hence, the desired function $s^*(x)$ is a weighted sum of the distance probability density functions of the individual cross sections. The contribution of the i-th cross section is proportional to its area S_i. Indeed, the probability to find a randomly chosen point inside the i-th cross section is proportional to S_i.

In theoretical calculations on infinitely large cross sections, the sums in Eq. (3.A1) can be replaced by integrals.

The function $s_S^*(R,x)$ for a randomly intersected sphere

The cross section of a sphere with radius R is a circle. When the distance between the intersecting plane and the sphere centre is written as z (the intersection height), the radius r of the circle is

$$r = \sqrt{R^2 - z^2}$$

The "inner perimeter" length $L(R,z,x)$ for a distance x from the edge becomes

$$\begin{cases} L(R,z,x) = 2\pi\left(\sqrt{R^2 - z^2} - x\right), & |z| \le z_m \\ L(R,z,x) = 0 & , \; |z| > z_m \end{cases}$$

with $z_m = \sqrt{R^2 - x^2}$. To get an average length this function is integrated over the height z and divided by the integration interval $2R$:

$$\overline{L}(R,x) = \frac{1}{2R}\int_{-R}^{+R} L(R,z,x)\,dz$$

The average circle surface $\overline{S}$ equals the sphere volume divided by $2R$. Then

$$s_S^*(R,x) \equiv \frac{\overline{L}(R,x)}{\overline{S}} = \frac{3}{4\pi R^3}\int_{-R}^{+R} L(R,z,x)\,dz =$$

$$= \frac{3}{4\pi R^3}\int_{-z_m}^{+z_m} 2\pi\left(\sqrt{R^2 - z^2} - x\right)dz =$$

$$= \frac{3}{R}\left\{\frac{\pi}{4} - \frac{x}{2R}\sqrt{1 - \left(\frac{x}{R}\right)^2} - \frac{1}{2}\arcsin\left(\frac{x}{R}\right)\right\}, \quad 0 \le x \le R$$

The function $s_C^*(R,x)$ for a randomly oriented cylinder

The cross section of a cylinder with radius R is an ellipse. Its shape depends on the angle θ between the ellipse axis and the intersecting plane. The points at a distance x from the ellipse edge form an "inner perimeter" with length $L(R,\theta,x)$.

The average length $\overline{L}(R,x)$ is calculated by integrating $L(R,\theta,x)$ over the angle distribution. In case of a random cylinder orientation (isotropy) the p.d.f. for θ is given by

$$p(\theta) = 2 \sin\theta \cos\theta$$

Then

$$\overline{L}(R,x) = \int_0^{\pi/2} L(R,\theta,x)\, p(\theta)\, d\theta$$

For certain values of R and x this integral has been calculated numerically by means of 7 point Gauss-Legendre integration (e.g. Press *et al.*,1986). For each of the 7 points the inner perimeter length $L(R,\theta,x)$ has been evaluated using elementary formula for an ellipse and step by step integration.

The average ellipse surface equals

$$\overline{S} = \int_0^{\pi/2} \frac{\pi R^2}{\sin\theta}\, p(\theta)\, d\theta = 2\pi R^2$$

And the desired function becomes

$$s_c^*(R,x) = \frac{\overline{L}(R,x)}{\overline{S}} \qquad (3.A2)$$

Note that the actual calculations need to be carried out only for $R=1$. For any other cylinder radius values of $s_c^*(R,x)$ follow from

$$s_c^*(R,x) = \frac{1}{R}\, s_c^*\left(1,\frac{x}{R}\right)$$

This formula also holds for the above analytical result for a sphere. A graph of $s_c^*(1,x)$ has been drawn in Fig. 3.1.

The calculation of cylinder volume fractions

Cylinder volume fractions can be calculated from (measured) distance probabilities p_i^* with Eq. (3.2). The radius R_j is chosen equal to the upper bound of the j-th distance class. The matrix element P_{ij}^* is calculated by integrating the function $s_c^*(R_j,x)$ (Eq. (3.A2)) over the i-th distance interval. For 8 distance classes of equal width on [0,1] the inverted matrix is.

$$\begin{pmatrix}
1.000 & -1.920 & 1.085 & -.289 & .124 & -.028 & .017 & -.000 \\
0 & 2.920 & -5.502 & 3.031 & -.803 & .346 & -.075 & .047 \\
0 & 0 & 5.416 & -10.118 & 5.517 & -1.462 & .627 & -.137 \\
0 & 0 & 0 & 8.376 & -15.576 & 8.449 & -2.241 & .962 \\
0 & 0 & 0 & 0 & 11.738 & -21.763 & 11.768 & -3.124 \\
0 & 0 & 0 & 0 & 0 & 15.458 & -28.600 & 15.430 \\
0 & 0 & 0 & 0 & 0 & 0 & 19.504 & -36.027 \\
0 & 0 & 0 & 0 & 0 & 0 & 0 & 23.850
\end{pmatrix}$$

The sum of the numbers in each column is 1. This, together with the unit sum of the probabilities p_i^*, guarantees that the sum of the cylinder volume fractions is also 1. For an increasing number of distance intervals new rows and columns are added to the inverted matrix, leaving unchanged the previously calculated elements. The above example for $N=8$ shows that, after the first few numbers, the absolute value of the numbers in each row rapidly decreases. This property leads to convergence when N increases. The volume fraction densities v_i/δ converge to a continuous function $v(R)$. Sphere volume fractions do not have that property as was shown in the Appendix of Chapter 2. That also holds for intersected spheres. The rows of the inverted matrix consist of numbers rapidly increasing in absolute size.

For plane sheets there is another difficulty. In the cross section of a plane sheet, there are points with a distance x to the edge exceeding the plane sheet radius R (unless the plane sheet is intersected at a right angle). When the intersection is (almost) parallel to the plane sheet, arbitrarily large distances x occur in the cross section. This implies that the distance p.d.f. $s^*(R,x)$ of a randomly oriented plane sheet gives a non-zero probability for all positive distances, irrespective of R. It is not possible then to set up a matrix equation analogous to Eq. (3.2) for the calculation of plane sheet volume fractions.

$s^*(x)$ for a set of spheres

The occurrence of different radius values is described by a probability density function $v_S(R)$. The product $v_S(R)\,dR$ describes the volume fraction occupied by spheres with a certain radius.

Calculating $s^*(x)$ for spheres with different sizes, one should imagine an infinitely large system with spheres at random positions in space. The probability of being hit by an intersecting plane is proportional to sphere radius. Once hit, the contribution of the intersection to the overall distance p.d.f. is proportional to the intersection surface (e.g. Eq.(3.A1)). Together that means that the spheres in a certain size class contribute to the overall function $s^*(x)$ in proportion to their volume. Hence, $s^*(x)$ is found by integrating the single sphere $s_S^*(R,x)$ over the volume distribution:

$$s^*(x) = \int_0^\infty s_S^*(R,x)\; v_S(R)\,dR$$

A lognormal radius distribution is characterized by a geometric mean radius R_g and a variability factor F. The underlying normal distribution has a mean μ and a variance σ^2. The relation between these parameters is given by

$$\mu = \ln R_g \quad , \qquad \sigma = \ln F$$

Expressions for the probability density of the sphere radius R, for the mean sphere volume and for the volume fraction density density $v_S(R)$ are given in Chapter 2.

Chapter 4

Measuring the diffusivity of oxygen in soil on a millimeter scale

Abstract. The diffusivity of oxygen in soil can be measured by making use of a concentration wave applied at the surface of a core sample. The gas above the sample is periodically changed from nitrogen to air and visa versa. The concentration wave is measured as function of depth with an oxygen electrode. For different Fourier components in the signal, phase shifts can be calculated as function of depth. The diffusivity follows from the increase of the phase shift with depth. It is shown theoretically that phase shifts are more suitable than signal amplitudes for the derivation of a diffusivity. Phase shifts are also easier to measure and do not require electrode calibration.

For a clayey soil with an air-filled porosity of about 5% a diffusivity of 0.9×10^{-9} $m^2 s^{-1}$ was measured. This low value can be explained by the presence of locally water-saturated clay. The measured diffusivity corresponds to a tortuosity (impedance factor) of 0.43 and to a diffusion coefficient of about 0.4×10^{-9} $m^2 s^{-1}$. This value is more than 100 times smaller than the macroscopic diffusion coefficients measured for whole core samples of the same soil type. This demonstrates the large difference in soil properties on different scales. The presence of water-saturated zones with a size of several millimeters in an otherwise unsaturated soil is relevant in describing diffusive transports and anaerobiosis.

INTRODUCTION

Currie (1961) pointed out that anaerobe zones may occur in a generally well aerated soil. That will be the case when vertical oxygen transport largely takes place through large gas-filled pores. Between the gas-filled pores oxygen transport may be too small to maintain aerobe conditions everywhere.

Another way of expressing this is that the diffusion coefficient of oxygen in soil depends on the scale on which it is measured. On a macroscopic scale, the diffusion coefficient is largely determined by the air-filled macropores. Transport of oxygen can be described then by means of a macroscopic diffusion coefficient and the respiratory activity of the soil on the same scale.

Table 4.1. Symbols, definitions and units.

symbol	description	units	Equation
A_0	amplitude of sine wave at the surface	mol m^{-3}	(4.1)
$A_n(x)$	amplitude of n-th component at depth x	mV	(4.8)
$a(x)$	relative amplitude at depth x	-	(4.4)
$a_n(x)$	sine part of n-th Fourier component	mV	(4.6)
$b_n(x)$	cosine part of n-th Fourier component	mV	(4.6)
$c(x,t)$	concentration as a function of x and t	mol m^{-3}	(4.2)
	or electrode signal	mV	(4.6)
c_{av}	average concentration	mol m^{-3}	(4.1)
D	diffusivity of oxygen in soil	m^2 s^{-1}	(4.3),(4.13)
D_S	oxygen diffusion coefficient in saturated soil	m^2 s^{-1}	(4.12)
D_W	diffusion coefficient in free water	m^2 s^{-1}	(4.12)
d	damping depth	m	(4.3)
f	impedance factor or tortuosity	-	(4.12)
θ	volumetric water content	-	(4.12)
M	order of trend function	-	(4.6)
m	number of trend component (=1,2,3...)	-	
N	number of Fourier components in fit	-	(4.6)
n	number of Fourier component (=1,2,3...)	-	
$P_m(t)$	polynomial of order m	-	
$\theta(x)$	phase shift at depth x	rad	(4.5)
$\theta_n(x)$	phase shift relative to surface signal	rad	(4.10),(4.11)
$\theta_n'(x)$	phase of n-th component at depth x	rad	(4.7),(4.9)
t	time		
ω	angular frequency	rad s^{-1}	
x	coordinate ; distance to the surface	m	
$z_m(x)$	coefficient in m-th trend component	mV	(4.6)

On a millimeter scale the situation may be very different. Most pores may be water-filled leading to a much lower oxygen diffusion and possibly to local anaerobiosis. The importance of this phenomenon depends on soil type, water content and respiratory activity. In this chapter a method is described for measuring the diffusivity of oxygen on a millimeter scale. The results for a clayey soil demonstrate the existence of water-saturated zones with a size of several millimeters.

The method is based on a phenomenon which is well known from heat transport. A periodic change of the oxygen concentration is applied to the surface of a cross section. That leads to periodicity in the signal of an oxygen electrode at a few millimeters from the surface. The amplitude of this "concentration wave" decreases with depth and the phase shift increases with depth. It is shown that

the diffusivity can be best derived from the phase shift. The use of concentration waves does not require electrode calibration nor longterm electrode stability.

Below, at first, the theoretical basis of the method is discussed and some experimental details are given. The method has been tested by measuring the diffusivity of oxygen in water. Finally, results are given for a clayey soil. Table 4.1 gives a description of the symbols used.

METHOD

At the surface of a cross section a sinusoidal "concentration wave" is applied. At a large depth, the concentration does not vary and approaches an average value c_{av}. The differential equation describing this is

$$\frac{\partial c(x,t)}{\partial t} = D\frac{\partial^2 c(x,t)}{\partial x^2}$$

with boundary conditions

$$\begin{cases} c(x,t) = c_{av} + A_0 \sin \omega t\,, & x = 0 \\ c(x,t) \rightarrow c_{av} & , \; x \rightarrow \infty \end{cases} \tag{4.1}$$

The solution for the concentration $c(x,t)$ at time t at a distance x from the surface is

$$c(x,t) = c_{av} + A_0\, e^{-x/d} \sin\left(\omega t - \frac{x}{d}\right) \tag{4.2}$$

The concentration $c(x,t)$ at a depth x depends on a characteristic length d, the damping depth. This depth is determined by the diffusivity D and the angular frequency ω according to

$$d = \sqrt{\frac{2D}{\omega}} \tag{4.3}$$

Koorevaar *et al.* (1983) give a derivation of this result for heat instead of mass.

Equation (4.2) expresses that the amplitude of the concentration wave decreases exponentially with depth. A relative amplitude $a(x)$ is defined as the ratio between the amplitude at a depth x and the amplitude A_0 at the surface. From Eq. (4.2) follows

$$a(x) = e^{-x/d} \tag{4.4}$$

The concentration wave at depth x also shows a phase shift $\theta(x)$, a delay relative to the surface wave. This phase shift increases linearly with x according to

$$\theta(x) = \frac{x}{d} \tag{4.5}$$

Both, the relative amplitude and phase shift, depend only on the ratio x/d, a

dimensionless depth. Hence, the damping depth d can be determined by measuring either $a(x)$ or $\theta(x)$. A measured damping depth leads to a value of the diffusivity D by making use of the (known) angular frequency and Eq. (4.3).

In principle, the relative amplitude and the phase shift should both lead to the same damping depth. In practice, however, measured functions $a(x)$ and $\theta(x)$ will not always be consistent. There are two reasons for preferring the phase shift $\theta(x)$ in such cases. The first reason is that the behavior of phase shifts is more robust against deviations of the plane geometry underlying Eq. (4.2). The second reason is that amplitudes are more difficult to measure than phase shifts. This is further discussed below.

The influence of macropores

The derivation above holds for a homogeneous soil and a flat geometry. A more realistic situation is drawn in Fig. 4.1. The oxygen electrode penetrates into an aggregate from the surface. The electrode is 1 mm thick and amplitudes and phase shifts are measured at several depths between 0 and 4 mm, for instance. At small depths the diffusion is dominated by the presence of the flat surface of the cross section. The air-filled macropores are relatively far away from the electrode. At larger depths the situation changes. Air-filled macropores represent open channels to the surface and when the electrode approaches a macropore, measured oxygen concentrations will certainly be influenced.

The problem is the extend to which the presence of macropores will influence the validity of Eqs. (4.4) and (4.5) near the surface. The presence of macropores implies that the assumption of a plane geometry does not hold. Consequently, some insight can be gained by studying the behavior of concentration waves for non-plane geometries.

For a sinusoidal concentration variation the diffusion equation has been solved numerically for a plane sheet with a thickness of $2R$, for a cylinder with radius R, and for a sphere with radius R. For these three object types the

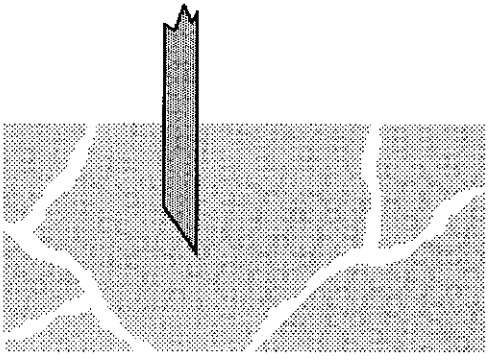

Figure 4.1. An oxygen electrode penetrating into water-saturated soil between air-filled pores.

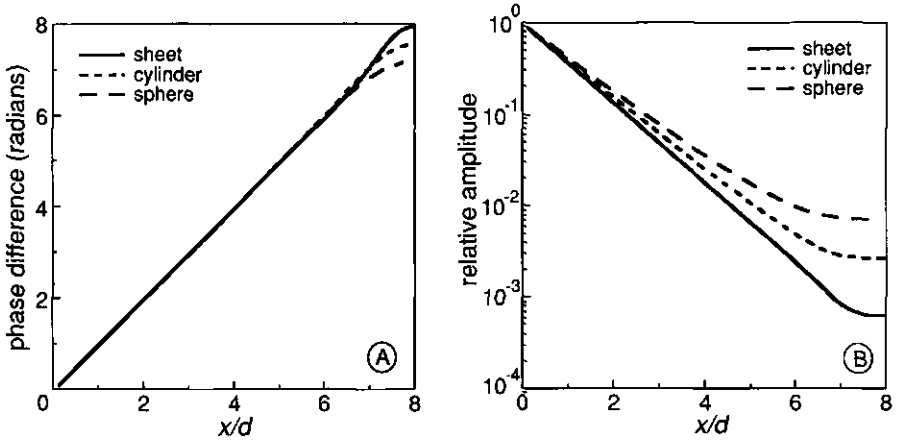

Figure 4.2. Numerical calculations for a sinusoidal concentration wave applied to the surface of a plane, cylindrical or spherical soil aggregate with $R = 8d$. The concentration wave inside the aggregate has shifted in phase and has a reduced amplitude. (A) Except in the center, the phase shift of the signal increases linearly with the distance x, independent of aggregate shape. (B) The decrease of the wave amplitude depends on aggregate shape.

relative amplitude and phase shift have been calculated as a function of the distance to the outer surface x. Figure 4.2 shows the results for R equal to 8 times the damping depth d. The graphs of $\theta(x)$ in Fig. 4.2a are the same for the three shapes except for the region close to the centre. Near the surface phase shifts are always accurately described by Eq. (4.5). The results for the relative amplitude in Fig. 4.2b show, from the surface onwards, considerable differences between the different shapes.

These results are relevant for understanding the situation of Fig. 4.1. As long as the distance to the macropore system is larger than the distance to the surface, phase shifts will be given by Eq. (4.5). The relative amplitude will be more sensitive to the presence of macropores. Consequently, the use of Eq. (4.5) has to be preferred.

A second reason for preferring phase shifts is that they are independent of slow changes in the oxygen electrode. In fact, for measuring phase shifts, there is no need to calibrate the electrode. When amplitudes are measured, however, the calibration constant of the electrode should not change with depth since absolute amplitudes are compared with the surface signal.

Some experimental details

For measuring oxygen concentrations polarografic electrodes have been used (Revsbach *et al.*, 1983). The platinum electrodes (with a sensing tip of approximately 10 μm) were protected against mechanical forces by sheathing them into

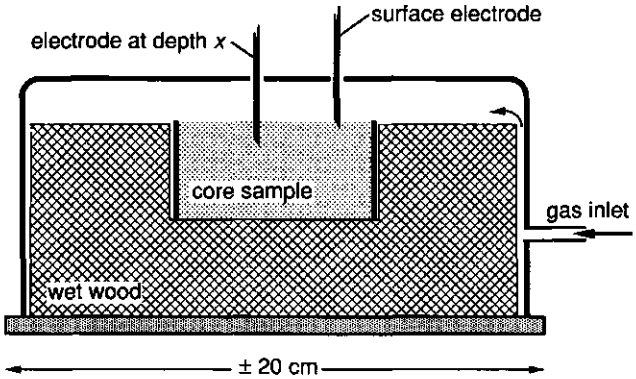

Figure 4.3. A core sample placed in a chamber in which the oxygen concentration is periodically changed. Oxygen electrodes are placed in the soil and at the soil surface. A calomel reference electrode is not shown. The electrode in the soil is pushed downward by attaching it to a small platform moved with a computer controlled stepper motor. The wet wood keeps the humidity high and reduces the chamber volume.

10 cm long stainless steel syringe needles with a diameter of 1 mm. To the platinum electrode a polarization potential was applied of –0.75 V. A calomel electrode closed the electrical circuit.

The current caused by the reduction of oxygen was measured by means of an operational amplifier used as a current to voltage converter with a feedback resistor of 100 MΩ (= 1 mV for each 10 pA current). The used amplifier should have a low input bias current. The AD 515J of Analog Devices was used, but more modern types are currently available. The amplifier circuitry floats at the polarization potential, which is (electronically) subtracted from the millivolt signal. The signal is further amplified using a dc amplifier and is finally led to a 12 bit analog to digital converter connected to a microcomputer. Due to a capacitor placed over the feedback resistor of the current to voltage converter, the characteristic reaction time of the system is about 1 second. This leads to a considerable noise reduction without being of any importance for measuring the much slower varying oxygen concentrations.

The concentration wave was applied to the flat surface of a core sample. The core sample was placed in a container with holes for electrode entry (Fig. 4.3). Through the container a small gas flow was maintained. By means of a relay operated gas switch the computer could switch between nitrogen and air. The switching was carried out with a period of 600 s, which corresponds to an angular frequency of 0.01047 rad s^{-1}.

The concentration changes at a few times the damping depth are small compared to the average signal (cf. Fig. 4.2b). The periodicity of the signal and the known frequency greatly simplify the detection of the signal, however. With

the electrodes and amplifiers used, sine waves have been detected being 1000 times smaller than the surface wave. This corresponds with a depth of about 7 times the damping depth in case of a plane geometry (cf. Fig. 4.2b and Eq. (4.4)).

Due to changes in the gas flow, the shape of the concentration wave at the surface could not be kept constant during longer periods. Consequently, the surface concentration had to be measured continuously for which a second oxygen electrode was placed at the surface (see Fig. 4.3).

Data analysis

Switching between air and nitrogen does apparently not lead to a concentration wave with a sinusoidal shape. The signal is still periodic, however, and may therefore be regarded as the sum of a number of sinusoidal components, the so-called harmonic or Fourier components of the signal. The angular frequencies of the Fourier components are $n\omega$ with $n = 1,2,3,\cdots$. As the diffusion equation is a linear differential equation, the different harmonic components of the concentration wave can be treated independently of each other. The n-th component leads to a damped oscillation at depth x with angular frequency $n\omega$. The signal measured at depth x is the sum of the concentration waves caused by the different harmonic components in the surface wave. Hence, by calculating the n–th harmonic component of both the surface signal and the signal at depth x, a phase shift can be determined belonging to a sine wave with angular frequency $n\omega$. Figure 4.4 shows phase shifts for the first, second and third harmonic component of signals measured at the surface (Fig. 4.4a) and at almost two times the damping depth (Fig. 4.4b). In the following paragraphs details of this figure and of the calculations are described.

The surface signal in Fig. 4.4a, and its first, second and third harmonic component, have been expressed as chamber concentrations between 0% and 21% oxygen gas. The shape of the signal shows that, after switching from air to nitrogen or from nitrogen to air, it takes a few minutes before the chamber concentration is stable. Therefore, the signal is not a symmetric square wave. Its decomposition into harmonic components is described as

$$c(0,t) = c_{av} + \sum_{n=1}^{\infty} \underbrace{\{a_n(0)\sin n\omega t + b_n(0)\cos n\omega t\}}_{n\text{-th harmonic component}}$$

The n-th harmonic component is written as the sum of a sine and cosine function and c_{av} is the average concentration.

In principle, the electrode signal measured at some depth x can be analysed in the same way. There is one difficulty, however. After moving the electrode to a greater depth its signal stabilized very slowly. Only after one or two periods of

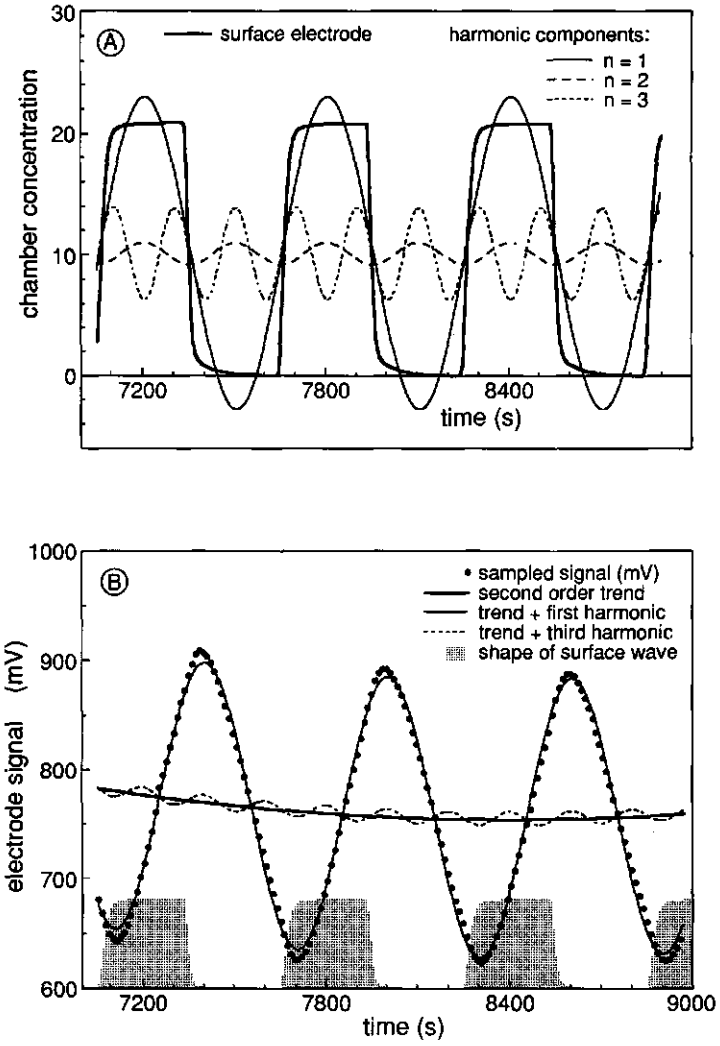

Figure 4.4. Fourier analysis of the concentration wave at the surface and in the soil. (A) The surface signal with a period of 600 s and its first three Fourier components. (B) The (uncalibrated) soil signal at almost two times the damping depth with its first and third Fourier component.

600 s, a neat periodicity appeared. Waiting for a completely stable periodic signal would have taken too much time. Usually, the measurements were interrupted after 4 or 5 periods in order to change depth again. During the last 2 or 3 periods, the relatively stable signal still had a trend superimposed on it as is shown in Fig. 4.4b. The periodic part of the signal has to be separated from the trend, which is accomplished by writing the signal at depth x as

$$c(x,t) = \underbrace{\sum_{m=0}^{M} z_m(x)\, P_m(t)}_{\text{trend function}} + \underbrace{\sum_{n=1}^{N} \{a_n(x)\sin n\omega t + b_n(x)\cos n\omega t\}}_{\text{periodic signal}} \qquad (4.6)$$

The periodic part consists of N harmonic components written again as the sum of a sine and cosine term. In theory N is infinite, but in practice only a few harmonic components can be calculated. The trend function is the sum of M polynomials $P_m(t)$ of order m. The simplest choice is $P_m(t) = t^m$, which makes the trend function a simple power series. When high order trends are used, it is advantageous to use Legendre polynomials as trend functions $P_m(t)$.

The Fourier coefficients $a_n(x)$ and $b_n(x)$ of the signal at depth x and the M parameters $z_m(x)$ of the trend function have been calculated by using Eq. (4.6) as a linear regression model. Chatfield (1975) showed that the Fourier components of a signal are equal to the least squares estimates derived with a linear regression model with sine and cosine terms. It is assumed here that this remains approximately true when a simple trend function is added to the regression model. Advantages of the regression technique are that the inclusion of a trend function is straightforward and that the data points need not to be equally spaced. It has the disadvantage of requiring more computing time than Fourier analysis. The least squares estimates of the $a_n(x)$, $b_n(x)$ and the trend parameters have been found by means of singular value decomposition as described in Press *et al.* (1986).

Surface signals as in Fig. 4.4a have been analysed by setting the order of the trend function M at zero (no trend, an average signal only) and the number of Fourier components N at 20. The signal in Fig. 4.4b consists largely of its first harmonic component. This component has shifted 196 seconds to the right relative to the first harmonic in the surface signal, which means a phase shift of 2.05 radians or about a third period. In the signal in Fig. 4.4b a second and third harmonic component are just detectable, the latter being shown in the figure. The third harmonic has shifted 93 seconds compared to the third harmonic in Fig. 4.4a. With a period of 200 seconds (= 600 / 3) this means a phase shift of 2.92 radians.

The amplitude of the third harmonic in Fig. 4.4a is about 30 percent of the size of the first component. In Fig. 4.4b the third harmonic is much smaller since its

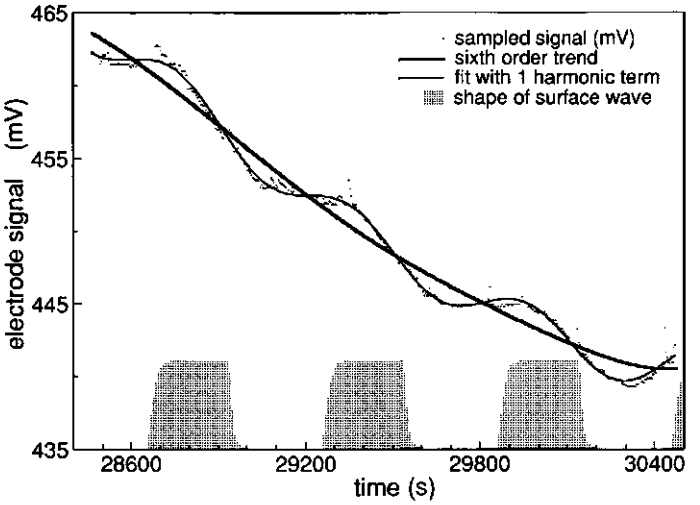

Figure 4.5. At larger depths the concentration wave is small and sinusoidal, since the higher order components have disappeared. A relatively large trend resulting from electrode instability is superimposed on the wave. The signal has been analysed with linear regression analysis (cf. Eq. (4.6)).

three times larger frequency leads to a damping depth which is a factor $\sqrt{3}$ smaller (cf. Eq. (4.3)). At larger depths, the higher order harmonic components disappear completely from the signal and only the sine wave of the first component remains. Figure 4.5 shows an example of this situation. The amplitude of the first harmonic component is about 300 times smaller than the average electrode signal (see the vertical axis). Clearly, it is only the periodic character of the signal which allows its separation from trend and noise. The concentration wave in Fig. 4.5 lies almost a full period (5.7 rad) behind the surface wave, which is drawn as hatched areas near the horizontal axis.

Some care is required in choosing the order M of the trend function. A 10-th order trend in Fig. 4.4b, for instance, would certainly describe also part of the periodic signal. In practice, the used value of M has been set at the smallest value consistent with a good fit. No attempt has been made to give this a precise mathematical meaning. Instead, graphs as Fig. 4.4b have been used to choose the lowest possible M by eye. A first or second order trend appeared to be sufficient in most cases.

In order to calculate phase shifts from the regression coefficients (instead of measuring them in graphs), the n-th order harmonic in Eq. (4.6) needs to be written as a single sine function according to

$$n\text{-th harmonic} = A_n(x)\sin\left(n\omega t - \theta_n'(x)\right) \tag{4.7}$$

Here $A_n(x)$ is the total amplitude of the n-th component at depth x, which is calculated from the regression parameters $a_n(x)$ and $b_n(x)$ as

$$A_n(x) = \sqrt{a_n^2(x) + b_n^2(x)} \tag{4.8}$$

The phase $\theta_n'(x)$ of the n-th component at $t=0$ is calculated by solving

$$\begin{cases} \cos\theta_n'(x) = +\dfrac{a_n(x)}{A_n(x)} \\ \sin\theta_n'(x) = -\dfrac{b_n(x)}{A_n(x)} \end{cases} \tag{4.9}$$

The phase shift $\theta_n(x)$ of the n-th harmonic component relative to the surface signal is found now as the difference between the phases of the sine functions at depths 0 and x:

$$\theta_n(x) = \theta_n'(x) - \theta_n'(0) \tag{4.10}$$

By substituting an angular frequency $n\omega$ in Eqs. (4.3) and (4.5), the expected behavior of $\theta_n(x)$ becomes

$$\theta_n(x) = \frac{x}{d}\sqrt{n} \tag{4.11}$$

in which d is the damping depth of the first harmonic. Hence, the ratio between the phase shift and $\sqrt{n}$ is equal to x/d for all harmonic components. This will be used to calculate values of the damping depth d and, finally, of the diffusivity D.

Testing the method

The electrode itself will disturb the concentration profile to some extent, since the needle is between the electrode tip and the surface. Especially for depths comparable to the needle diameter, deviations from a simple linear increase of the phase shift may be expected.

To get an impression of the importance of this effect, measurements were carried out in water with a small amount of agar agar added to it (0.5 g/l). The agar agar prevents convective mixing. Figure 4.6 shows the measured phase shifts as function of electrode depth. Only components larger than a thousandth part of the surface signal have been used. Smaller Fourier components did not have any significance. Phase shifts have been calculated only for the first five harmonic components. As a consequence of the shape of the applied surface wave, the first and third component are always the largest ones.

Figure 4.6 shows that the phase shifts start to increase from an offset depth of about 0.3 mm. The reason is that the platinum electrode tip lies somewhat behind the needle tip. After hitting the surface, the electrode has to go down a little further before the phase shift starts to increase. From the offset depth on, the increase is linear . No special behavior at small depths could be observed.

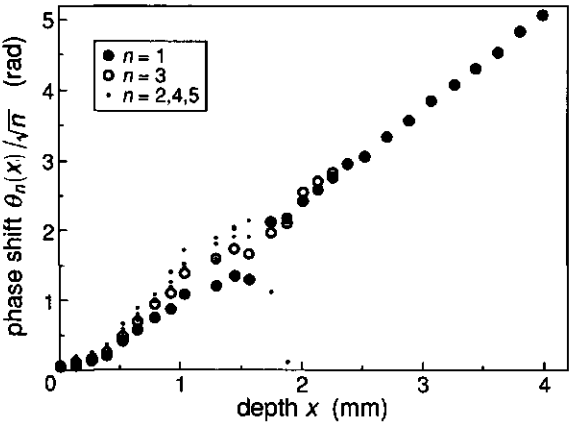

Figure 4.6. Phase shifts measured in water with agar agar (0.5 gram/liter). Results for different harmonic components have been combined in one graph by dividing the shifts by $\sqrt{n}$. The oxygen diffusivity derived from this graph is $(2.95 \pm 0.06) \times 10^{-9}$ m^{2}s^{-1}.

A straight line has been fitted through the measured phase shifts for $n=1$ and $n=3$ (without using the data points for the lowest three depths, cf. Fig. 4.6). The resulting damping depth d is 0.750 ± 0.013 mm. Then, with a wave period of 600 s, Eq. (4.3) gives a diffusivity of $(2.95 \pm 0.06) \times 10^{-9}$ m^{2}s^{-1}. The water temperature has been 23 °C.

This result can be compared to values in the literature. Glinski and Stepniewski (1983) use 2.10×10^{-9} m^{2}s^{-1} at 20 °C and 2.38×10^{-9} m^{2}s^{-1} at 25 °C. Grable (1966) reports a larger value, 2.60×10^{-9} m^{2}s^{-1} at 25 °C. Hence, the value found in this paper is probably about 20% too large. No clear explanation could be found. The error seems not to be serious, however, in interpreting the measurements for soil samples.

RESULTS

Figure 4.7a shows the results of measurements in a core sample of clayey soil with an air-filled porosity of 0.073. Phase shifts have been calculated for harmonic components larger than a thousandth part of the surface signal. The regression line is based on the phase shifts for the first four depths and corresponds to a diffusivity of $(0.81 \pm 0.06) \times 10^{-9}$ m^{2}s^{-1}. The offset depth for the measurements in soil corresponds to $x = 0.89$ mm. Using that value, the measurements shown in Fig. 4.7b can be interpreted consistently (the same electrode was used). The line in that figure leads to a diffusivity of 0.96×10^{-9} m^{2}s^{-1}. The deviations for $x = 1.2$ mm and $x = 1.5$ mm may have been caused by leakage

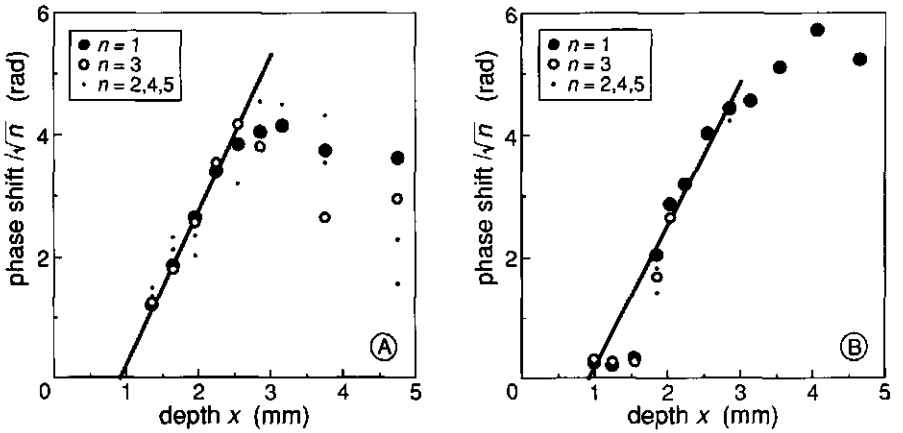

Figure 4.7. Phase shifts for different harmonic components measured in soil. The two regression lines have a common offset depth of 0.89 mm and lead to diffusivities of (A) 0.81×10^{-9} m^2s^{-1} and (B) 0.96×10^{-9} m^2s^{-1}.

along the electrode (for larger depths this leakage was prevented by the grease applied to the electrode needle). The air-filled porosity of the second core sample was 0.038.

In both graphs of Fig. 4.4, the measured phase shifts stop increasing at 2 or 3 millimeters from the surface. This probably reflects the influence of air-filled pores (cf. Fig. 4.1). The observed distance of a few millimeters indicates the size of the saturated zones between the air-filled pores.

For whole core samples macroscopic diffusion coefficients have been measured using the method described by Bakker & Hidding (1970) and Rolston (1986). The oxygen concentration is measured in a diffusion chamber placed above the core sample. Initially, the chamber is filled with oxygen. This oxygen diffuses into the sample and the diffusion coefficient is calculated from the decreasing concentration in the chamber. For 10 soil samples with air-filled porosities between 0.02 and 0.07 the measured macroscopic diffusion coefficients varied between 13×10^{-9} m^2s^{-1} and 310×10^{-9} m^2s^{-1} with an average value of 75×10^{-9} m^2s^{-1}.

DISCUSSION

The diffusivity of about 0.9×10^{-9} m^2s^{-1} measured with the oxygen electrodes on a millimeter scale is an extremely low value for unsaturated soil. A simple calculation shows that this value can be explained by assuming local saturation

of the soil with water. The diffusion coefficient D_s of a solute (e.g. dissolved oxygen) in saturated soil can be written as

$$D_s = \theta D_w f \tag{12}$$

in which θ is the volumetric water content (total porosity), D_w is the diffusivity in free water and f is a tortuosity or impedance factor (see also Table 4.1). According to this equation the diffusivity can be written as

$$D = \frac{D_s}{\theta} = D_w f \tag{13}$$

Dividing the measured diffusivity by D_w ($=2.10 \times 10^{-9}$ m^{2}s^{-1}, Glinski & Stepniewski, 1983) a tortuosity of 0.43 is found. This is a realistic value. Nye and Tinker (1977) mention that values between 0.4 and 0.7 have been obtained for saturated soil.

The average diffusion coefficient of 75×10^{-9} m^{2}s^{-1} measured for whole core samples is consistent with data on gaseous diffusion in the literature. Glinski and Stepniewski (1983) give an empirical model relating the diffusion coefficient in soil to the coefficient in free air. An air-filled porosity of 0.05, a value of 2 for their parameter μ (values between 0.8 and 4 have been reported), and a diffusion coefficient for oxygen in air of 2.0×10^{-5} m^{2}s^{-1} (20 °C) give a diffusion coefficient in soil of 40×10^{-9} m^{2}s^{-1}. This value has the same order of magnitude as the measured diffusion coefficients.

The local diffusion coefficient for oxygen can be estimated by multiplying the measured diffusivity by the local water content of about 0.4, which gives $D_s \approx 0.4 \times 10^{-9}$ m^{2}s^{-1}. This value is more than 100 times smaller than the macroscopic value for whole core samples of the same soil. It should therefore be emphasized that macroscopic coefficients describe transport over macroscopic distances and nothing more.

The size scale associated with the small saturated zones between air-filled pores is a few millimeters in the clayey soil used here. In combination with a diffusivity as low as the measured value, this length scale is large enough to cause anaerobiosis between individual air-filled pores. In general, the importance of small saturated zones will depend on the size of these zones compared with the distance characterizing the transport process studied. Hence, an important characteristic of soil structure is the geometry of the air-filled part of the pore system as function of the water content.

In principle, an oxygen electrode may also be used to measure the diffusivity at a centimeter scale. The electrode then passes air-filled pores and the phase shift will fluctuate. The average phase shift, however, will increase slowly expressing a macroscopic diffusivity. Whether or not this diffusivity is the same as the diffusivity for a hole core sample is unknown. The electrodes used were too fragile to be driven into the clayey soil more than a few millimeters.

Chapter 5

A simple model of non-uniform respiration in a soil aggregate

Abstract. The consequences of non-uniform respiration in a soil aggregate are studied. A simple model is made for a plane aggregate with a single layer of active soil in it. For this aggregate, the overall respiration is calculated for a zero-order respiration process as function of the position of the active zone. The result is used to find the respiration for a collection of aggregates with a randomly located active zone. If a small portion of the soil is active, say 10%, the overall soil respiration may be several orders of magnitude smaller than the potential respiration in the (largely anoxic) active zones. Hence, a large local soil activity is consistent with a moderate soil respiration rate. The reason behind this result is the diffusive resistance of the inactive soil surrounding the active zones. This picture of soil respiration is consistent with the concept of hot spots used in soil biology.

INTRODUCTION

Anaerobiosis may occur in a soil aggregate in which a zero-sink respiration process takes place. Greenwood (1961) and Currie (1961) described this with a diffusion model for a homogeneous, spherical soil aggregate. Smith (1980) used spheres with different sizes to describe anaerobiosis in an aggregated soil. Denitrification can be described by extending the model with equations describing the transport and reduction of nitrate (Arah & Smith, 1989). Two important assumptions made in these models are a spherical aggregate shape and homogeneity.

The spherical aggregate shape is not a problem. In Chapter 2 it has been shown that diffusion in an aggregated soil can be approximately described as diffusion in spherical, cylindrical or plane aggregates. The geometry used in actual model calculations will generally have a minor influence on the results.

The assumption of homogeneity represents a more serious problem. Figure 5.1 shows a uniform and a non-uniform distribution of biological activity in a soil aggregate. Several differences between the distribution of oxygen in the

Table 5.1. Symbols, definitions and units.

symbol	description	units
α	ratio between Q and Q_0	-
c	concentration as a function of x	mol m^{-3}
C	concentration outside the aggregate	mol m^{-3}
d	characteristic diffusion length	m
d_0	value of d for homogeneous aggregate	m
D	diffusion coefficient	m^2 s^{-1}
e	inactive fraction of the aggregate ("empty")	-
H	half the aggregate thickness	m
h	the ratio H/d	-
h_0	the value of h for a homogeneous aggregate	-
p	position parameter	-
q	respiration relative to respiration for homogeinity	-
θ	probability of anaerobiosis	-
Q	potential respiration rate of the active soil	mol m^{-3} s^{-1}
Q_0	value of Q for a homogeneous aggregate	mol m^{-3} s^{-1}
r	respirating fraction of the aggregate	-
r_0	respirating fraction of homogeneous aggregate	-
t	defined as eh	-
x	coordinate ; distance to the surface	m
x_1, x_2	distance between surface and anaeroob soil	m
z_1, z_2	distance between surface and active zone	m

two aggregate types are intuitively clear. In case of homogeneity, the anoxic zone, if present, will always lie in the centre. This zone is surrounded by active, oxic soil in which the respiration takes place. The respiring soil is bounded by the surface of the aggregate.

The heterogeneous aggregate in Fig. 5.1 will behave quite differently. The soil is largely inactive and anaerobiosis can occur in relatively small active zones only. Soil respiration takes place in the oxic, outer parts of these active zones. Although the active zones may have a large potential for oxygen consumption, the resistance of the inactive soil around them largely prevents the flow of oxygen. As a consequence, the actual soil respiration may be very small compared with the potential use of oxygen by the active parts of the soil. The importance of this effect depends on the spatial distribution of the active zones.

The consequences of heterogeneity are demonstrated in this chapter by means of a simple model. Instead of solving a difficult transport problem for an aggregate as in Fig. 5.1, a plane aggregate with a single active zone has been used. The plane aggregate in Fig. 5.2 is the one-dimensional analogue of the

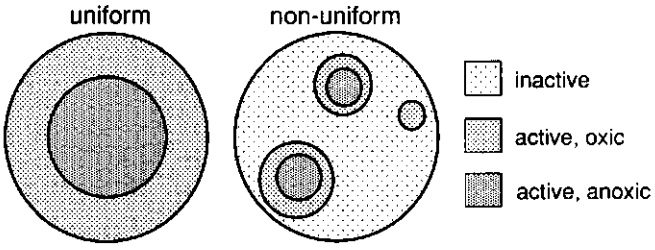

Figure 5.1. Soil aggregates with a uniform and a non-uniform activity. Anoxic soil (dark) can only occur in an active zone.

non-uniform aggregate in Fig. 5.1. Only a single active zone is present, because, in one dimension, oxygen cannot flow around one active zone towards another. The asymmetry of the system is represented by an excentric position of the active zone. After exploring the basic properties of the model, some results on anaerobiosis are derived for a random position of the active zone. Table 5.1 gives a list of symbols used, with definitions and units.

MODEL

The drawing in Fig. 5.2 shows the cross section of a plane soil aggregate with a thickness $2H$. Edge effects are neglected and oxygen transport is assumed to take place in the x-direction only. The position of the active zone is arbitrary. It lies somewhere between the two outer surfaces of the aggregate and oxygen will reach the zone from the left and right side. That leads to two oxic layers and, depending on the model parameters, to an anoxic centre. In the oxic layers, a zero-order respiration process takes place, which is characterized by a respiration coefficient Q. Expressions will be derived for the widths of the oxic and anoxic parts, and for the respiration rate of the aggregate.

If the active zone contains an anoxic part, the diffusion problem can be solved for the two sides of the aggregate independently. Below, the concentration profile at the left side of the anoxic zone is calculated. Using the distance x to the outer surface as a coordinate the differential equation describing the steady state is

$$D\,\frac{d^2c(x)}{dx^2} = \begin{cases} 0\,, & 0 \le x < z_1 \\ Q\,, & z_1 \le x \le x_1 \end{cases} \qquad (5.1)$$

in which the distance x_1 is a yet unknown penetration distance. The boundary conditions are

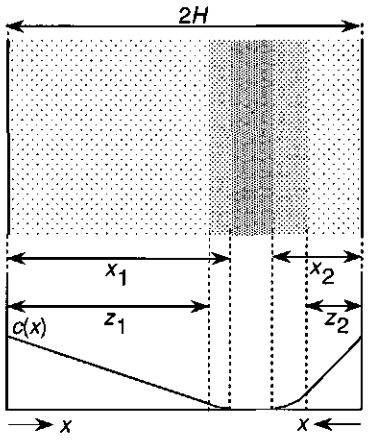

Figure 5.2. A plane soil aggregate with a partly anoxic active zone. The graphs show oxygen concentration profiles at the left and right side of the anoxic zone.

$$c(x) = 0\,,\ {dc(x)}/{dx} = 0 \quad \text{for } x = x_1 \quad \text{and} \quad c(0) = C\,.$$

The length z_1 describes the position of the active zone (see Fig. 5.2) and can be expressed in terms of the inactive fraction of the soil e and a position parameter p:

$$z_1 = eH(1+p) \tag{5.2a}$$

Similarly, for the length z_2 at the right side of the anoxic zone,

$$z_2 = eH(1-p) \tag{5.2b}$$

The value of p is 0 for a central position of the active zone and 1 for a position at the outer surface of the aggregate. The solution of Eq. (5.1) for the oxygen concentration $c(x)$ at the left side of the active zone is

$$\begin{cases} c(x) = \dfrac{Q}{2D}(x_1-z_1)^2 + \dfrac{Q}{D}(x_1-z_1)(z_1-x)\,, & 0 \le x < z_1 \\ c(x) = \dfrac{Q}{2D}(x_1-x)^2 \qquad\qquad\qquad\qquad\quad , & z_1 \le x \le x_1 \end{cases} \tag{5.3}$$

In the inactive part of the aggregate, the concentration decreases linearly with the distance to the surface x (see the graphs in Fig. 5.2). This corresponds to a constant flux of oxygen in the direction of the active zone. In the active zone itself, oxygen is consumed and the concentration falls quadratically to zero. The concentration at the right side is described by a similar expression.

In the derivation of Eq. (5.3) only the first two boundary conditions have been used. Substituting Eq. (5.3) in the third condition leads to an algebraic equation for the unknown penetration distance x_1. Solving this equation, and a similar equation for x_2, yields

$$\begin{cases} x_1 = \sqrt{z_1^2 + 2\,d^2} \\ x_2 = \sqrt{z_2^2 + 2\,d^2} \end{cases} \tag{5.4}$$

in which

$$d \equiv \sqrt{\frac{DC}{Q}} \tag{5.5}$$

The length d is a characteristic length belonging to the respiration process. In case of uniform activity (e=0), Eq. (5.4) reduces to a penetration distance $\sqrt{2}\,d$ (cf. Chapter 2). In the presence of an inactive outer layer, Eq. (5.4) shows that the square of the thickness z of this layer is added to the square of the penetration depth for uniform activity.

It is useful to express the size of the aggregate relative to the characteristic length d. The dimensionless aggregate size h is

$$h \equiv \frac{H}{d} \tag{5.6}$$

When the sum of x_1 and x_2 exceeds the aggregate thickness $2H$, the aggregate is fully oxic. For this situation no concentration profile has been derived. The respiration rate of the aggregate can be found immediately, however, from the size of the active layer and the potential respiration rate Q.

The respiration rate of the aggregate

The quantity which is usually measured as "soil respiration" is not a local, potential respiration rate Q, but an overall respiration rate of the soil. For the aggregate in Fig. 5.2, respiration takes place only in the oxic part of the active zone. The respiring fraction of the aggregate $r(e,h,p)$ is (cf. Fig. 5.2):

$$\begin{cases} r(e,h,p) = \dfrac{(x_1 - z_1) + (x_2 - z_2)}{2H} = \dfrac{x_1 + x_2}{2H} - e\,, & x_1 + x_2 \le 2H \\ r(e,h,p) = (1 - e) & , \; x_1 + x_2 > 2H \end{cases} \tag{5.7}$$

The first part of this equation can be expanded by substituting Eq. (5.4) for x_1 and x_2. The second part of Eq. (5.7) refers to the situation without anaerobiosis. The respiration rate of the aggregate is found by multiplying the respiring fraction $r(e,h,p)$ by Q. Only when there is no inactive soil and the aggregate is fully oxic, the soil respiration is equal to Q.

Figure 5.3 shows graphs of $r(e,h,p)$ as function of p for an inactive fraction e of 0.9 and for different choices for h. The graphs demonstrate that oxygen use is largest when the active zone lies near the aggregate surface. An active zone in the centre of an aggregate tends to be largely anoxic, as it is surrounded

by inactive soil with a resistance for oxygen transport.

Due to the presence of inactive soil, the respiration of a non-uniform aggregate will always be smaller than the respiration of a uniform aggregate with the same potential respiration Q. Studying the consequences of non-uniform activity, however, the respiration rates of the uniform and non-uniform aggregate should be kept equal. This can be done by choosing a value of Q for the non-uniform aggregate which is α times as large as the value Q_0 for a uniform aggregate. Then, later, the value of α which is required for equal respiration rates is calculated.

In derivations below, the respiring fraction of a uniform aggregate is used. It follows from Eq. (5.7) by setting the inactive fraction e to 0 and the potential respiration to Q_0. The result is

$$\begin{cases} r_0(h_0) = \dfrac{\sqrt{2}}{h_0} = \dfrac{\sqrt{2DC/Q_0}}{H}, & h_0 \geq \sqrt{2} \\ r_0(h_0) = 1, & h_0 < \sqrt{2} \end{cases} \tag{5.8}$$

in which h_0 is defined by using Q_0 instead of Q in Eqs. (5.5) and (5.6).

A random position of the active zone

A random position of the active zone can be described by a uniform distribution of the position parameter p between 0 and 1. The average respiration is calculated then as the integral of $Qr(e,h,p)$ over the p–interval

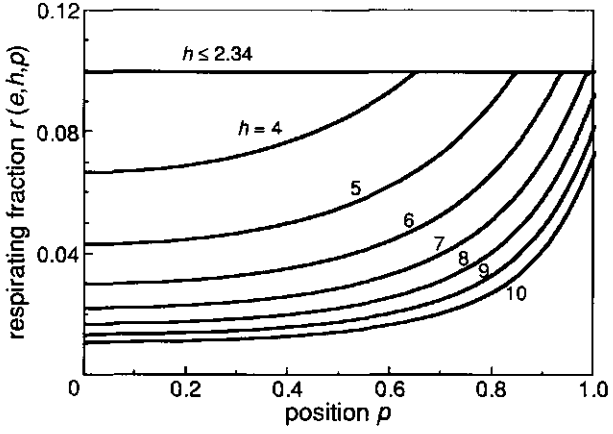

Figure 5.3. The respiring fraction of the aggregate is larger when the active zone lies close to the surface. The graphs have been calculated for an active zone occupying 10% of the soil volume (e=0.9).

[0,1]. Dividing the result by the respiration of a uniform aggregate leads to a relative respiration rate q. With a potential respiration Q being α times larger than Q_0 is

$$q(\alpha,e,h) \equiv \frac{\alpha Q_0 \overline{r(e,h,p)}}{Q_0 r_0(h_0)} = \frac{\alpha}{r_0(h_0)} \int_0^1 r(e,h,p)\,dp \qquad (5.9)$$

For $\alpha=1$ and for different values of h, the relative respiration $q(\alpha,e,h)$ has been calculated as function of the inactive fraction e. The results are drawn in Fig. 5.4 as function of the product eh.

As an example, the curve for $h=4$ is discussed. For $e=0$, the full aggregate is active and $q(1,0,4)$ is equal to 1. The straight, thin line between $eh=0$ and $eh=4$ indicates a reduction of the respiration proportional to e. This line would be followed if the respiring proportion of the active zone would be independent of e. In that case an inactive fraction of, say 40%, would simply lead to a 40% reduction of the respiration rate. The actual graph of $q(1,e,4)$, however, shows a steep decrease due to the resistance of the inactive layers between the respiring zones and the outer surface. For increasing e the active zone becomes so small that it is completely oxic for most, or all, values of p. Then $q(1,e,4)$ lies above the line for a proportional decrease.

For the common part of the ten curves in Fig. 5.4 an analytical expression exists. It has been derived by substituting Eqs. (5.2) and (5.4) in the first part of Eq. (5.7) and substituting the resulting expression for $r(e,h,p)$ in Eq. (5.9). The result is

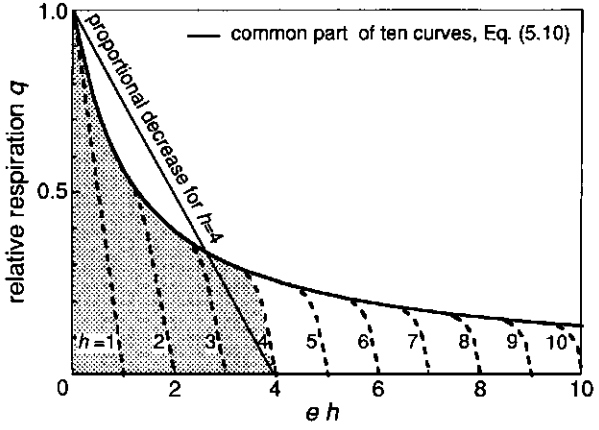

Figure 5.4. Average respiration for a random position of the active zone as a function of eh for different values of h. The common part of the ten curves is described by Eq. (5.10) with $\alpha=1$.

$$q(\alpha,e,h) = \frac{\sqrt{\alpha}}{2}\left[\frac{1}{t\sqrt{2\alpha}}\ln\left(\sqrt{2\alpha t^2+1} + t\sqrt{2\alpha}\right) + \sqrt{2\alpha t^2+1} - t\sqrt{2\alpha}\right] \quad (5.10)$$

in which t is equal to the product eh. This expression is valid only when there is an anoxic zone for all positions p in [0,1] and when also the reference value $r_0(h_0)$ in Eq. (5.8) is less than 1.

THE PROBABILITY OF ANAEROBIOSIS

Consider a random point in the plane aggregate at a distance x from the outer surface ($0 \le x \le H$). The probability that this point lies in the anoxic part of the active zone is calculated for a random position of the active zone. When the point lies in the right half of the aggregate (cf. Fig. 5.2), the active zone may lie at the same or at the opposite side. This is described by choosing the position parameter p in the interval [−1,+1]. Then, the random point lies in the anoxic zone when

$$x_1 \le 2H - x \quad \text{and} \quad x_2 \le x$$

With Eqs. (5.2) and (5.4) these conditions lead to a p-interval for which the point is anoxic. This interval is given by

$$p_2 \le p \le p_1$$

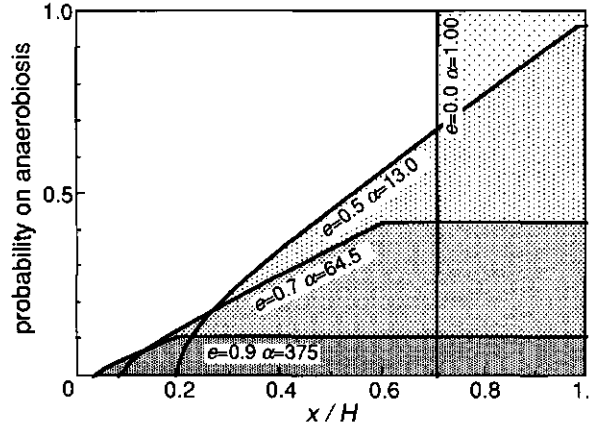

Figure 5.5. Probability of anaerobiosis according to Eqs. (5.11) and (5.12) as a function of the distance x to the surface, calculated for h=2 and for different values of e. The active zone has a random position and the average soil respiration is the same for the four graphs. The case e=0 describes a uniform aggregate.

in which

$$\begin{cases} p_1 = \min\left[+1,\ -1+\frac{1}{e}\sqrt{\left(2-\frac{x}{H}\right)^2-2\left(\frac{d}{H}\right)^2}\ \right], & (2H-x)^2 \geq 2d^2 \\ p_2 = \max\left[-1,\ +1-\frac{1}{e}\sqrt{\left(\frac{x}{H}\right)^2-2\left(\frac{d}{H}\right)^2}\ \right], & x^2 \geq 2d^2 \end{cases} \tag{5.11}$$

As always $x \leq H$, a sufficient condition for the existence of both p_1 and p_2 is $x^2 \geq 2d^2$. The probability that the point is anoxic is then equal to the width of the position interval $[p_2,p_1]$ relative to the range $[-1,+1]$ of p. Hence, the probability $\theta(x)$ that the point is anoxic becomes

$$\begin{cases} \theta(x) = \frac{p_1-p_2}{2}, & x^2 \geq 2d^2 \\ \theta(x) = 0, & x^2 < 2d^2 \end{cases} \tag{5.12}$$

For $h=2$ and for different choices of the inactive fraction e, Fig. 5.5 shows graphs of $\theta(x)$ as function of x. The vertical line for $e=0$ describes a homogeneous aggregate with a potential soil respiration rate Q_0. Points closer to the surface than $\sqrt{2}\,d$ are always oxic and points in the centre of the aggregate are anoxic.

For larger values of e, the potential respiration rate Q has been increased in order to compensate for the presence of inactive soil. The respiration rate is kept constant by making Q a factor α larger than Q_0. The value of α is found from (cf. Eq. (5.9))

$$q(\alpha,e,h) = 1$$

Large values of α are required for keeping the overall respiration constant (see Fig. 5.5). The graphs show that a deterministic relation between the distance x and the aeration status no longer exists. Instead, there is only a probability on anaerobiosis which increases with the distance x to the surface. For $e=0.9$, ten percent of the soil is active. Only close to the surface the soil is never anoxic and there is practically no relation between the probability of anaerobiosis and x. The anoxic zones tend to occur randomly, with about the same distribution as the active parts of the soil themselves.

CONCLUSIONS

The assumption of a non-uniform soil has important implications for a model of anaerobiosis. Inactive zones act as a barrier reducing the diffusion of oxygen to the active parts of the soil. Active soil easily becomes anoxic and respiration takes place then in a tiny fraction of the soil only. That implies that local

respiration rates can be several orders of magnitude larger than the average respiration rate, which is measured for a macroscopic soil sample. Extremely large local activities may be consistent with a moderate, overall respiration rate. In soil biology small active zones are well-known and are sometimes called "hot spots" (e.g. Seech & Beauchamp, 1988). Hot spots may evolve around concentrations of plant residues or manure, or may be related to the presence of root exudates. Bouwman *et al.* (1990) reported 100 times larger nematode densities for the soil around wheat seedling roots.

A consequence of non-uniform activity is that there is no longer a fixed relation between the distance to the aggregate surface and the aeration status of a point. There is only a probability on anaerobiosis, determined by the distribution of soil activity. In case of a random distribution of small, highly active zones, there will be practically no relation between distance and the probability on anaerobiosis. When the activity is concentrated near the edge of the soil aggregates, the correlation between distance and anaerobiosis may even be negative.

Differences in soil activity of a factor 100 or more cannot be described by adapting a model for homogeneous soil. The occurrence of hot spots is a major factor with qualitative consequences for the behavior of the system. The description of anaerobiosis and denitrification in hot spots requires a new class of transport models for soil aggregates.

Chapter 6

Anaerobiosis in a clayey soil

with A.Th.Helmink

Abstract. The aeration of a clayey soil is studied by comparing the position of the cracks with the distribution of anoxic soil. A weak relation is found between the crack pattern and the distribution of anoxic soil. Locally, anoxic soil occurs even within 1 mm from a crack surface. Assuming that clay is locally saturated with water, the measured macroscopic soil respiration allows a penetration depth for oxygen of 10 mm. It is therefore concluded that soil activity is not uniform. Local activity exceeds the bulk respiration by at least a factor 100. This also explains the absence of a relation between the crack pattern and the distribution of anoxic soil. A consequence of the presence of anoxic soil close to cracks is that denitrification may take place without diffusion of nitrate towards the inner parts of an aggregate. Highly active and anoxic soil may absorb dissolved nitrate from water flowing through it.

INTRODUCTION

The occurrence of anaerobiosis in a soil is determined by its oxygen use and by the transport of oxygen from the atmosphere to the soil. This transport is influenced by the soil structure. Oxygen enters the soil from the surface and from gas-filled macropores. When, locally, the oxygen consumption is larger than the maximum flux to that region, the soil becomes anoxic. Greenwood (1961) and Currie (1961) gave a model for anaerobiosis in a homogeneous and spherical aggregate. When the oxygen flux from the surface is too small to maintain respiration in the entire aggregate, the centre becomes anoxic.

Application of this model to an aggregated soil implies that the soil close to the macropores will be oxic and that anoxic soil occurs in the centre of the aggregates. Even in the presence of some variability in the properties of the soil aggregates, there should still be a correlation between the aeration status of a point and its distance to the nearest crack. In Chapter 5 it has been shown that this is no longer true if the soil aggregates themselves are not homogeneous.

Table 6.1. Description of symbols used in the text.

symbol	description	units
α	solubility of oxygen in water	-
c_g	oxygen concentration in gaseous phase	mol m^{-3}
c_s	oxygen concentration in aquous phase	mol m^{-3}
C	oxygen concentration in atmosphere or crack	mol m^{-3}
D_g	oxygen diffusion coefficient for non-saturated soil	m^2 s^{-1}
D_s	oxygen diffusion coefficient for saturated soil	m^2 s^{-1}
D_w	oxygen diffusion coefficient in water	m^2 s^{-1}
f	turtuosity factor	-
λ_g	penetration depth for non-saturated soil	m
λ_s	penetration depth for saturated soil	m
Q	potential respiration rate of the soil	mol m^{-3} s^{-1}
θ	total soil porosity ; satrurated water content	-
t	time	s
x	coordinate ; distance to the surface	m

In this chapter the aeration of a cracked clayey soil is studied. For a number of horizontal intersections, the distribution of anoxic soil is compared with the crack pattern. Additionally, the macroscopic (vertical) transport of oxygen is described by measuring respiration rates and diffusion coefficients. The field work has a somewhat explorative character, but the results show that the clay aggregates are heterogeneous. The assumption of homogeneity is too far from reality to be useful in an aeration model. Some consequences for the description of denitrification are discussed.

METHODS

Macroscopic diffusion coefficients and respiration rates were measured in order to get some insight into the penetration of oxygen into the soil profile. On the aggregate scale, the crack pattern and the anaerobiosis were observed by means of colouring techniques. To describe quantitatively the relation between anaerobiosis and the distance of the soil to the nearest crack, digitized images of the crack pattern and the anoxic soil are compared. In subsections below, details are given of the various techniques used. A list of symbols is given in Table 6.1.

Field site and soil

The field measurements were carried out on the experimental farm "De Bouwing" in Randwijk, about 1 km south of the river Lower Rhine. The farm is located on a wide natural old river levee (De Visser, 1958). The soil can be characterized as a non-calcareous, well-structured, medium textured soil with a coarse sandy subsoil below 0.4 m to 1.2 m depth. The clay content in the upper part of the soil is estimated between 25 and 35 percent (<2 μm). This corresponds with heavy loam ("zware zavel") to light clay ("lichte klei") in the Dutch texture classification (De Bakker & Schelling, 1966), and with loam to clayloam in the international terminology (Soil Survey Staff, 1951).

In the legend of the soil map of the Netherlands the soil is placed in the unit Rn95C-GtVI described as non-calcareous River clay "Poldervaag" soils, heavy loam and light clay, with a groundwater table fluctuating seasonally between 0.4 m and 1.2 m (Stichting voor Bodemkartering, 1973). These soils are very extensive in the alluvial plains of the Rhine and the Meuse. According to the USDA Soil Taxonomy (Soil Survey Staff, 1975) they are classified as "Typic Fluvaquent".

The field work has been carried out in the first week of September 1988. Cracks were visible at the surface. The typical clod diameter was 10 cm.

Macroscopic soil respiration

The macroscopic soil respiration has been determined by measuring the oxygen consumption of soil that was put in a bottle. On subsequent days the oxygen concentration in the bottle was measured by means of the equipment shown schematically in Fig. 6.1. With two surgery needles the gas content of the bottle was connected to a closed circuit containing a small pump and a Clark type oxygen electrode. After pumping about 20 seconds the stabilized electrode signal was measured. In order to treat all bottles in the same way, the gas circuit was flushed with air before connecting it to a next bottle.

Figure 6.2 shows the result for one bottle. After about 15 days the oxygen consumption obviously decreases and the concentration rises as a result of leakage through the increasing number of needle punctures in the cap of the bottle. The gas volume in the bottle has been calculated from the wet and dry weight of the soil, the density of the solid phase and the bottle volume. Respiration has then been calculated from the initial decrease in concentration.

Each time a concentration is measured, some oxygen is pumped into the bottle, which leads to a systematic underestimate of the respiration rate. In principle, a correction can be calculated from the measured concentrations and the total circuit volume of 8 cm^3. This correction, leading to respiration rates which are roughly 30% larger, has not been carried out, however. The reason is

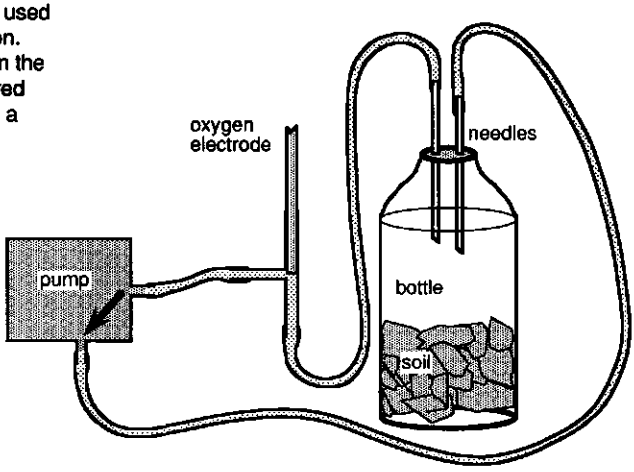

Figure 6.1. The equipment used for measuring soil respiration. The oxygen concentration in the air above the soil is measured with an oxygen electrode in a closed gas circuit.

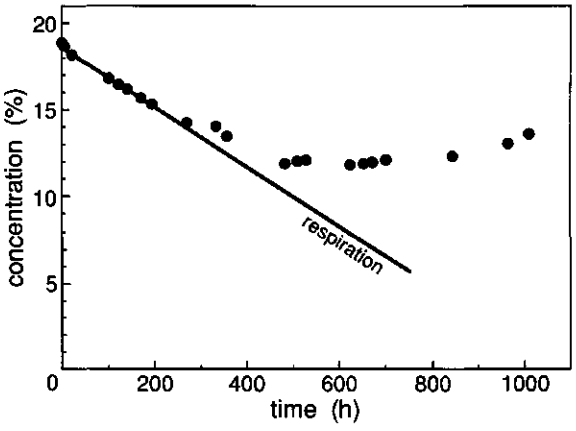

Figure 6.2. Oxygen concentration as measured for one particular bottle (cf. Fig. 6.1). Soil respiration is calculated from the initial decrease in concentration.

the large variability in the measured respiration, and the fact that the results are used only as an indication of the order of magnitude of the bulk respiration.

Oxygen diffusion

In the DISCUSSION of this chapter, order of magnitude calculations are made for situations in which either the oxygen transport in the liquid phase or the oxygen transport in the gaseous phase can be neglected.

Unless the soil is almost saturated with water, oxygen diffusion is dominated by the transport through gas-filled pores. This is usually the case for macroscopic, downward oxygen transport (Glinski & Stepniewski, 1985 ; Bakker *et al.*,

1987) and the oxygen flux can be written as

$$\text{flux} = -D_g \frac{\partial c_g}{\partial x}$$

in which D_g is the diffusion coefficient (m^2s^{-1}) and c_g the oxygen concentration in the soil air (mol m^{-3}). In these terms, the differential equation for a steady-state, zero-sink respiration process in a flat, aerated layer with thickness λ_g becomes

$$D_g \frac{d^2 c_g(x)}{dx^2} = Q$$

with boundary conditions

$$c_g(x) = 0\,, \quad {dc_g(x)}/{dx} = 0 \quad \text{for } x = \lambda_g \quad \text{and} \quad c_g(0) = C\,.$$

The oxygen penetration depth λ_g depends on C, D_g and Q in the following way (cf. Chapters 2 and 5)

$$\lambda_g = \sqrt{\frac{2 C D_g}{Q}} \tag{6.1}$$

For a number of core samples, the macroscopic diffusion coefficient D_g has been measured using a method described by Rolston (1986). The oxygen concentration is measured in a diffusion chamber placed above the core sample. Initially, the chamber is filled with oxygen. This oxygen diffuses through the sample to the atmosphere and a diffusion coefficient is calculated from the decreasing concentration in the chamber. The results are used to calculate the

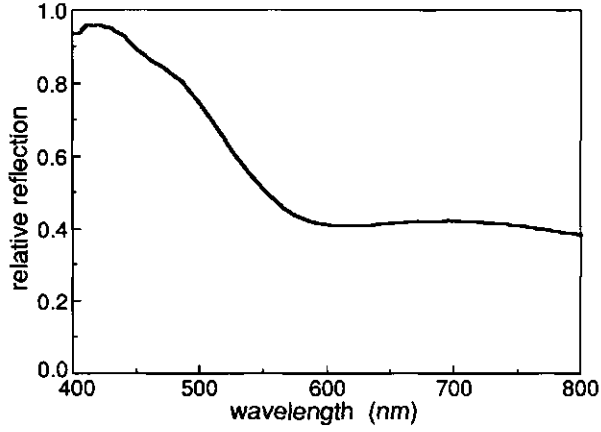

Figure 6.3. The ratio between the reflection of blue colored anoxic soil and the reflection of oxic soil as function of wavelength. Both surfaces were treated with potassium ferricyanide, which forms a stable blue precipitate (Turnbull's blue) with ferrous iron.

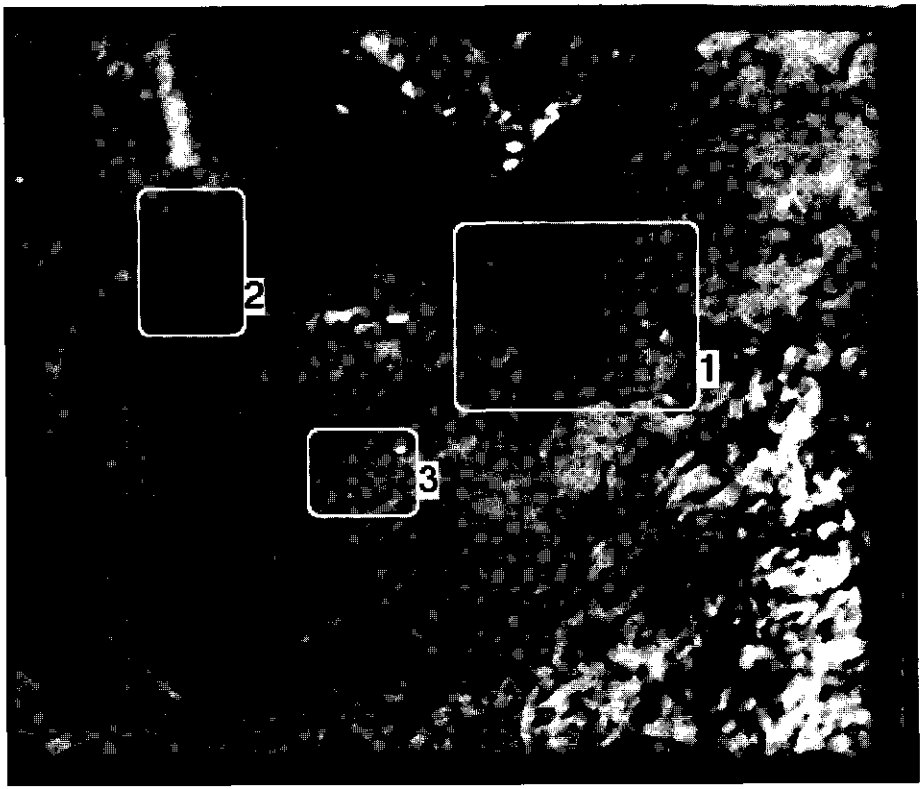

Figure 6.4. (A) (left) A sample area of 18.0×14.5 cm treated with potassium ferricyanide. By placing a red filter (cut-off wavelength 610 nm) in front of the camera, the blue precipitate on anoxic soil appears as dark areas on the photograph. The numbered spots are referred to in the text. (B) (on next page) The digitized crack pattern belonging to the same sample area.

macroscopic penetration depth λ_g with Eq. (6.1). It is assumed that, on the scale of a core sample, the macroscopic respiration can be neglected. This assumption can be verified by comparing the calculated depth λ_g with the core sample dimensions.

A clay soil may remain locally saturated with water, even in the presence of air-filled cracks and macropores (Bronswijk, 1991). For the clayey soil used in the field work it has been shown experimentally in Chapter 4 that the size of the water-saturated zones may be several millimeters. On that scale the diffusion of oxygen is determined by diffusion through water-saturated pores only. The equations describing the oxygen transport are analogous to the above equations for gas diffusion: oxygen concentrations c_s are expressed now as the dissolved

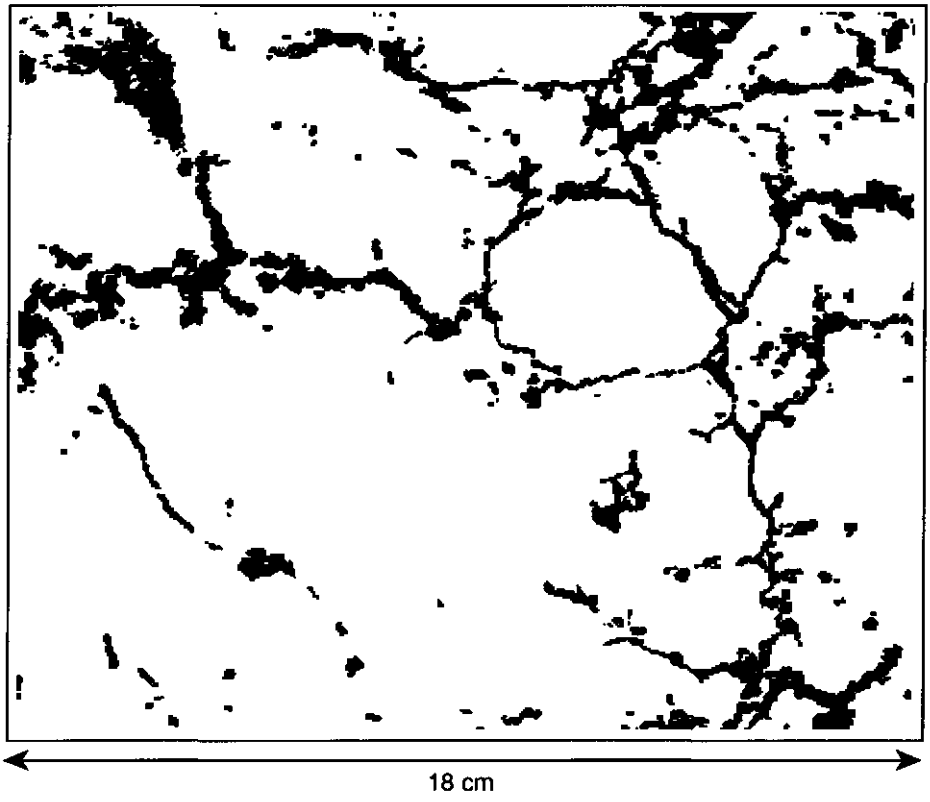

amount of oxygen per unit volume of the soil solution and the penetration depth for saturated soil λ_s becomes

$$\lambda_s = \sqrt{\frac{2\alpha C D_s}{Q}} \tag{6.2}$$

in which α is the solubility of oxygen in water.

In order to make use of the diffusivity measured in Chapter 4, Eq. (6.2) needs to be rewritten. The diffusion coefficient for saturated soil D_s can be expressed as (e.g. Nye & Tinker, 1977)

$$D_s = \theta D_w f \tag{6.3}$$

in which θ is the water content, D_w the diffusion coefficient in water and f a tortuosity factor (see also Table 6.1). The penetration depth becomes

$$\lambda_s = \sqrt{\frac{2\alpha C \theta D_w f}{Q}} \tag{6.4}$$

In Chapter 4 the diffusivity D_s/θ has been measured. According to Eq. (6.3), the diffusivity is equal to $D_w f$. The penetration depth for water saturated soil can be calculated then with Eq. (6.4) from values for $D_w f$, α, C, θ and Q.

Detection of anaerobiosis

It has been assumed that a prolonged lack of oxygen leads to the formation of ferrous iron. The presence of ferrous iron has been detected by applying a solution of potassium ferricyanide $K_3Fe(CN)_6$ to the surface of a soil intersection. With ferrous iron it forms a deep blue and stable precipitate called Turnbull's blue, $Fe_3[Fe(CN)_6]_2$. Photographs of the pattern of blue spots on the intersection surface have been made and analysed later.

Before starting the field work the reflection spectrum of blue coloured soil (containing ferrous iron) was compared to the spectrum belonging to oxic soil. The spectra were made using a spectrometer with a barium sulfate coated integrating sphere (the LI–1800 of LI–COR). Figure 6.3 shows the ratio between the two reflection coefficients as a function of wavelength. In the blue part of the spectrum the difference between the reflection coefficients is small (the ratio lies close to unity). The reflection of red light, however, is considerably suppressed by the Turnbull's blue precipitate. Consequently, the contrast in black and white photographs can be enhanced by using the red light only. We used a red filter with a cut-off wavelength of 610 nm (the Red Sharp Cut-off Glass Filter RG610 of Melles Griot).

Intersections of about 0.5 m^2 were made at a depth of about 10 cm. The last millimeters of soil were removed carefully with a sharp knife. To the exposed surface the colour test on ferrous iron was applied as quickly as possible. Since the Turnbull's blue is formed only in an acid solution, the intersections were first "wetted" with a spray of diluted HCl (0.15 mol/l). Then a 5% solution of ferricyanide was applied, also as a spray. After a few seconds stable blue spots appeared on the reduced parts of the soil.

The relation between the cracks and the positions of blue spots has been studied in sample areas of 18.0×14.5 cm. From these areas black and white photographs were made with the red filter. In choosing the sample areas we have not attempted to get statistically representative samples of blue spots or cracks. Therefore, the quantitative results of the analysis, the anoxic surface fractions for instance, will not and cannot be used as a property of the whole field.

A second reason for not using the results for the whole field is that the blue spots did not occur everywhere on the intersection. Blue spots occurred only in broad, parallel zones with a width of about 20 cm and about 40 cm apart. Within these zones the above mentioned sample areas have been chosen to study the cracks and blue spots. Between the broad zones, cracks were present but the

blue spots were lacking. This larger scale structure has not been studied in detail. It has probably resulted from soil tillage.

Soil structure

Of each sample area a second photograph was made on which only cracks are visible. The sample area was covered with a layer of white wall paint on a latex base. Over the paint a plexiglass cap was placed enclosing the sample area of 18.0 × 14.5 cm. Then, with a simple hand pump some pressure was applied to the sample area causing the white paint to penetrate a few millimeters into cracks and large pores. After removing the cap, the paint dried, and on the next day the top layer of dry paint was removed with a scalpel knife. The cracks became visible as clear white lines and contrast rich photographs were easily made. Finally the polluted soil was removed from the field.

Image processing

Prints of all photographs have been made in an ordinary darkroom. The photographs of the blue precipitate have been digitized as grey value images, which will be referred to as the "oxygen images". The oxygen image files contain 307 200 grey values organized as an image of 600 × 512 pixels. To reduce noise a so called 5 × 5 median filter has been applied, which means that every grey value is replaced by the median value of the 25 pixels in the square around it. As

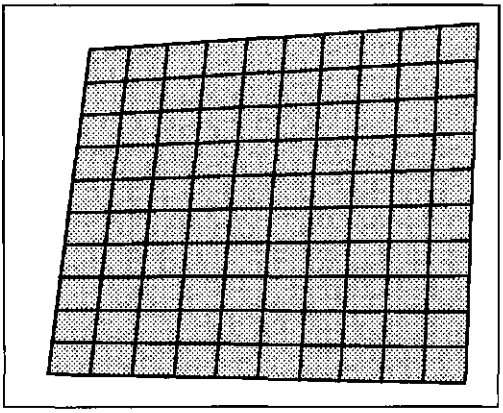

Figure 6.5. The grey area shows, with exaggerated distortion, the shape of a rectangular sample area on the photographs. Blue spots and crack pattern have been compared by using non-rectangular coordinate systems for both photographs.

an example, an oxygen image is shown in Fig. 6.4a.

The contrast in the crack photographs was so large that they were immediately converted into binary image files, containing only 1 bit per pixel (being 0 for soil and 1 for the white cracks). The crack images contain 642 240 bits, organized as a binary image of 892×720 pixels. On a few places of the images isolated white pixels occurred, being rests of paint lying on the surface or other noise. Isolated white pixels have a profound influence on distance calculations since the distance to the nearest "crack" is strongly reduced in the neighborhood of, even, a single white pixel. They were removed from the image by requiring that in the 25×25 square around each white pixel should lie at least 24 other white pixels. A few hundred white pixels of the roughly 50 000 in each crack image have been removed in this way. Figure 6.4b shows the clear crack image belonging to the oxygen image in Fig. 6.4a.

Image analysis

Comparing an oxygen image with a crack image, a solution had to be found for the different scales of the images and the distortion of the rectangular sample area on both images. Due to a slightly excentric position of the camera, the rectangular shape of the sample area is distorted on the photographs. On both pictures the sampling area is visible as a quadrangle (cf. the right edge of Fig. 6.4a). Figure 6.5 schematically shows the shape of a sampling area on a digitized image. The shape of the quadrangles is different for the two images. Although the distortion is exaggerated in Fig. 6.5, the deviations are too large to ignore when an oxygen image and a crack image are compared with each other. The problem has been solved by using "field coordinates". The field x-coordinate and the field y-coordinate describe the position of a point within the real, rectangular sampling area of 180 x 145 mm in the field. The four corners of each image can obviously be identified with the corners of the real sample area, with positions in field coordinates (0,0), (180,0), (180,145) and (0,145). The field coordinates of the other pixels of the image are found then by means of interpolation according to the grid of lines shown in Fig. 6.5. The crack image in Fig. 6.4b is in fact a plot of the field coordinates of all crack pixels.

By assigning field coordinates to the pixels in both images, the oxygen and the crack image of a sample area can be compared. The crack pixels of Fig. 6.4b, for instance, can be projected on the oxygen image of Fig. 6.4a. Figure 6.6 shows the result.

The next step is to choose test points in the oxygen image. The field coordinates of each test point are calculated and the distance to the nearest crack is found by comparing the point's position with the position of all white

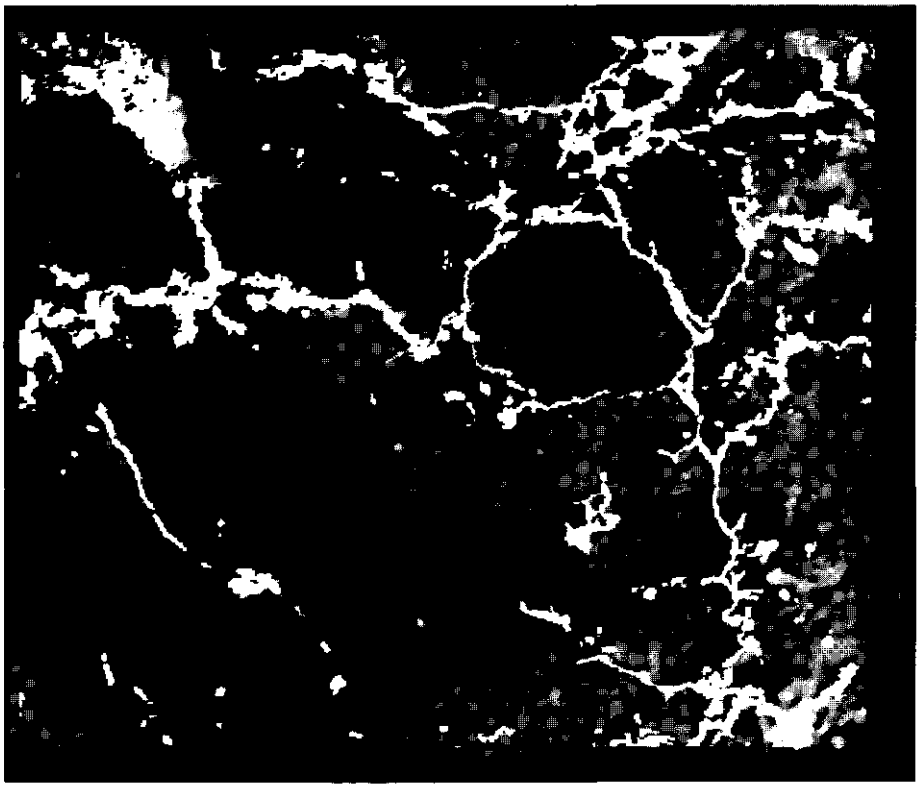

Figure 6.6. The cracks of Fig. 6.4b projected on the "oxygen image" of Fig. 6.4a.

pixels of the crack image. That involves about 50 000 distance calculations and is therefore an inefficient procedure. The procedure is easy to program, however, and computer time has been reduced by using integer coordinates based on a length unit of 0.1 mm. The distance calculations are actually carried out then by using integer arithmetic. The calculation of the distance to the nearest crack for a thousand sample points took about 20 minutes on an Apple Macintosh II.

RESULTS

The macro-scale oxygen distribution

For 16 soil samples, the respiration rate varied between 1.2×10^{-6} and 6.5×10^{-6} mol $m^{-3}s^{-1}$ with an average value of 3.5×10^{-6} mol $m^{-3}s^{-1}$. For 10

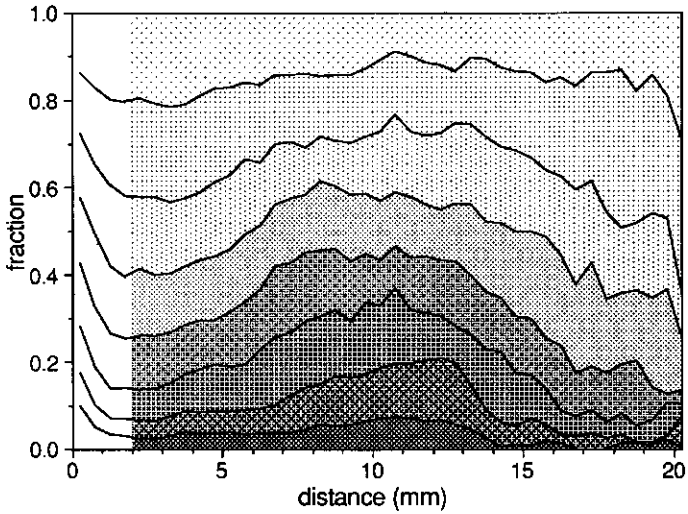

Figure 6.7. Grey value fractions as function of the distance to the nearest crack for the sample area in Fig. 6.4a and Fig. 6.6. For distances below 2 mm, the contribution of dark ("anoxic") soil is overestimated as a result of non-painted parts of the cracks and errors in calculated coordinates.

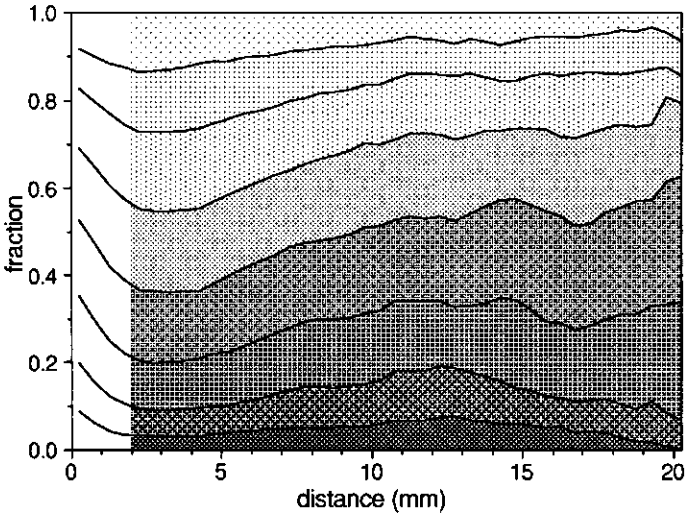

Figure 6.8. Grey value fractions as function of the distance to the nearest crack. The lumped result for 9 sample areas of 18.0×14.5 cm. The total area covered by test points is 0.143 m^2.

core samples with an air filled porosity between 0.02 and 0.07 the measured macroscopic diffusion coefficients varied between 26×10^{-9} and 567×10^{-9} $m^2 s^{-1}$ with an average value of 145×10^{-9} $m^2 s^{-1}$. Substituting the average values in Eq. (6.1), together with an atmospheric oxygen content of 9.3 mol m^{-3}, the penetration depth for oxygen becomes 0.88 m.

This value implies that the cracks at 10 cm depth, the depth of the intersecting planes, are well aerated, which is a necessary condition for treating the soil as aggregated. The soil consists of aggregates surrounded by cracks in which large concentration gradients are not likely to occur. The penetration depth of 0.88 m is also considerably larger than the height of the core samples (0.05 m) for which the diffusion coefficient D_g has been measured. This justifies the neglection of soil respiration in calculating D_g.

The meso-scale oxygen distribution

Before giving the quantitative results of the image analysis, some qualitative remarks can be made on the oxygen images. In Fig. 6.4a three small areas have been marked as 1, 2 and 3. In area 1 the influence of the crack on the aeration status of the soil is clearly visible. The anoxic zone is located close to the centre of the aggregate. Area 2 shows anoxic soil at the edge of cracks and area 3 lies far from the cracks without being anoxic. The picture appearing is that there is no strong relation between the aeration status of a point and its distance x to the nearest crack. The influence of cracks is clearly visible at specific locations, but a statistical relation between distance and grey value will be weak or absent.

This qualitative conclusion is confirmed by a quantitative analysis. Figure 6.7 gives the probability of finding certain grey values in Fig. 6.4a, as function of the distance to the nearest macropore. For very small distances (<2 mm), the fraction of dark test points decreases with increasing distance. This results from the remaining errors in distance measurements. On the oxygen image, cracks are dark and may therefore appear as anoxic points in the sample when they fall just besides the white parts of the crack image. This may be caused by incompletely painted cracks or by errors in the match between the two images.

Above a distance of 2 mm the probability of finding a dark, anoxic test point increases with distance. Above about 12 mm the probability decreases again. This pattern results partly from the small sample size. Only a few clods are present in Fig. 6.4a and the position of the anoxic parts in these clods determines the result in Fig. 6.7.

The analysis has been repeated for 8 other photographs. The total area covered with test points is 0.143 m^2 with a test point density of 258 points per square centimeter. The graph in Fig. 6.8 shows the lumped result of the 9

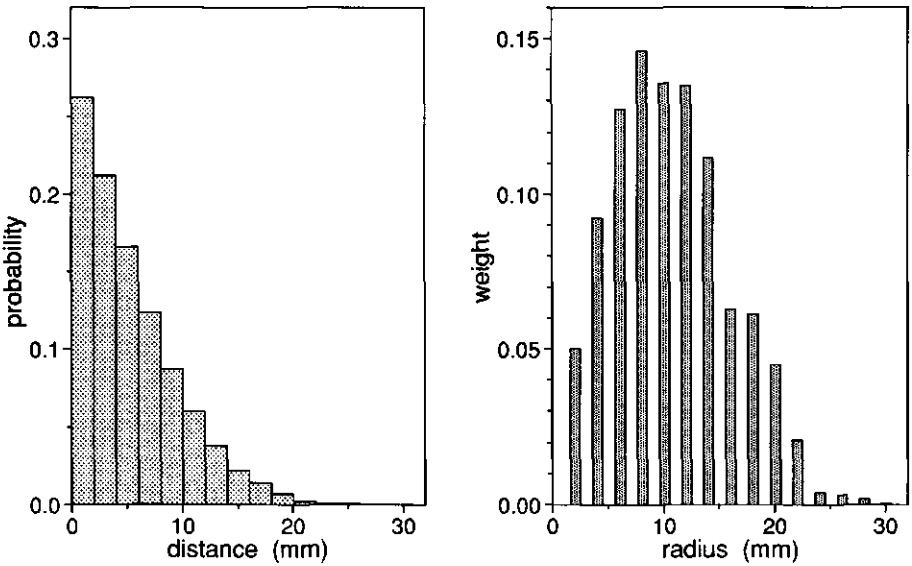

Figure 6.9. (left) Distance probabilities, lumped for 9 sample areas.

Figure 6.10. (right) Weights (or volume fractions) belonging to a model soil consisting of plane sheets with different radii.

photographs. Again, the decreasing probabilities for distances below 2 mm should be neglected. Then, up to a distance of about 10 mm, the fraction of dark test points slightly increases. This means that the probability on anaerobiosis slightly increases with the distance to the nearest crack. For the darkest (and certainly anoxic) points there is a slight decrease in probability for large distances, as in Fig. 6.7. For the less dark soil, however, this effect is absent. On the whole, the relation between distance and grey value is weak.

Model systems

The distances x on the horizontal axis of Fig. 6.8 are not equally abundant. In Fig. 6.9 a histogram of distance probabilities is shown, consisting of lumped results for the nine photographs analyzed. From the distance probabilities a model system consisting of plane sheets has been calculated with the method developed in Chapter 2. Figure 6.10 gives the volume fractions or weights belonging to each plane sheet radius in the model system (the radius of a plane sheet is defined as half its thickness). Diffusion models can be much more easily applied to the plane sheets of the model system than to the real soil. The simple

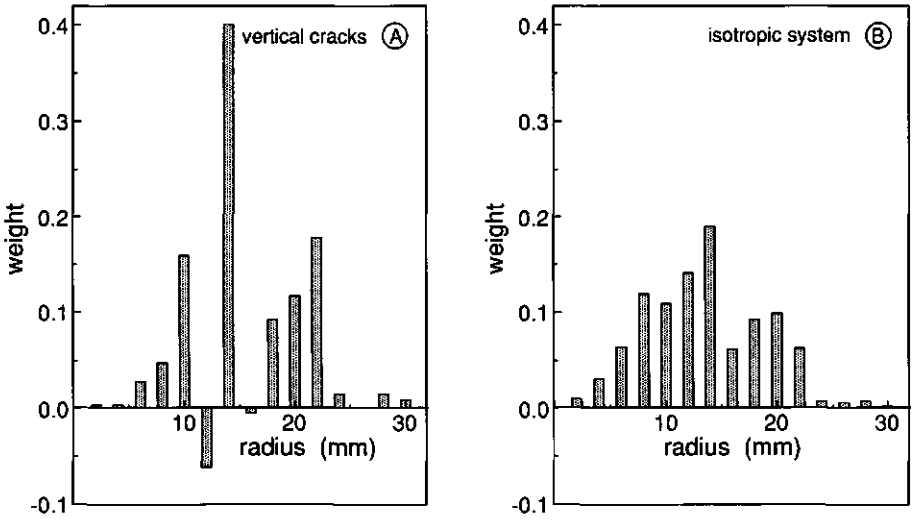

Figure 6.11. Weights (or volume fractions) belonging to a model soil consisting of cylinders. (A) Assuming the cracks to be vertical ; (B) For an isotropic system. See the text for comments.

diffusion models discussed in Chapter 2, but also the model for non-uniform respiration developed in Chapter 5, can be directly applied.

Figure 6.11 gives weights for two model systems consisting of cylinders. Assuming the cracks to be vertical leads to the left histogram (Fig. 6.11a). The right histogram has been calculated for an isotropic system, using the technique described in Chapter 3.

A remark has to be made about the negative weights in Fig. 6.11a for cylinder radii of 12 and 16 mm. The cylinder weights are closely related to the second-order derivative of the distance probability density function of the system (see Chapter 2). This leads to sensitivity for statistical variation in the measured distance probabilities in Fig. 6.9. This sensitivity causes a few weights to become negative. In case of the model system in Fig. 6.11a, however, the negative weights would probably not be a problem in applying a diffusion model. Their effect will be compensated by the large positive weights for nearby radii. When problems arise in such cases, a continuous distance probability density function has to be estimated from which a continuous non-negative weight function can be found.

The weights of the isotropic model system in Fig. 6.11b are more stable than the weights in Fig. 6.11a. This stability has a purely mathematical origin, however, (see the Appendices of Chapters 2 and 3). In the field, the larger cracks were vertical and the soil is probably better described by the system in Fig. 6.11a.

DISCUSSION

On the analyzed photographs there soil aggregates are visible in which oxygen diffusion may well take place according to the model for a uniform soil aggregate. There is a more or less uniform activity, the soil close to the cracks is oxic and at some distance from the crack an anoxic zone begins. The lack of correlation between distance and probability on anaerobiosis is obviously caused by the presence of anoxic soil close to cracks and by the presence of oxic soil far from cracks. These two types of places will be discussed separately.

Anoxic soil close to cracks

On many photographs anoxic soil is visible within 1 mm from a crack. A small penetration depth can be realized by a low diffusion coefficient, a low oxygen concentration in the crack or a large respiration rate of the soil. By means of simple order of magnitude calculations the importance of these three factors can be investigated.

Local diffusion coefficients may indeed be very small. Shrinking clay remains locally water-saturated, even in the presence of air-filled cracks and macropores (Bronswijk, 1991). Equation (6.4) allows the calculation of a penetration depth for saturated soil, making use of the results of Chapter 4. The measured values of the diffusivity $D_w f$ lie close to 1.0×10^{-9} $m^2 s^{-1}$. Then, with $\alpha C = 0.63$ mol m^{-3} for atmospheric air in the cracks (at 15 °C, Benson & Krause, 1980), an estimated volumetric water content of 0.3 and a mean bulk respiration of 3.5×10^{-6} mol $m^{-3} s^{-1}$, the local penetration depth becomes 10 mm. This value, based on the lowest possible diffusion coefficient, is at least a factor 10 too large. This implies that either the local respiration rate lies a factor 100 above the bulk value for the soil, or that the local oxygen concentration in the crack is close to zero.

The crack system as a whole is certainly not anoxic. It has been shown above that the macroscopic penetration depth for oxygen is 0.88 m, which implies that the oxygen concentration in most cracks and macropores at 10 cm from the surface is close to the atmospheric concentration. Only when cracks are not connected to the atmosphere, local concentrations may fall to zero. Although this may be the case for a few isolated macropores, it does not provide an explanation for the occurrence of anaerobiosis close to cracks. Cracks close to the surface will usually form as a result of soil evaporation and transport of water vapor through the cracks to the soil surface. This implies gas continuity, and therefore anoxic cracks will be rare. In addition to this physical argument, Fig. 6.12 shows that oxic and anoxic soil may both be adjacent to the same crack

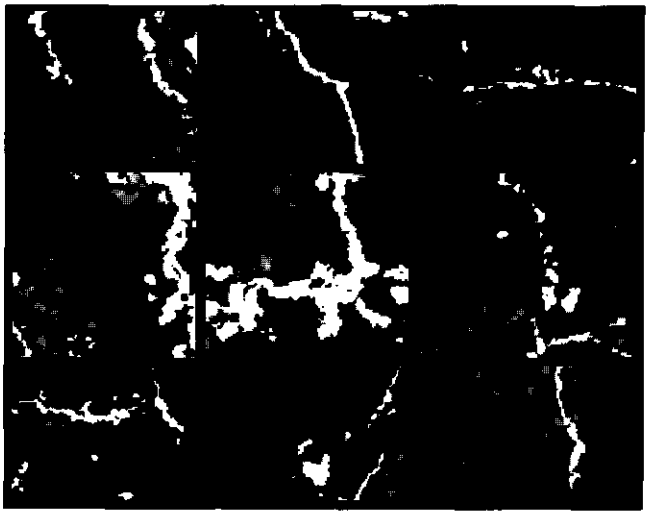

Figure 6.12. A collection of details showing that oxic soil (light) and anoxic soil (dark) may both be adjacent to the same crack or macropore (white).

or macropore. The anaerobiosis cannot be caused then by a lack of oxygen in the crack.

The conclusion is that the occurrence of anaerobiosis close to cracks is caused by a local soil activity exceeding the bulk value by at least a factor 100. This leads to a thin oxic layer at the crack surface and behind that layer, the soil is anoxic.

Oxic soil far from cracks

The presence of oxic soil at 20 or 30 mm from the cracks can be explained in different ways. On that scale air-filled pores occur and the diffusion coefficient will lie between the extremely low value for water-saturated soil and the measured macroscopic values. In combination with the macroscopic respiration rate, the penetration depth for oxygen lies somewhere between 10 mm and tens of centimeters. Hence, it cannot be concluded that oxic soil far from cracks is not active at all. An activity level comparable with the macroscopic respiration is consistent with available data. A much larger activity, however, cannot exist in oxic soil, since it would lead to anaerobiosis between the air-filled pores.

More can be said about the activity of oxic soil by measuring the oxygen diffusivity on the scale of a few centimeters. As reported in Chapter 4, mechani-

cal difficulties with the oxygen electrodes used prevented such measurements. In the meantime (autumn 1991) better electrodes have been designed.

The distribution of soil activity

The field results show that highly active soil ("hot spots") occurs close to cracks, but do not allow conclusions with respect to the activity of anoxic soil at larger distances. Different assumptions can thus be made on the distribution of hot spots. If the activity of anoxic soil is independent of the distance to the nearest crack, the hot spots are randomly distributed over the soil. In a cylinder or plane sheet model system, this can be represented by a random distribution of hot spots over the model system. For plane sheets a model has been developed in Chapter 5.

If hot spots occur only close to cracks, one should be aware of the difference between the real soil aggregates and the cylinders or plane sheets of a model system. The small cylinders, or small plane sheets represent the soil in small aggregates, but also the soil at the surface of large aggregates with an irregular shape. Hence, by simply using a high activity for the small cylinders or sheets leads, the model soil already represents a soil with hot spots close to cracks.

The assumption of a non-random distribution of hot spots is in agreement with observations made by Seech and Beauchamp (1988). They observed a relatively large denitrification in small aggregates, explained by a lack of carbon substrate in the larger aggregates. A simple explanation for a non-random distribution of activity is the presence of plant residues and manure close to cracks or macropores. Cracks may also form at those places where leaves, for instance, are burried in the soil.

Some consequences of non-uniform activity

Some consequences of non-uniform activity have already been investigated in Chapter 5 by means of a simple model. In this model, a large local activity is indeed consistent with a relatively low bulk respiration rate, since much of the highly active soil is anoxic and does not consume oxygen. The distribution of anoxic soil almost coincides with the distribution of soil activity.

The fact that highly active parts of a clayey soil are largely anoxic has consequences for the description of processes such as mineralization and immobilization. In a clayey soil, the biological activity associated with plant residues will take place under anoxic conditions, irrespective of the soil structure. In a sandy soil, local gas diffusion coefficients will seldom be as low as in clay. The aeration of plant residues depends then more strongly on the soil structure

and the plant residues will more often be oxic.

The occurrence of anoxic soil close to cracks has also consequences for denitrification. In case of uniform activity, nitrate diffuses to the anoxic zones in the centres of the aggregates. There, under anoxic conditions, denitrification occurs (e.g. Leffelaar, 1987). The presence of hot spots close to cracks and macropores, however, leads to a different picture of the process. When water passes an anoxic zone at the surface of a crack, there is hardly any barrier between dissolved nitrogen and the anaerobic organisms. In this picture, denitrification occurs when dissolved nitrate meets anoxic soil, by chance.

A denitrification model then consists of a description of the movement of water with dissolved nitrogen in relation with the distribution of the anoxic hot spots. The flow of water through a hot spot leads to denitrification, since the dissolved nitrate is immediately used by the anaerobic organisms in the hot spot. The denitrification rate of the soil will depend on the size and the number of hot spots, and their position relative to places with a large nitrate flux. Clearly, the role of diffusion in such a system is smaller than in a model for homogeneous soil.

The formulation of process models is certainly more difficult for a non-uniform soil activity than for homogeneous soil aggregates. A variability of a factor 100 or more, however, will generally lead to a qualitatively different behavior of the system. One may simplify the situation by assuming that soil does, or does not use oxygen. In Chapter 5 an example of this approach is presented.

Chapter 7

Application of nutrient uptake models to non-regular distributions of roots

Abstract. Detailed transport models exist for water and nutrient uptake by a single root located along the axis of a soil cylinder. An approximate method has been developed that enables the application of such uptake models to a root system with an arbitrary geometry. The root system is replaced by a model system consisting of soil cylinders with different radii. The soil cylinders do not represent the soil around specific roots, however. Each cylinder radius represents a distance scale that occurs in the system and a weight function expresses the relative abundance of each scale. The nutrient uptake by the root system is calculated as a weighted sum of uptakes from the soil cylinders of the model system.

The weight function can be obtained from the statistical distribution of the distance from a point in the soil to the nearest root. Equations are given for deriving a continuous weight function from a continuous distance distribution, and for deriving a number of discrete weights from measured distances.

The method is worked out for a zero-sink uptake model. Fractional uptakes calculated for random and clustered root distributions agree with electrical analogue data from the literature. In addition to its utility in describing root systems, the method can be applied to worm burrows, networks of blood capillaries, and similar systems.

INTRODUCTION

Detailed models exist for the nutrient uptake by a single root. Usually, the root is located along the axis of a soil cylinder and a differential equation is solved. Various assumptions on the nutrient transport in the soil and on the behavior of the root can be made and the cylindrical symmetry allows an analytical solution in many cases. Some references to these models and their backgrounds are Bouldin (1961), Barber (1962), Olsen & Kemper (1968), Nye & Tinker (1977), and De Willigen & Van Noordwijk (1987). A cylinder model can be easily applied to a root system consisting of parallel and equidistant roots. Uptake calculations for a

Table 7.1. Description of symbols used in the text. The subscripts "c" and "s" stand for "cylinder" and "root system", respectively. Symbols used only in the Appendix have not been included.

symbol	description	units	Equation
a	dimensionless, quadratic cylinder size	-	(7.10)
a_i	series of a values, $i = 1,...,N$	-	(7.31)
β	time constant in an approximate formula	s	(7.46)
A_c	initial amount of nutrient in cylinder	$kg\,m^{-3}$	(7.36)
A_s	initial amount of nutrient in root system	$kg\,m^{-3}$	(7.42)
α	radius of Poisson clusters	m	
b	numerical constant related to λ	-	(7.18)
c	concentration in the liquid phase	$kg\,m^{-3}$	
c_0	initial concentration	$kg\,m^{-3}$	
δ	width of the first distance interval	m	
D	diffusion coefficient of the nutrient in soil	$m^2\,s^{-1}$	
g	function in zero-sink model	-	(7.A2)
G	time integral of g	-	(7.A3)
H	cylinder height, used only in Eq. (7.1)	m	
K	absorption constant	-	
L	root length density	m^{-2}	
λ	radius of close-packed cylinders	m	(7.18)
μ	mean number of points in Poisson clusters	-	
N	number of distance and cylinder classes	-	
v_c	root volume fraction in cylinder	-	(7.35)
v_s	root volume fraction in root system	-	(7.41)
p_i	distance probability, $i = 1,...,N$	-	
P_{ij}	matrix element, $i,j = 1,...,N$	-	(7.22)
θ	water content	-	
r	coordinate	m	
R	cylinder radius	m	
R_0	root radius	m	
R_i	series of R values, $i = 1,...,N$	m	(7.20)
$s(x)$	distance probability density function	m^{-1}	
$\sigma(y)$	reduced surface function	-	(7.9)
t	time	s	
τ_c	time constant for cylinder system	s	(7.34)
τ_s	time constant for root system	s	(7.40)
τ_s^*	characteristic soil depletion time	s	(7.49)
u_c	uptake rate per unit cylinder volume	$kg\,s^{-1}\,m^{-3}$	
u_s	uptake rate per unit system volume	$kg\,s^{-1}\,m^{-3}$	
U_c	cumulative uptake per unit cylinder volume	$kg\,m^{-3}$	
U_s	cumulative uptake per unit system volume	$kg\,m^{-3}$	
VM	variance over mean (clustering parameter)	-	
$v(R)$	weight of cylinder radius R	m^{-1}	(7.6)

(Continuation of Table 7.1)

symbol	description	units	Equation
v_i	weight belonging to R_i, $i = 1,...,N$	-	
$w(a)$	weight function	-	(7.12)
w_i	weight belonging to a_i, $i = 1,...,N$	-	(7.30)
x	distance	m	
x_i	series of x values, $i = 0,...,N$	m	
y	dimensionless, quadratic distance	-	(7.8)
y_i	series of y values, $i = 0,...,N$	-	(7.31)

more complicated root system, however, require a method which takes into account the geometry of the system.

Barley (1970) proposed the application of Dirichlet tesselation (or Voronoi polygons) to parallel, non–regular roots. To each root a "region of influence" is assigned which is replaced by a cylinder with equal volume. The soil around each individual root is thus represented by its own equivalent cylinder to which an uptake model is applied. Baldwin *et al.* (1972) studied experimentally the effects of root pattern by means of an electrical analogue and found much lower uptakes than Barley (1970) for a similar root distribution.

In this paper a theoretical method is developed, which can be applied to non–parallel roots as well. The method is more efficient than Dirichlet tesselation and is in agreement with Baldwin's electrical analogue data. The method makes use of an overall geometric property of the root system.

Various authors have characterized the structure of a root system by the (statistical) distribution of the distance from a randomly chosen point to the nearest root (e.g. Barley, 1970; De Willigen & Van Noordwijk, 1987; Tardieu, 1989). Clearly, this distance distribution expresses how close the soil is to the roots and therefore is related to "travel distances" of water and nutrients. The relation with transport processes is not just a qualitative one. In Chapter 2 it is shown that quantitative diffusion models for an aggregated soil can be based on a distance distribution and that the method developed can be applied to root systems as well. The method for root systems is elaborated in this chapter.

In the next section the method is described and motivated. The analysis of measured distances is treated in a following section. As an example, a zero–sink uptake model is applied to different root distributions. The results are compared with data of Baldwin *et al.* (1972) for an electrical analogue, and the failure of Dirichlet tesselation is discussed. Table 7.1 gives a list of symbols with definitions and units.

METHOD

The method is most easily understood by considering the real root system and its model as two, initially independent systems. The purpose of the simple model system is to replace the real root system in uptake calculations. Clearly, in order to have approximately equal nutrient uptakes, the model system and the root system should have certain geometrical properties in common. The property proposed in this paper is the (statistical) distribution of the distance from a point of the soil to the nearest root. Hence, the model system used has the same distance distribution as the real root system.

A suitable model system consists of soil cylinders with different radii, each with a root along its axis. The relative abundance of the cylinders with radius R is expressed by the value of a weight function $v(R)$. This weight function is derived from the requirement that model system and root system have equal distance distributions.

The soil cylinders of the model system do not represent the soil around specific roots. Instead, the cylinder radius R can be interpreted as a characteristic length scale occurring in the root system and $v(R)$ as the abundance of this scale. The square radius R^2 is proportional to the characteristic time scale for diffusion in a soil cylinder, suggesting the use of square distances and square cylinder radii. Suitable quadratic scales are introduced in the subsection *Quadratic Scales*. The resulting equations have a simple form and are easily made dimensionless. Examples are given for a regular and for a random root distribution.

The distance probability density function $s(x)$

Figure 7.1 shows the cross section of a straight root located along the axis of a soil cylinder with radius R. Diffusive transports to and from the root take place through surfaces around the root. At a distance x from the root axis, the area of the cylindric surface is $2\pi Hx$ in which H is the cylinder height. The surface area is normalized by dividing it by the volume πHR^2 of the root plus surrounding soil. The surface to volume ratio as function of R and x becomes

$$\begin{cases} s_c(R,x) = \dfrac{2\pi Hx}{\pi HR^2} = \dfrac{2x}{R^2} & , \ 0 \le x \le R \\ s_c(R,x) = 0 & , \ x > R \end{cases} \tag{7.1}$$

The fraction of the cylinder volume Δv that lies between a distance x_1 and a distance x_2 from the root axis is

$$\Delta v = \int_{x_1}^{x_2} s_c(R,x)\,dx = \frac{x_2^2 - x_1^2}{R^2} \tag{7.2}$$

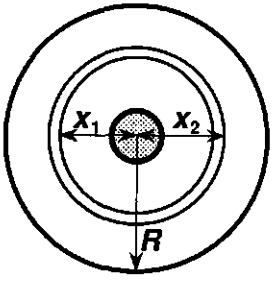

Figure 7.1. The cross section of a soil cylinder with a root along its axis. Concentric surfaces are indicated at a distance x_1 and at a distance x_2 from the root axis.

This volume fraction can be interpreted as the probability that a randomly chosen point lies between the two concentric surfaces. Thus, Eq. (7.2) also expresses the fact that the surface to volume ratio $s_c(R,x)$ is the probability density belonging to a distance x. That property can be used to define a function $s(x)$ for a root system in general: The distance x is the spatial distance from a randomly chosen point to the nearest root axis and $s(x)$ is the probability density of x. The general form of Eq. (7.2) is

$$\Pr(x_1 < x < x_2) = \int_{x_1}^{x_2} s(x)\,dx \tag{7.3}$$

In this paper, the positions of randomly distributed roots are described as infinite lines with a random position and orientation. For such a system Ogston (1958) showed that

$$s(x) = 2\pi L x\, e^{-\pi L x^2} \tag{7.4}$$

in which L is the root length per unit soil volume. It is also illustrative to consider, in this case, the relation between $s(x)$ and the concentric surfaces around the

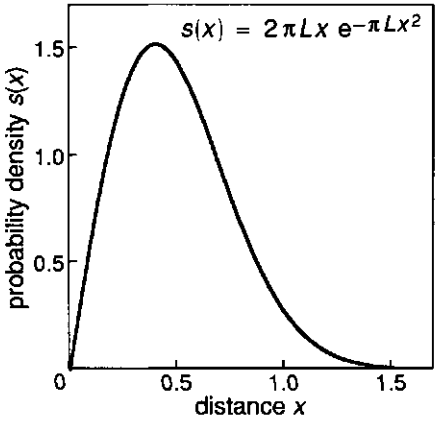

Figure 7.2. The distance probability density function $s(x)$ for randomly distributed roots (Eq. (7.4)) for the root length density $L = 1$.

roots. For small distances the graph in Fig. 7.2 shows a linear increase of $s(x)$ with x. This corresponds to the linearly increasing size of concentric surfaces around all individual roots. For larger distances the concentric surfaces around neighboring roots touch each other and the total surface area at a distance x from the roots increases more slowly, and eventually decreases with x. The long tail of the function $s(x)$ represents regions of the soil that are situated at exceptionally large distances from the roots.

Derivation of the weight function $v(R)$

The model system consists of soil cylinders with different radii, each with a root along its axes. The cylinders are hypothetical objects without a position or an orientation. They are taken so long that end effects in transport processes can be neglected. A weight function $v(R)$ describes how the total volume of the model system is distributed over soil cylinders with different radii. The soil cylinders with a radius between R_1 and R_2, for instance, occupy the volume fraction

$$\Delta v = \int_{R_1}^{R_2} v(R)\,\mathrm{d}R$$

which expresses that $v(R)$ is the volume fraction density function of the model system.

The model system representing a real root system must meet the criterion that the distance probability density functions of the model system and the real root system are equal. To derive a model system with such a prescribed function $s(x)$, the relation between $s(x)$ and $v(R)$ must be known. The roots of the model system are situated along the cylinder axes. Hence, for each soil cylinder separately, Eq. (7.1) gives the distance probability density function. The function $s(x)$ for the whole model system becomes

$$s(x) = \int_0^\infty s_c(R,x)\,v(R)\,\mathrm{d}R = \int_x^\infty \left(\frac{2x}{R^2}\right) v(R)\,\mathrm{d}R \qquad (7.5)$$

The integrand in this expression can be regarded as the product of two probabilities. The first is the probability $v(R)\mathrm{d}R$ that a randomly chosen point lies in a soil cylinder with a radius in the interval $[R, R+\mathrm{d}R]$. The second is the probability (density) $s_c(R,x)$ that a point inside such a cylinder actually has a distance x to the cylinder axis. The integral sums the contributions of all cylinders to find the overall probability density $s(x)$ for the model system.

Equation (7.5) can be treated as an equation with known $s(x)$ (the function for the root system) and with unknown weight function $v(R)$. In the Appendix it is shown that the solution is

$$v(R) = \tfrac{1}{2}s(x) - \tfrac{1}{2}x\frac{ds(x)}{dx}\Big/_{x=R} \qquad (7.6)$$

As the root system and the model system have equal functions $s(x)$, integrals of $s(x)$ (volume fractions) are also conserved. In other words, each volume fraction lying between a distance x_1 and a distance x_2 from the root system, will be correctly reproduced by the model system.

Justification for the conservation of $s(x)$

The distance probability density function $s(x)$ is the only geometrical property shared by root and model system. The first reason for choosing $s(x)$ as the conserved property is the close relation between $s(x)$ and surface to volume ratios. Approximate calculations on diffusion in a non-regular particle can be based upon the ratio between its outer surface and its volume (e.g. Bird *et al.*, 1960, section 17.6). In Chapter 2 the method for a single particle or clod has been generalized in order to describe diffusion in aggregated soil. Theoretical calculations described in that chapter suggest that systems with equal functions $s(x)$ behave similarly with respect to diffusion processes.

The second reason for the choice of $s(x)$ is related to the nutrient uptake in the absence of interaction between roots. The roots absorb nutrients from the soil close around them without initially influencing the uptake by neighboring roots. The system behaves as a set of independent roots, each with soil around it. This limiting situation will be correctly described by the model system, since the conservation of $s(x)$ guarantees that the soil volume at some (relatively small) distance from the roots is the same in root and model system.

The third reason is simply that the method works. Below, in the section APPLICATION OF A ZERO-SINK UPTAKE MODEL, data from Baldwin *et al.* (1972) for an electrical analogue are favorably compared with results calculated for model systems.

The application of an uptake model

A nutrient uptake model is applied to a model system by calculating

$$u_s(t) = \int_0^\infty u_c(R,t)\, v(R)\, dR \qquad (7.7)$$

The subscripts "c" and "s" stand for "cylinder" and "root system", respectively (cf. Table 7.1). The function $u_c(R,t)$ in the integrand is the uptake rate for a root in a soil cylinder as function of the cylinder radius R and time. The uptake rate should be expressed as an amount per unit time and per unit cylinder volume. In

Eq. (7.7) it is integrated over the cylinder radius, using the volume fraction density function $v(R)$ as a weight function. Note that the equation remains unchanged when cumulative uptakes are used instead of uptake rates.

The function $u_c(R,t)$ may be based on different assumptions for the transport process and the root behavior. It may be the analytical solution of a diffusion equation or the result of numerical calculations. Besides time and cylinder radius, the uptake rate will depend on the parameters of the transport model used, such as diffusivity, adsorption constant etc. Also the root radius is treated as a parameter of the transport model.

Quadratic scales

In order to simplify the mathematical treatment and the analysis of measured distances, a new distance scale and a new cylinder size are adopted, which are taken proportional to the square of x and the square of R, respectively. Additionally, the new variables are made dimensionless. These changes require new, dimensionless functions replacing the distance probability density $s(x)$ and the weight function $v(R)$. It is emphasized that neither the root system nor the model system change by introducing new variables and functions. Only the mathematical description of the root and model system becomes different, leading to somewhat abstract, but surprisingly simple equations. The diagram in Fig. 7.3 summarizes the relation between the functions used in the preceding sections, $s(x)$ and $v(R)$, and the new ones, $\sigma(y)$ and $w(a)$.

The new, dimensionless distance variable y is defined by

$$y \equiv \pi L x^2 \tag{7.8}$$

The variable y plays the same role as the distance x. For a randomly chosen point the value of the "distance" y can be calculated from Eq. (7.8). The probability density of y, written as $\sigma(y)$, is derived below from the probability density function $s(x)$. The quadratic relation between x and y implies that the shape of the functions $s(x)$ and $\sigma(y)$ will be different. Integrals of both functions, however, are volume fractions of the root system that should not be affected by the variable change. Therefore, the new function $\sigma(y)$ must satisfy

$$\sigma(y)\,dy = s(x)\,dx$$

leading to the following relation between $s(x)$ and $\sigma(y)$

$$\sigma(y) = \left(\frac{dx}{dy}\right) s(x) = \frac{s(x)}{2\pi L x} \tag{7.9}$$

Equation (7.9) expresses that $s(x)$ must be divided by $2\pi Lx$ before x can be replaced by y according to Eq. (7.8). The denominator $2\pi Lx$ requires some attention. The cylindric surface at a distance x from a certain root has a size of

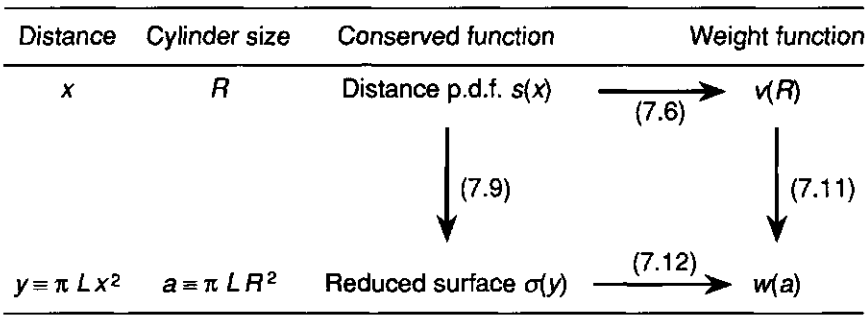

Figure 7.3. The functions belonging to the distance x and the cylinder size R on one hand, and to the quadratic variables y and a on the other hand. Numbers of the transformation equations are given near the arrows.

$2\pi x$ per unit root length. Hence, $2\pi Lx$ is the total cylinder surface at a distance x around all roots per unit system volume. It would be the value of $s(x)$ when the roots would not interact. In reality, the concentric surfaces around neighboring roots touch each other and $s(x)$ is reduced (cf. the explanation following Eq. (7.4)). The limiting value $2\pi Lx$ can still be used, however, to make $s(x)$ dimensionless. The resulting function $\sigma(y)$ expresses the reduction of the surface due to the presence of other roots. It will therefore be called the reduced surface function.

For a root system consisting of a single root along the axis of a soil cylinder, the root length density L is $1/\pi R^2$. Because the surfaces around the root are actually full cylinders, there is no surface reduction and $\sigma(y)$ is equal to 1 for "distances" y not exceeding the soil cylinder radius. Equations (7.1) and (7.9) indeed lead to

$$\begin{cases} \sigma(y) = 1 \ , \ 0 \le y \le 1 \\ \sigma(y) = 0 \ , \ y > 1 \end{cases}$$

In case of an arbitrary root distribution, $\sigma(y)$ will be 1 for $y = 0$. Then, for increasing y, the function either remains constant or decreases. For a system of randomly distributed roots, for instance, Eqs. (7.4) and (7.9) yield $\sigma(y) = \exp(-y)$.

Equation (7.8) suggests a similar expression for the radius R of a soil cylinder. The dimensionless size a of a soil cylinder in the model system is defined by

$$a \equiv \pi L R^2 \tag{7.10}$$

Again, a weight function describes the relative importance of different cylinder sizes in the model system. The new weight function $w(a)$ can be derived from $v(R)$ by means of a transformation analogous to Eq. (7.9):

$$w(a) = \left(\frac{dR}{da}\right) v(R) = \frac{v(R)}{2\pi L R} \tag{7.11}$$

It can also be derived directly from the requirement that the reduced surface function $\sigma(y)$ is conserved (like $s(x)$). In the Appendix it is shown that this leads to

$$w(a) = -y \frac{d\sigma(y)}{dy} \Big/_{y=a} \tag{7.12}$$

The dimensionless weight function $w(a)$ is characteristic of a certain type of root distribution. It is the same function, for instance, for all random root distributions, irrespective of the actual root length density.

An uptake model is applied to the model system by means of the following equation, equivalent to Eq. (7.7),

$$u_s(t) = \int_0^\infty u_c(a,t)\, w(a)\, da \tag{7.13}$$

The uptake $u_c(a,t)$ is easily derived from $u_c(R,t)$ by substituting $\sqrt{a/\pi L}$ for the cylinder radius R (cf. Eq. (7.10)). Equation (7.13) will be used in the section APPLICATION OF A ZERO-SINK UPTAKE MODEL.

The time constant associated with diffusion processes in a cylinder, is proportional to the square cylinder radius R^2 (cf. Eq. (7.34)). Hence, when cylinder size is expressed as a, the time constant belonging to a soil cylinder is proportional to its size and the new weight function $w(a)$ describes the range of different time scales in the root system. This is a physical justification for the use of a quadratic size scale instead of merely a dimensionless radius (as $\sqrt{a}$ would be).

Examples

Root distributions may be either regular, random or clustered. The random distribution, lying between the other two possibilities, is often used as a reference in describing the nature of an observed root distribution. For infinite lines with a random position and orientation Ogston (1958) derived the following expression for the distance distribution:

$$\Pr(\text{distance} < x) = 1 - e^{-\pi L x^2} \tag{7.14}$$

The probability density function $s(x)$ is found from the distribution function by differentiation. The result was given already as Eq. (7.4). Equation (7.14) is easily rewritten in terms of the quadratic distance variable y (cf. Eq. (7.8)). Then $\sigma(y)$ is:

$$\sigma(y) = \frac{d(1-e^{-y})}{dy} = e^{-y} \tag{7.15}$$

With Eq. (7.12) the weight function $w(a)$ becomes

$$w(a) = a e^{-a} \tag{7.16}$$

Figure 7.4 shows a graph of this simple weight function. It reaches a maximum when $a=1$. The wide range of a values occurring in the model system represents the different scales on which transport takes place in a system of randomly distributed roots. A clustered root distribution would require to an even wider range of cylinder sizes.

As a second example, the system consisting of a hexagonal grid of parallel roots is analyzed. For relatively small distances x, the size of the cylindric surface around each root increases linearly with x. At a distance λ, equal to half the distance between two neighboring roots, the surfaces just touch each other and form close-packed cylinders. For distances larger than λ, the size of the surface decreases steeply, reaching zero for $x = 2\lambda/\sqrt{3}$. Some geometry leads to

$$\begin{cases} s(x) = L x\, 2\pi & , 0 \le x < \lambda \\ s(x) = L x\, 2\left\{\pi - 6 \arccos\left(\frac{\lambda}{x}\right)\right\} & , \lambda \le x \le 2\lambda/\sqrt{3} \end{cases} \tag{7.17}$$

The distance λ is given by

$$\pi L \lambda^2 = b \tag{7.18}$$

where $b = \pi/2\sqrt{3} \approx 0.907$, the volume fraction occupied by close packed

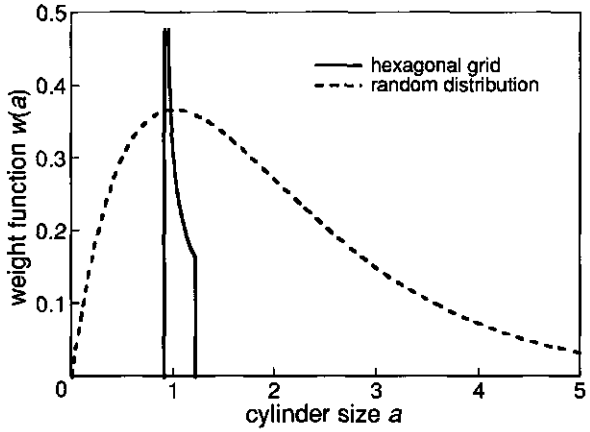

Figure 7.4. The dimensionless weight function $w(a)$ for randomly distributed roots (Eq. (7.16)) and for equidistant, parallel roots in a hexagonal grid (Eq. (7.19), values divided by 10).

cylinders. The reduced surface function $\sigma(y)$ is found by applying to Eq. (7.17) the transformation Eq. (7.9). The result is

$$\begin{cases} \sigma(y) = 1 & , 0 \le y \le b \\ \sigma(y) = 1 - \frac{6}{\pi} \arccos\left(\sqrt{b/y}\right) & , b < y \le \frac{4}{3}b \end{cases}$$

This expresses that the surfaces around the roots are full cylinders until y reaches the value b. For larger y values the size of the surface is reduced.

The model system is obtained again by applying Eq. (7.12) to $\sigma(y)$. The non–zero part of the weight function becomes

$$w(a) = \frac{3}{\pi}\sqrt{\frac{b}{a-b}}\ , \ b < a \le \frac{4}{3}b \qquad (7.19)$$

A graph of this function has been drawn in Fig. 7.4. All cylinder sizes lie in a narrow range around $a=1$. This narrow size range reflects the regularity of the hexagonal root distribution. Basically, the only length scale occurring in the system is the average value of a, which is $5\pi/9\sqrt{3} \approx 1.0077$. This value is close to $a=1$ and thus corresponds to the cylinder radius derived from $\pi R^2 = L^{-1}$, a usual choice for regular distributions (e.g. Barley, 1970).

THE ANALYSIS OF MEASURED DISTANCES

The above results were obtained for theoretically derived functions $s(x)$ or $\sigma(y)$. In this section it is shown how a model system can be obtained from measured distances. For a large number of test points in the root system the spatial distance to the nearest root axis needs to be determined. The test points may either be randomly distributed or may form a dense grid. Distance intervals

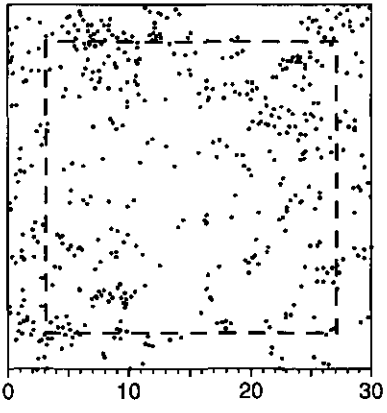

Figure 7.5. Example of observed root positions (De Willigen and Van Noordwijk, pers. comm.). In the central square of 24x24 cm test points have been chosen for which the distance to the nearest root has been calculated.

are chosen and each class will contain a fraction of the measured distances. These fractions will be referred to as distance probabilities.

As an example, Fig. 7.5 shows the positions of 505 roots in an intersecting plane (data from De Willigen and Van Noordwijk, pers. comm.). For simplicity, it is assumed that the roots are parallel and perpendicular to the intersecting plane. Distances in the plane can be treated then as true, three dimensional distances. Distance measurements have been carried out by a computer and Fig. 7.6a shows the result.

A model system with the same distance probabilities as the observed root system is derived. The derivation starts with some definitions. There are N distance classes and the i-th class is written as $[x_{i-1}, x_i]$. The value of x_0 is set at 0 and x_N is the largest distance occurring in the system. The probability of finding a distance in the i-th distance class is written as p_i. The model system consists of cylinders with N discrete cylinder radii. These are chosen equal to the upper bounds of the distance classes. Hence,

$$R_i = x_i, \quad i = 1,...,N \tag{7.20}$$

Each cylinder class occupies a fraction v_j of the total volume ($j = 1,...,N$). These (still unknown) volume fractions v_j replace a continuous weight function and will act as weights belonging to the radii R_j.

The measured probabilities p_i are set equal to the distance probabilities of the model system by

$$p_i = \sum_{j=1}^{N} P_{ij} v_j, \quad i = 1,...,N \tag{7.21}$$

This equation can be understood as follows. The weight (or volume fraction) v_j is the probability that a randomly chosen point lies in the j-th cylinder class. P_{ij} is the probability that, given a point in a cylinder with radius R_j, the distance belonging to that point falls in distance class i. Hence, Eq. (7.21) expresses the measured probability p_i as a sum of contributions from all cylinder classes. It forms a set of N linear equations with N unknown weights. The matrix elements or probabilities P_{ij} are (cf. Eq. (7.2))

$$\begin{cases} P_{ij} = \displaystyle\int_{x_{i-1}}^{x_i} \frac{2x}{R_j^2}\, dx = \frac{1}{R_j^2}(x_i^2 - x_{i-1}^2), & i \le j \\ P_{ij} = 0 \qquad\qquad\qquad\qquad\qquad\qquad , & i > j \end{cases} \tag{7.22}$$

After solving Eq. (7.21) for the weights v_j, the application of an uptake model is straightforward. Analogous to Eq. (7.7), the uptake $u_s(t)$ by the model system is calculated as a weighted sum according to

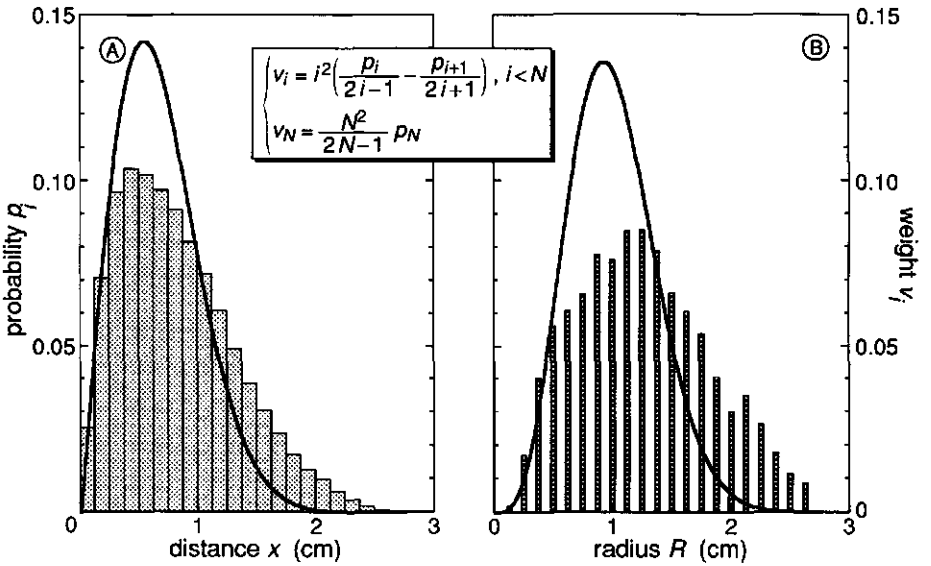

Figure 7.6. (A) Distance probabilities calculated with the root positions in Fig. 7.5 for equal distance intervals of 0.125 cm ; (B) the weights belonging to the cylinders of the model system (Eq. (7.26)). The curves indicate the shape of similar histograms for a random root distribution.

$$u_s(t) = \sum_{j=1}^{N} v_j\, u_c(R_j,t) \tag{7.23}$$

Equation (7.21) can be solved numerically for arbitrary class bounds x_i. Two useful choices, however, are further discussed: classes of equal width on a linear distance scale (as in Fig. 7.6a) and classes of equal width on a quadratic distance scale. These choices allow an analytical solution of Eq. (7.21) leading to expressions of weights, directly in terms of measured distance probabilities.

A linear distance scale

The class bounds are written as

$$x_i = \delta i, \quad i = 0,\ldots,N \tag{7.24}$$

with δ being defined as the width of the first interval. The intervals specified by Eq. (7.24) all have the same width and the cylinder radii R_j are equal to δj (cf. Eq. (7.20)). The matrix elements P_{ij} become

$$\begin{cases} P_{ij} = \frac{1}{j^2}\left\{i^2-(i-1)^2\right\} = \frac{2i-1}{j^2}, & i \le j \\ P_{ij} = 0 \qquad\qquad\qquad\quad , & i > j \end{cases} \tag{7.25}$$

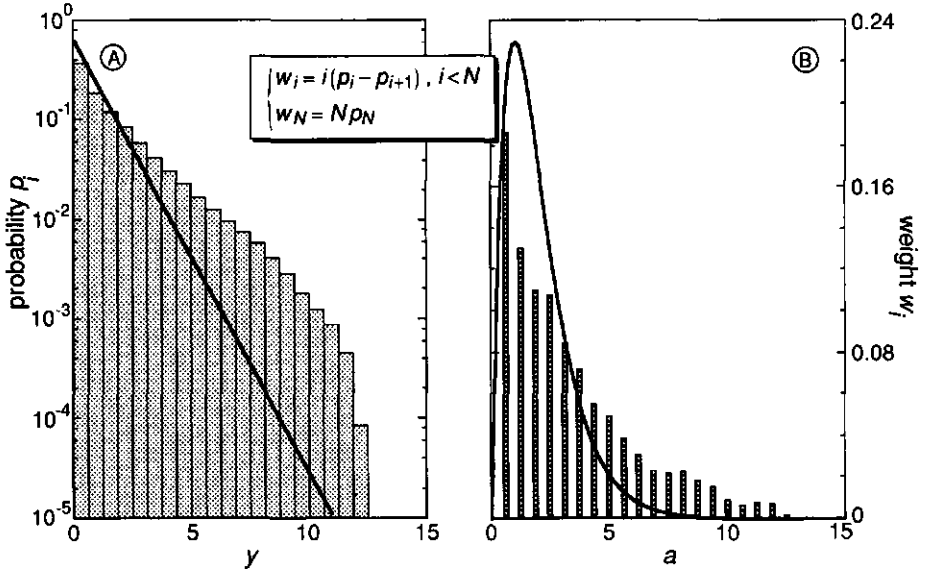

Figure 7.7. (A) Distance probabilities for equal intervals of 0.625 on a dimensionless, quadratic distance scale (see Eq. (7.28)) ; (B) the weights belonging to the cylinders of the model system (Eq. (7.30)). The curves indicate the shape of similar histograms for a random root distribution.

In the Appendix the inverse matrix is given, leading to weights calculated as

$$\begin{cases} v_i = i^2\left(\dfrac{p_i}{2i-1} - \dfrac{p_{i+1}}{2i+1}\right), & i<N \\ v_N = \dfrac{N^2}{2N-1}p_N \end{cases} \tag{7.26}$$

The histogram in Fig. 7.6b shows the weights obtained with Eq. (7.26) from the distance probabilities in Fig. 7.6a. The curves in Fig. 7.6 show the shape of the functions $s(x)$ and $v(R)$ for randomly distributed roots (cf. Eqs. (7.4) and (7.6)). Function values have been multiplied by the class width δ (= 0.125 cm) in order to obtain numerical values comparable with distance probabilities and weights, respectively. Comparison of the histograms to the curves in Fig. 7.6 shows that the roots in Fig. 7.5 are somewhat clustered. In the CONCLUSIONS some remarks are made on this clustering.

A quadratic distance scale

The class bounds are written as

$$x_i^2 = \delta^2 i, \quad i = 0,\ldots,N \tag{7.27}$$

Distance probabilities can be calculated by classifying square distances according to Eq. (7.27) and calculating the fraction in each class. Figure 7.7a

shows the result for the roots in Fig. 7.5, using $\delta^2 = 0.355$ cm^2. The class bounds on the horizontal axis of the graph have been multiplied by $\pi L (= 1.76$ cm$^{-2})$ in order to get a dimensionless y-scale with class bounds y_i according to (cf. Eq. (7.8))

$$y_i = \pi L x_i^2 = (\pi L \delta^2) i, \quad i = 0,...,N \tag{7.28}$$

A model system is derived by substituting the class bounds x_i into Eqs. (7.20) and (7.22). The matrix elements become

$$\begin{cases} P_{ij} = \dfrac{1}{j}, & i \le j \\ P_{ij} = 0, & i > j \end{cases} \tag{7.29}$$

The inverse of this matrix is simple (see Appendix) and the weights, written as w_i, are

$$\begin{cases} w_i = i(p_i - p_{i+1}) & , \; i \le N-1 \\ w_N = N p_N \end{cases} \tag{7.30}$$

The cylinder sizes belonging to these weights are (cf. Eq. (7.10))

$$a_j = y_j = \pi L x_j^2 = (\pi L \delta^2) j, \quad i = 1,...,N \tag{7.31}$$

In combination with these cylinder sizes, the weights w_j resemble the continuous weight function $w(a)$, which explains the use of the symbol "w". Figure 7.7b shows the weights calculated with Eq. (7.30) from the distance probabilities in Fig. 7.7a.

The clustering of the roots in Fig. 7.5 again leads to a clear difference between the shapes of the histograms in Fig. 7.7 and the graphs of $\sigma(y)$ and $w(a)$ for randomly distributed roots (Eqs. (7.15) and (7.16)). Again, in order to obtain numerical values comparable with the histograms, the functions have been multiplied by the class width $\pi L \delta^2 (= 0.625)$.

The use of Eqs. (7.26) and (7.30) requires that, for an infinite number of distance classes, the weights converge to continuous functions $v(R)$ and $w(a)$. This convergence is proven in the Appendix.

APPLICATION OF A ZERO-SINK UPTAKE MODEL

The method described in the previous sections will now be used to calculate the zero–sink uptake for various root distributions. The applied uptake model originates from Youngs & Gardner (1963). The analytical expression for the uptake by a root in a soil cylinder can be written as function of three parameters: a time constant, the volume fraction occupied by roots and the initial amount of

nutrients. The expression for the uptake by a root system contains one additional quantity, a weight function $w(a)$. Numerical results are given for three different root distributions, a comparison is made with electrical analogue data from Baldwin *et al.* (1972) and the use of Dirichlet tesselation is discussed.

The model for a root in a soil cylinder

The nutrient transport is described as diffusion in an infinite hollow cylinder with a zero-sink condition at the root surface $r = R_0$ and no flux at the outer surface $r = R$. The function $c(r,t)$ is the concentration in the liquid phase in which the diffusion takes place. The contribution of mass flow is neglected, and the adsorption to the solid phase is assumed to be proportional to the solute concentration. The differential equation describing this process is

$$(K+\theta)\frac{\partial c(r,t)}{\partial t} = \frac{D}{r}\frac{\partial}{\partial r}\left(r\frac{\partial c(r,t)}{\partial r}\right) \tag{7.32}$$

with boundary conditions

$$t = 0\ ,\ c(r,t) = c_0\ ,\ R_0 \le r \le R$$

$$t > 0\ ,\ c(r,t) = 0\ \ ,\ r = R_0$$

$$\frac{\partial c(r,t)}{\partial r} = 0\ \ ,\ r = R$$

The second boundary condition expresses the behaviour of the root: the concentration at the root surface is zero. This so-called zero-sink condition describes a limiting situation in which the root always maximizes its uptake.

The diffusion coefficient of the solute, D, may be written as the product of the coefficient in free solution, the water content and a tortuosity factor (e.g. Rowell, *et al.* 1967). Other model parameters are the (constant) water content θ, the adsorption constant K, and the initial concentration in the liquid phase c_0 (see also Table 7.1). Following De Willigen & Van Noordwijk (1987), the buffer capacity is written as $K+\theta$.

Youngs & Gardner (1963) gave the solution of Eq. (7.32) for a more general boundary condition. In case of zero-sink root behavior their expression for the flux at the root surface can be written as

$$u_c(R,t) = \frac{D}{R^2}\, c_0\, g\left(\frac{R_0^2}{R^2}, \frac{Dt}{R^2(K+\theta)}\right) \tag{7.33}$$

Here, g is a dimensionless function with two (dimensionless) arguments, which is given in the Appendix (Eq. (7.A2)). In the derivations below the full expression for g is not used, however. It has been evaluated only for obtaining the

numerical results in the graphs.

The second argument of g contains the time constant τ_c defined by

$$\tau_c \equiv \frac{R^2(K+\theta)}{D} \tag{7.34}$$

Due to the first boundary condition, the solution depends also on the root radius R_0. This dependency is expressed by the first argument of g which is defined as

$$\nu_c \equiv \frac{R_0^2}{R^2} \tag{7.35}$$

The number ν_c is equal to the fraction of the cylinder volume occupied by the root. Finally, the quantity A_c is defined as the initial amount of nutrients per unit cylinder volume. A_c is related to the initial concentration c_0 in the liquid phase by

$$A_c = (K+\theta)(1-\nu_c)\, c_0 \tag{7.36}$$

The last three definitions (Eqs. (7.34), (7.35) and (7.36)) are used to write Eq. (7.33) as

$$u_c(R,t) = \frac{A_c}{\tau_c(1-\nu_c)}\, g\left(\nu_c, \frac{t}{\tau_c}\right) \tag{7.37}$$

Equation (7.37) expresses the uptake rate as an amount per unit of time and per unit of cylinder volume (A_c/τ_c), multiplied by the time dependent function g. The term $(1-\nu_c)$ will usually be close to unity.

The cumulative uptake can be derived by integrating Eq. (7.37) over time. The result is

$$U_c(R,t) = \frac{A_c}{(1-\nu_c)}\, G\left(\nu_c, \frac{t}{\tau_c}\right), \tag{7.38}$$

where G is the integral of g over its second argument (see Appendix, Eq. (7.A3)).

The approximate solution for a root system

The square cylinder radius R^2 in Eq. (7.33) can be replaced by $a/\pi L$ (cf. Eq. (7.10)). The uptake is then expressed as a function of the dimensionless cylinder size a and can be substituted into Eq. (7.13) for a model system. This leads to

$$u_s(t) = \int_0^\infty \frac{\pi L D\, c_0}{a}\, g\left(\frac{\pi L R_0^2}{a}, \frac{\pi L D\, t}{(K+\theta)\, a}\right) w(a)\, da \tag{7.39}$$

This equation is simplified in the same way as the solution for a single soil cylinder. The time constant in the second argument of g is

$$\tau_s \equiv \frac{K+\theta}{\pi L D} \tag{7.40}$$

The fraction of the total soil volume occupied by the roots is defined by

$$v_s \equiv \pi L R_0^2 \tag{7.41}$$

And finally, instead of the initial concentration c_0, the initial amount of nutrients per unit system volume A_s is used. Similar to Eq. (7.36) is

$$A_s = (K+\theta)(1-v_s)\, c_0 \tag{7.42}$$

Using the definitions of τ_s, v_s and A_s, Eq. (7.39) simplifies to

$$u_s(t) = \frac{A_s}{\tau_s(1-v_s)} \int_0^\infty \frac{w(a)}{a}\, g\left(\frac{v_s}{a}, \frac{t}{a\tau_s}\right) da \tag{7.43}$$

As in case of a single soil cylinder, the uptake rate is expressed as an amount per unit of time and per unit system volume (A_s/τ_s), multiplied by a dimensionless number (cf. Eq. (7.37)). This dimensionless number (the integral) depends on the function g derived for a single cylinder, on the time t, and on the root system properties τ_s, v_s and $w(a)$. The weight function $w(a)$ characterizes the type of root distribution and is independent of the actual root length density L. The influence of L is completely contained in the values of τ_s and v_s.

The product $a\tau_s$ in the second argument of g (Eq. (7.43)) is the time constant for diffusion in a soil cylinder with size a. Hence, the value of the weight function $w(a)$ expresses the importance of the time constant $a\tau_s$ in the root system.

The cumulative uptake of a root system becomes (cf. Eq. (7.38))

$$U_s(t) = \frac{A_s}{(1-v_s)} \int_0^\infty w(a)\, G\left(\frac{v_s}{a}, \frac{t}{a\tau_s}\right) da \tag{7.44}$$

The fractional uptake, which is the cumulative uptake relative to the initial amount of nutrients, is simply found as $U_s(t)/A_s$.

Uptake calculations for three root distributions

The fractional zero-sink uptake $U_s(t)/A_s$ has been calculated with Eq. (7.44) for a system of parallel and equidistant roots, for randomly distributed roots and for the distribution of parallel roots in Fig. 7.5. The three thick curves in Fig. 7.8 show the results as function of the dimensionless time t/τ_s, and for a root volume fraction $v_s = 0.01$. The differences in uptake between the three root distributions are considerable. Nutrients are taken up most easily by regularly distributed roots. The clustered roots lead to the lowest uptakes, and randomly distributed

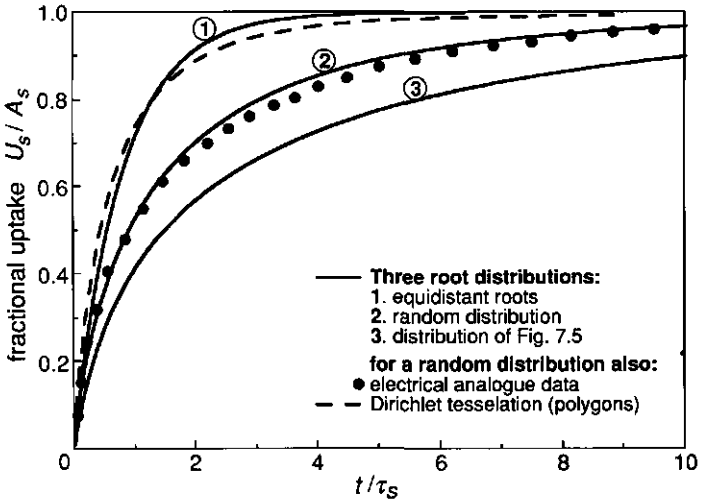

Figure 7.8. The fractional zero-sink uptake for three root distributions, calculated with a model system. The middle curve, calculated for $w(a) = a \exp(-a)$, is compared with electrical analogue data of Baldwin *et al.*(1972) and with the result of Dirichlet tesselation. The calculations and measurements have been carried out for $v_s = 0.01$.

roots take an intermediate position. Before continuing the description of Fig. 7.8, some details of the calculations are given.

The uptake by parallel and equidistant roots has been calculated by considering a cylinder with size $a=1$ only (see the text following Eq. (7.19)). Equation (7.44) for the root system reduces then to the solution for a single root in a soil cylinder.

The uptake by randomly distributed roots has been calculated by substituting the weight function $w(a) = a\exp(-a)$ into Eq. (7.44) (see Eq. (7.16)). The integrand in the resulting expression contains $\exp(-a)$ and can be efficiently evaluated by means of Gauss-Laguerre integration (e.g. Scheid, (1968) ; Abramowitz & Stegun (1970)). The middle curve in Fig. 7.8 has been obtained with the 12 point Gauss–Laguerre formula.

Fractional uptakes for the root distribution in Fig. 7.5 have been calculated by using the model system given in Fig. 7.7b (cf. Eqs. (7.27), (7.30) and (7.31)). The 14 cylinder sizes a_j and associated weights w_j have been substituted into

$$U_s(t) = \frac{A_s}{(1-v_s)} \sum_{j=1}^{N} w_j \, G\left(\frac{v_s}{a_j}, \frac{t}{a_j \tau_s}\right) \qquad (7.45)$$

This expression is similar to Eq. (7.44) and can be formally derived from Eq. (7.23) by substituting the zero-sink solution for a single soil cylinder.

Comparison with electrical analogue data

Baldwin, *et al.* (1972) used an electrical analogue for simulating a system of 40 randomly positioned, parallel roots. The simulated root volume fraction is 0.010 and their result is shown in Fig. 7.8 as a series of data points read from curve b in Fig. 7.4 of their paper. Their times, expressed as DLt, have been multiplied by π in order to get values of t/τ_s (the buffer capacity $K+\theta$ can be set at 1 since it does not occur in their differential equation, cf. Sanders *et al.* 1970).

The distance distribution for randomly positioned parallel roots is the same as for roots with a random distribution in three dimensions. Hence, the electrical analogue is described by the weight function $w(a) = a\exp(-a)$ and the middle curve in Fig. 7.8 may be compared with the data points. The theoretical curve is in close agreement with the measured uptakes.

Comparison with Dirichlet Tesselation

Barley (1970) introduced the use of Dirichlet tesselation in uptake calculations for parallel roots. To each root belongs a region of influence. These regions appear as "Voronoi polygons" on a plane intersecting the roots at right angles. For the root in each polygon the nutrient uptake is calculated by means an equivalent soil cylinder with a cross sectional area πR^2 equal to the area of the polygon.

In case of equidistant roots, all polygonal areas are equal to L^{-1}, which leads to equivalent cylinders with dimensionless size 1. As shown above, in the subsection *Examples*, this practically coincides with the use of a weight function. Hence, in case of equidistant roots the two methods will always lead to the same result.

For randomly positioned, parallel roots the zero-sink uptake has been calculated with Dirichlet tesselation, using 799 equivalent cylinders. Figure 7.8 shows the result as a dashed line close to the uptake for equidistant roots. This small difference with the uptake by equidistant roots was also found by Barley (1970) and led him to the conclusion that a central position of the roots in the equivalent cylinders is not realistic. A central position leads to a reduction of the effective size of the region of influence and therefore to overestimated uptakes. The method described in this paper, however, also makes use of a central root position and leads to lower and realistic uptakes. This requires an explanation.

Dirichlet tesselation for randomly positioned roots leads to dimensionless cylinder sizes a ($=\pi L R^2$) with mean 1 (as the total surface remains unchanged) and variance 0.280 (Gilbert, 1962). These values can be compared with the weight function for the same system. The function $w(a)$ in Eq. (7.16) corresponds to a gamma distribution of a with mean 2 and variance 2 (e.g. Hogg

& Craig, 1978). The conservation of $s(x)$, on which $w(a)$ is based, apparently requires an increase of a and its variance relative to the size of the "regions of influence". This allows a central root position without leading to overestimated uptakes. In other words, the weight function describes the length scales in the system in terms of cylinders with a central root.

Comparison with data for clustered root patterns

When a square is randomly positioned over a two-dimensional root pattern, different numbers of roots may lie in it. The variance–to–mean ratio *VM* of this number can be used to measure the degree of clustering. It is 0 for equidistant roots, 1 for a random pattern and larger than 1 for clustered patterns. Baldwin *et al.* (1972) also arranged their 40 "roots" in clustered patterns and measured the fractional uptake as a function of *VM*(still, with $v_s = 0.01$). Figure 7.9 shows their results for three different values of t/τ_s. The data points are compared to zero-sink uptakes calculated with weight functions $w(a)$ for a so-called Poisson cluster process.

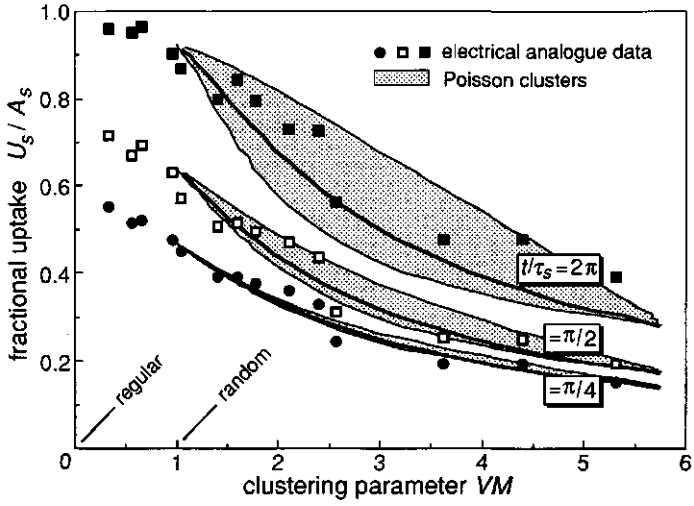

Figure 7.9. The fractional zero-sink uptake of as function of the clustering statistic *VM* (see text) for three values of t/τ_s. The points are electrical analogue data for 40 "roots" from Baldwin *et al.* (1972). The hatched areas are feasible ranges for Poisson clustered roots. For each value of t/τ_s, the lower boundary of the hatched area has been calculated by keeping the number of roots per cluster (μ) at 40 and varying the size of the clusters, the thick curve in the middle by keeping the cluster radius α at $1.19/\sqrt{L}$ and varying μ, and the upper boundary by varying both parameters while keeping the root density in the clusters ($\mu/\pi\alpha^2$) at $9L$. For each choice of μ and α, the ratio *VM* has been calculated for test squares with an area of $40L^{-1}/59$, the same area that was used by Baldwin.

Poisson clusters (Diggle, 1983) can be generated in a plane by choosing random points which act as "parents". Each parent point is the centre of a cluster consisting of "offspring". For each cluster, the number of offspring is taken from a Poisson distribution with mean μ. The positions of the offspring are randomly chosen within a circle with a fixed radius α around each parent point. The parents only play a role in the generation process and the offspring represents root positions. Generated root patterns lie between highly clustered and random, depending on μ and α. Diggle (1978) gives an expression for the distance distribution. With the help of that expression and Eq. (7.12), values of the weight function $w(a)$ can be calculated numerically, which allows the calculation of zero-sink nutrient uptakes by applying Eq. (7.44). Some details are given in the Appendix.

The most clustered root pattern formed by Baldwin *et al.* (1972) consisted of a single cluster of 40 roots with a local root density of $9L$. The Poisson clusters representing this distribution have been formed by setting μ at 40 and the root density within the clusters ($\mu/\pi\alpha^2$) at $9L$. Because the Poisson clustering process has two independent parameters (for a given L), one may proceed in different ways from strongly clustered to random. Three methods have been used, each resulting in a different relation between the calculated zero-sink uptake and the clustering statistic *VM*. In Fig. 7.9 the results are shown as three curves for each value of t/τ_s. The hatched areas between the upper and lower curves indicate feasible ranges for the uptake by clustered roots. The data points lie within, or close to, these ranges.

The characteristic soil depletion time

The zero-sink uptake from a soil cylinder can be accurately described by means of a single time constant. This is not the constant τ_c, however, since the uptake depend also on the root volume fraction v_c (cf. Eq. (7.37)). Suitable time constants were derived by Baldwin *et al.* (1973) and De Willigen & Van Noordwijk (1987), who used an approximate steady-state and an approximate steady-rate model, respectively.

In both derivations the concentration profile around the root is assumed to have a constant shape. Smaller uptake rates require smaller gradients and concentrations, but the shape of the profile remains the same. The expression for the concentration leads then to a relation between the amount of nutrients in the soil cylinder and the uptake rate. The amount of nutrients, however, decreases as result of that same uptake rate, which leads to a simple, ordinary differential equation. The fractional uptake becomes

$$\frac{U_c(t)}{A_c} = 1 - e^{-t/\beta} \tag{7.46}$$

in which β is the characteristic time constant for the zero-sink uptake from a soil cylinder. In the limit for $\nu_c \ll 1$ the steady-state approximation leads to (Baldwin *et al.* 1973 ; Nye & Tinker, 1973, expression 7.13)

$$\beta = \frac{\tau_c}{4}\left\{\ln\left(\frac{1}{\nu_c}\right) - 1\right\} \tag{7.47}$$

and the steady-rate approximation to (De Willigen & Van Noordwijk, 1987, expression 12.8)

$$\beta = \frac{\tau_c}{4}\left\{\ln\left(\frac{1}{\nu_c}\right) - \frac{3}{2}\right\} \tag{7.48}$$

Especially Eq. (7.48) represents an excellent approximation of the zero-sink uptake from a soil cylinder.

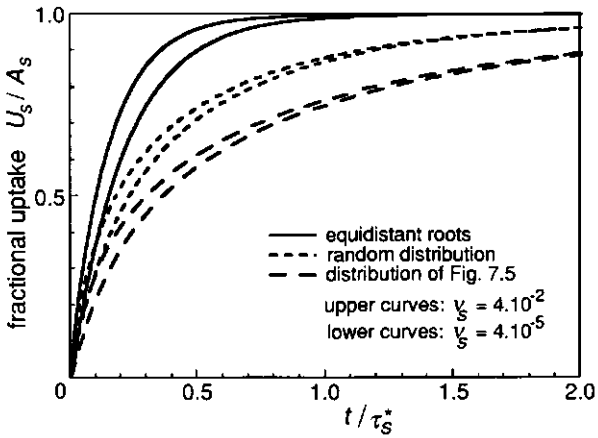

Figure 7.10. The fractional zero-sink uptake for three root distributions, calculated with Eqs. (7.44) and (7.45) as function of the dimensionless time t/τ_s^* (Eq. (7.49)). The upper and lower curve for each distribution have been calculated with values of the root volume fraction ν_s (Eq. (7.41)) of 4×10^{-2} and 4×10^{-5}, respectively.

For a root system, an approximate expression in the form of Eq. (7.46) does not exist. Initially, when the roots do not interact, the uptake rate is always as large as for equidistant roots. Later, only the larger cylinders of the model system contribute to the uptake rate and the process takes place more slowly. Although a simple exponential expression for the uptake does not exist, It is still possible, to characterize the time scale of the process. A characteristic soil depletion time can be defined as

$$\tau_S^* \equiv \tau_s \ln\left(\frac{1}{v_s}\right) = \frac{K+\theta}{\pi L D} \ln\left(\frac{1}{\pi L R_0^2}\right) \tag{7.49}$$

which is a simplified form of Eqs. (7.47) and (7.48), generalized for a root system.

Figure 7.10 shows fractional uptakes for equidistant roots, for randomly distributed roots, and for the distribution of parallel roots in Fig. 7.5. The curves have been calculated for two widely differing values of the root volume fraction v_s, 4×10^{-2} and 4×10^{-5} and the time axis has been scaled with τ_S^* defined in Eq. (7.49).

For each of the three root distributions the two curves are close. For a random root distribution about 88% of the nutrients is taken up at $t = \tau_S^*$, which means that the time τ_S^* practically coincides with the 90%-point of the uptake process. For equidistant roots the 90%-point is reached at least twice as fast and for clustered root distributions it takes (much) longer before 90% of the nutrients is taken up. Note that the curves in Fig. 7.10 are independent of the root length density and the parameters of the uptake model. Quantitative use of Fig. 7.10 only requires values for the initial amount of nutrients A_s and the characteristic soil depletion time τ_S^*.

Clearly, the curves for equidistant roots could be scaled better with a time constant analogous to Eq. (7.48). Then, for larger times, the results for non–regular distributions become much worse. The simple form of Eq. (7.49) was therefore preferred.

Some typical parameter values are (taken from De Willigen & Van Noordwijk, 1987) $K = 0$ (for nitrate), $\theta = 0.3$, $L = 1$ cm^{-2}, $D = 0.1$ cm^2/day and $R_0 = 0.025$ cm. These lead to $\tau_S^* = 6.0$ day, which gives an idea of the order of magnitude of τ_S^*. The characteristic soil depletion time may be compared with characteristic times of other processes in the studied system, for instance, with times associated with the supply of nutrients.

CONCLUSIONS

Approximate uptake calculations for a root system can be based on the distribution of the spatial distance from a point to the nearest root axis. The uptake process needs to be described for a single root with a cylinder of soil around it. The uptake model can then be applied to a set of cylinders forming a model of the root system. These cylinders represent the different length and time scales occurring in the system. In fact, the model system only consists of a weight function specifying the relative importance of the different scales (cylinder radii). The uptake by the root system is thus calculated as a weighted sum of the

results for all scales. Calculations for zero-sink root behavior agree well with uptakes determined by Baldwin *et al.* (1972) for an electrical analogue. It is therefore concluded that the use of a distance distribution leads to simple, approximate solutions with a good accuracy. In practice, there will be no need to use the real geometry of a root system in a large numerical model.

The weight function is derived from the requirement that the model system has the same distance distribution as the root system. This implies that surfaces and volume fractions at certain distances from the roots are conserved in the model system. The negligence of individual root positions in the actual uptake calculations allows efficient calculations. In practice, more than 20 cylinder radii will rarely be required. The use of quadratic length scales is advantageous, both in theoretical calculations and for the analysis of measured distances. Equations become more elegant because the time constant for diffusion processes in a cylinder is proportional to its square radius.

The analysis of Dirichlet tesselation supports the conclusion of Barley (1970). The use of Voronoi polygons leads to overestimated uptakes due to a central root position in combination with the conserved size of the regions of influence. De Willigen & van Noordwijk (1987) overcame this problem by deriving excentric root positions for the equivalent cylinders. The cylindrical symmetry is lost then and much more complicated uptake models are required. Conservation of the distance distribution solves the problem in a much simpler way.

The method described in this paper has been elaborated for a zero-sink uptake model. Any numerical or analytical uptake model, however, which is formulated for a soil cylinder can be applied to a root system. De Willigen & Van Noordwijk (1987), for instance, give an analytical description of the nutrient uptake by a root in partial contact with the soil.

The method can also be used for clustered root distributions. The calculations for a zero-sink uptake process showed that no unique relation exists between the used clustering statistic *VM* and the fractional uptake. A clustering statistic with a higher predictive value remains yet to be found. Without such a statistic, a distance probability density function remains necessary for every root distribution.

The calculations in this paper make use of a homogeneous soil. Especially in case of clustered root distributions, however, the soil around the roots is likely to be heterogeneous. Adaptations can be made for various types of heterogeneity. Nutrient concentrations need not be taken equal in the different cylinders, for instance. They may be taken larger in the small cylinders, simulating larger root densities in richer soil. Model properties may also be subjected to random variation. Root radii, for instance, may be chosen randomly, with or without a correlation with the cylinder radius. The consequences of soil structure can also be taken into account. When the distance x from an arbitrary point to the nearest root is measured, roots at the opposite side of a crack can be neglected. In that

way, the presence of cracks influences the measured distance probabilities. The cylinders of the model system will be larger than for a homogenous soil with the same root positions.

These examples show that the use of a model system based on a distance distribution constitutes a flexible method. Various assumptions on soil and root behavior can be investigated. When adapting the method to special needs, however, one should be aware of the character of the method: the cylinders form an abstract model system and do not represent individual roots. The analysis of the Dirichlet tesselation shows how easily errors are made as a result of straightforward simplification. Approximate calculations need to be based on insight in the described system and not on its reconstruction in the form of a huge computer model with an unknown accuracy.

The developed method can also be applied to wormhole systems, networks of blood capillaries and similar systems.

APPENDIX

The weight functions $w(a)$ and $v(R)$

Equation (7.1) gives the distance probability density function of a single cylinder with radius R. Its reduced surface function, following from the transformation Eq. (7.9), is equal to a^{-1} for "distances" y less than a. Hence, for a model system with weight function $w(a)$, the overall reduced surface function is (cf. Eq. (7.5))

$$\sigma(y) = \int_y^\infty \frac{1}{a} w(a)\, da \qquad (7.A1)$$

The reduced surface function $\sigma(y)$ of the model system is set equal to the known reduced surface function of the root system. Then Eq. (7.A1) becomes an equation with unknown $w(a)$. The solution, given as Eq. (7.12), can be found by differentiating Eq. (7.A1) with respect to y (cf. the solution for the "plane sheet model soil" in Chapter 2). Note that Eq. (7.A1) implies that the average value of a^{-1} is 1 (since $\sigma(0)=1$).

Equation (7.6) for $v(R)$ can be found now from $w(a)$, using Eqs. (7.9), (7.10), (7.11) and (7.12):

$$v(R) = \frac{da}{dR} w(a) = -2\pi L R\, a \frac{d\sigma(a)}{da} =$$

$$= -\pi L R^2 \frac{d(s(R)/2\pi L R)}{dR} = \frac{1}{2}\left\{s(R) - R\frac{ds(R)}{dR}\right\}$$

The matrix solutions

In case of equal distance classes on a quadratic scale, the inverse matrix is

$$\begin{cases} P_{ij}^{-1} = +i & , j = i \\ P_{ij}^{-1} = -i & , j = i+1 \\ P_{ij}^{-1} = 0 & , j < i \text{ or } j > i+1 \end{cases}$$

This can be proven by carefully calculating the product $P^{-1}P$ (cf. Eq. (7.29)). The weights in Eq. (7.30) are found by multiplying the inverse matrix by the vector of distance probabilities. In Chapter 2 it has been proven that, for a class width approaching zero, the weights in Eq. (7.30) converge to the continuous function $w(a)$ in Eq. (7.12) (the convergence proof for the "plane sheet model soil" applies).

In case of equal distance classes on a linear scale (Eq. (7.24)), the inverse matrix is

$$\begin{cases} P_{ij}^{-1} = \frac{+i^2}{2i-1} & , j = i \\ P_{ij}^{-1} = \frac{-i^2}{2i+1} & , j = i+1 \\ P_{ij}^{-1} = 0 & , j < i \text{ or } j > i+1 \end{cases}$$

Also this can be proven by calculating the product $P^{-1}P$ (cf. Eq. (7.25)).

The convergence proof for the volume fractions in Eq. (7.26) is given for a fixed distance x and for a class width δ approaching zero. At first, the expression for v_i in Eq. (7.26) is rewritten as

$$v_i = \frac{i^2}{4i^2-1}[2i(p_i - p_{i+1}) + (p_i + p_{i+1})]$$

Then, with $i = x/\delta$, the the limit of the volume fraction density v_i/δ is

$$\lim_{\delta \downarrow 0}\left(\frac{v_i}{\delta}\right) = \lim_{\delta \downarrow 0}\left[\frac{i^2}{4i^2-1}\left\{2i\left(\frac{p_i}{\delta} - \frac{p_{i+1}}{\delta}\right) + \frac{(p_i + p_{i+1})}{\delta}\right\}\right] =$$

$$= \frac{1}{4}\left\{-2x\frac{ds(x)}{dx} + 2s(x)\right\}$$

which is equal to the solution for $v(R)$ in Eq. (7.6).

Details of the zero-sink uptake model

The expressions given by Youngs & Gardner (1963) describe zero-sink root behavior when their parameter σ is set at 0 and their parameter K is set at 1. Their equation for the flux at the root surface is then multiplied by $2\pi R_0/\pi R^2$ in order to get the nutrient uptake per unit cylinder volume. That leads to Eq. (7.33) for the uptake rate in which

$$g(A_1,A_2) = \sum_{i=1}^{\infty} \frac{4\, J_1^2(\rho\alpha_i)}{J_0^2(\alpha_i) - J_1^2(\rho\alpha_i)} \exp\left(-\alpha_i^2\rho^2 A_2\right) \qquad (7.A2)$$

with $\rho = \sqrt{1/A_1}$. This equation expresses g as function of its two arguments A_1 and A_2 only (cf. Eq. (7.33)), which simplifies its numerical evaluation. The coefficient α_i is the i-th nonzero root of

$$J_0(\alpha)\, Y_1(\rho\alpha) - Y_0(\alpha)\, J_1(\rho\alpha) = 0$$

The Bessel functions have been calculated with programs from Press *et al.* (1986) and the roots α_i have been found iteratively by bisection.

Note that the first argument A_1 is always the root volume fraction of the soil cylinder for which g has to be evaluated (cf. Eqs. (7.33) and (7.39)). The second argument A_2 is a dimensionless time, based on the cylinder radius R as a length scale.

The function $G(A_1,A_2)$ was introduced in Eq. (7.38) as the integral of $g(A_1,A_2)$ over its second argument. Hence,

$$\begin{aligned} G(A_1,A_2) &= \int_0^{A_2} g(A_1,A_2)\, dA_2 = \\ &= \sum_{i=1}^{\infty} \frac{1}{\alpha_i^2\rho^2} \frac{4\, J_1^2(\rho\alpha_i)}{J_0^2(\alpha_i) - J_1^2(\rho\alpha_i)} \left(1 - \exp\left(-\alpha_i^2\rho^2 A_2\right)\right) \end{aligned} \qquad (7.A3)$$

The weight function for poisson clusters

Diggle (1978) derived the distribution function $F(x)$ of the distance x for Poisson clusters with a cluster density ρ, a cluster radius α and a mean number of points per cluster μ. His expression for $F(x)$ can be written as

$$F(x) = 1 - e^{-E(x)}$$

in which the exponent $E(x)$ is given by

$$\begin{cases} E(x) = \pi\rho \left\{1 - \exp\left(-\dfrac{\mu x^2}{\alpha^2}\right)\right\}(\alpha - x)^2 + 2\pi\rho Q(x)\,, & 0 \le x \le \alpha \\ E(x) = \pi\rho \left\{1 - \exp\left(-\mu\right)\right\}(x - \alpha)^2 + 2\pi\rho Q(x) \quad , & x > \alpha \end{cases}$$

where

$$Q(x) = \int_{|x-\alpha|}^{x+\alpha} \left[1 - \exp\left(-\frac{\mu A(x,\alpha,r)}{\pi\alpha^2}\right)\right] r\,dr$$

and $A(x,\alpha,r)$ is the area of intersection of two circles with radii x and α with their centers a distance r apart. Values of $Q(x)$ have been calculated with Gauss-Legendre integration. Using $y = \pi L x^2 = \pi\rho\mu x^2$, the exponent E and the distribution function F can be calculated as function of the quadratic distance variable y. Values of the weight function are then found from (cf. Eq. (7.12))

$$w(a) = -y\frac{d\sigma(y)}{dy} = -y\frac{d^2F(y)}{dy^2} =$$

$$= y\,\exp(-E(y))\left\{\left(\frac{dE(y)}{dy}\right)^2 - \frac{d^2E(y)}{dy^2}\right\} \Big/_{y=a}$$

Numerical values of the derivatives of E have been obtained in the elementary way, using values of E with 8 byte precision and a y-interval of 0.005. Fractional zero-sink uptakes have been calculated with Eq. (7.44), using 16 point Gauss-Legendre integration on [0,1] and 12 point Gauss-Laguerre integration on [1,∞] (with actual integration variable $t = \sqrt{2a} - \sqrt{2}$ on [0,∞]).

Chapter 8

Worm burrows in a homogeneous clay soil

Abstract. A sulfide containing, black clay soil has become partly oxic due to the presence of worm burrows from which oxygen has entered the soil. The oxidized soil has a light color. The pattern formed by the worm burrows and the light and dark soil has been recorded by making photographs of horizontal cross sections. The photographs are analyzed with the help of a simple oxidation model made for randomly positioned burrows and accounting for the observed anisotropy of the burrow system. Assuming a constant distance over which oxygen has entered the soil, predictions can be made about the pattern of oxidized soil visible at a cross-sectional surface. These model results are compared with the photographs made in the field. The assumption of a fixed penetration distance does not explain fully the observed patterns. Other factors, such as differences in burrow size and burrow age play a role. This has not been studied further.

INTRODUCTION

A clay soil has been studied in which worm burrows occur, which have a profound influence on the soil aeration. Far from the burrows the soil contains sulfide and is black. Close to the burrows the sulfide has oxidized and the soil has a much lighter color. Except the worm burrows, the soil does not show any structure on a relevant scale and is assumed to be homogeneous. The aim of this chapter is to compare, in this relatively simple situation, observed patterns of oxidized soil with results of an aeration model. Observations have been made by analyzing digitized photographs of horizontal cross sections.

Oxygen diffusion and sulfide oxidation have not been studied in detail, however, and the oxidation model applied is a purely geometrical one. It is simply assumed that the sulfide has oxidized up to a certain distance from the worm burrows. From this assumption, properties of a cross section can be derived. These properties are compared with real cross sections in order to test the assumption of a fixed penetration distance.

Table 8.1. Description of symbols used in the text. The subscripts "v" and "s" stand for "volume" and "surface" properties, respectively.

symbol	description	units	Equation
d	entry distance for oxygen	m	(8.7)
$\mathbf{d}$	distance vector of unit length	m	(8.9)
$\mathbf{e}_{1,2}$	basis vectors of plane perpendicular to $\mathbf{d}$	m	(8.10)
F	distribution function	-	(8.8)
$\mathbf{h}$	position vector	m	(8.11)
$\mathbf{h}'$	intersection of line with plane $z = 0$	m	(8.12)
L_s	burrow density in intersecting plane	m^{-2}	
L_v	burrow length density in clod	m^{-2}	
p_s	probability density of θ in intersection	-	(8.1)
p_v	probability density of θ in clod	-	(8.2)
θ	polar angle	rad	
r_i	random number, uniform in [0,1]	-	
R	radius of sphere containing model system	m	
s_s	distance p.d.f. for intersecting plane	m^{-1}	
s_v	distance p.d.f. for clod	m^{-1}	
$\mathbf{t}$	testpoint in intersecting plane	m	
x_s	distance to nearest burrow intersection	m	
x_s^*	dimensionless value of x_s	m	
x_v	spatial distance to nearest burrow	m	
x_v'	distance to intersection of nearest burrow	m	
x_v^*	dimensionless value of x_v	m	
z	vertical coordinate	m	

At first a general description of the clay soil is given. Then, for a three-dimensional model of the burrow system, relations between volume and surface properties are derived. Finally, digitized photographs of a few cross sections are analysed and compared with the model results. Table 8.1 gives a list of symbols used in this chapter.

DESCRIPTION OF THE SOIL

The soil studied is situated on the island Schiermonnikoog in the Dutch part of the Wadden Sea. Between the dike along the southern part of the island and the tidal flats lies a strip of salt marsh. On this salt marsh small depressions occur with a typical size of 20 × 40 meter. They are a few years old and have been created as about one meter deep clay excavations during a recent dike

reconstruction. During periods of inundation a new layer of clay has been deposited on the bottom. The clay is black, due to the sulfide formed under anoxic conditions.

In spring and summer prolonged periods of drought occur. Water evaporates from the excavations, the clay soil becomes dry and about 20 cm deep cracks have developed. The cracks form the pattern which is characteristic for a cracked clay soil. In autumn and winter the evaporation is lower and the depressions are usually inundated. The water probably has a strongly varying salinity and comes in during storm tides and rainfall.

The soil in the depressions is bare. No pioneer plants in the region have been able to withstand the harsh conditions. The only larger organism present is the ragworm *Nereis diversicolor* living in burrows inside the clay prisms. These worms are able to survive dry periods by hiding up to 30 cm below the surface where the soil remains wet throughout the year.

A horizontal cross section of a clay prism shows a number of worm burrows (Fig. 8.1). Around the burrows there are lighter zones. Apparently, oxygen has

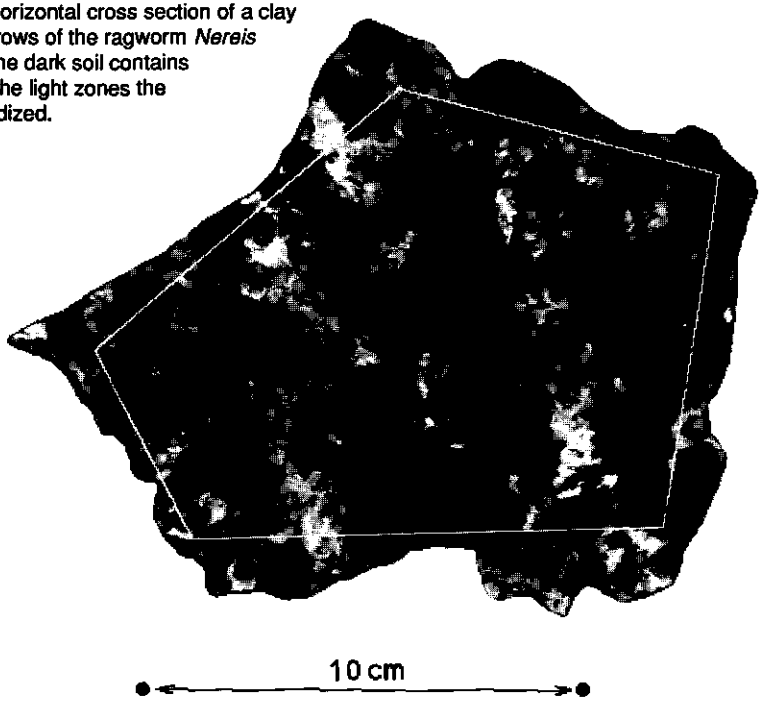

Figure 8.1. Horizontal cross section of a clay prism with burrows of the ragworm *Nereis diversicolor*. The dark soil contains sulfide and in the light zones the sulfide has oxidized.

entered the soil from the worm burrows, leading to the oxidation of sulfide and the local disappearance of the black color.

A GEOMETRICAL MODEL

If the statistical distribution of the distance from a random point of the soil to the nearest burrow axis is known, a model system can be derived with the method developed in the Chapters 2 and 7. Such a model system consists of soil cylinders with different diameters, each with a worm burrow along its axis. A model of oxygen transport and sulfide oxidation can be applied to these cylinders.

In the plane of a cross section no three-dimensional distances can be measured, however. Figure 8.2 shows a schematic drawing of the situation. To a certain point of a cross section belongs a spatial distance x_v to the nearest burrow. In the cross-sectional plane two more distances can be distinguished. The first is the distance x_v' to the intersection of the nearest burrow. This distance is related to x_v and the burrow orientation. The second distance is x_s, the distance to the nearest burrow intersection, which is not necessarily the intersection of the nearest burrow! Hence, the distances x_v' and x_s need not to be equal and their distributions will differ.

If the worm burrows have a random position in the soil, a simple relation exists between the distribution of x_s, which can be easily measured, and the distribution of x_v, upon which a cylinder model system can be based. Hence, in case of a random burrow position, a model system can be derived from distance

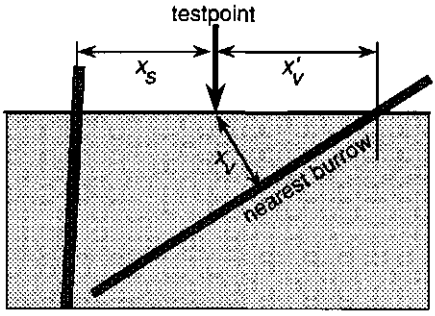

Figure 8.2. A test point in an intersecting plane has a spatial distance x_v to the nearest worm burrow, a surface distance x_v' to the intersection of the nearest burrow and a surface distance x_s to the nearest burrow intersection.

measurements in a cross section.

When an oxidation model is applied to a model system, the result is a probability on anaerobiosis as function of x_V. After assigning orientations to the cylinders, the model system can also be intersected (cf. Chapter 3). That results in a probability on anaerobiosis as function of the distance x_V' from a point to the intersection of the nearest burrow. In a real cross section of the soil, however, properties can be measured only as function of x_S, the distance to the nearest burrow intersection. Unfortunately, distances x_S do not exist in the model system, because the model system consists of separate cylinders. The worm burrows in the different cylinders have no position relative to each other.

In short, a model system can be used to apply oxidation models to the burrow system. It cannot be used, however, to predict surface properties measured as function of the distance x_S. In this paper, for a very simple oxidation model, surface pattens are calculated with a more detailed model of the system structure. Before describing these calculations, the burrow length density of the system is related to the cross-sectional density.

Volume and surface densities

The orientation of a straight worm burrow can be described with a polar angle θ and an azimuthal angle φ. The polar angle is measured relative to a vertical axis. The system is assumed to possess azimuthal symmetry, which means that all values of φ between 0 and 2π are equally abundant. An important property is the burrow length L_V per unit soil volume. The corresponding property of a horizontal cross section is L_S, the number of intersected burrows per unit surface area. When all burrows are parallel and perpendicular to the intersecting plane, L_S is equal to L_V. In general, however, L_S and L_V have different values and their relation depends on the distribution of the polar angle θ.

The burrow length (per unit volume) with a polar angle θ in the interval $[\theta, \theta+\mathrm{d}\theta]$ is $L_V\, p_V(\theta)\,\mathrm{d}\theta$. Here $p_V(\theta)$ is a probability density function describing the relative abundance of the different angles θ. An analogous function $p_S(\theta)$ is defined for a cross section. It describes the orientation of intersected burrows. The relation between $p_V(\theta)$ and $p_S(\theta)$ is

$$L_S\, p_S(\theta) = L_V\, p_V(\theta) \cos\theta \tag{8.1}$$

This equation expresses that the (relative) presence of burrows in an intersecting plane decreases with $\cos\theta$. The reason is that burrows with a large angle θ are rarely intersected by a horizontal plane.

From Eq. (8.1) practical relations are derived. Values of $p_V(\theta)$ can be found from the distribution of angles θ measured at the surface by using

$$p_V(\theta) = \frac{1}{(L_V/L_S)} \frac{p_S(\theta)}{\cos\theta} \tag{8.2}$$

Before Eq. (8.2) can be used, the ratio L_V/L_S needs to be found. As the integral of Eq. (8.2) should be equal to unity, is

$$\frac{L_V}{L_S} = \int_0^{\pi/2} \frac{p_S(\theta)}{\cos\theta} \mathrm{d}\theta \tag{8.3}$$

Using Eqs. (8.2) and (8.3) volume properties can be calculated from a measured surface density L_S and from angles measured at the surface of an intersecting plane.

For an isotropic system all orientations are equally probable. The ratio L_V/L_S is 2 and the probability density functions for the angle θ become

$$p_S(\theta) = 2 \sin\theta \cos\theta \tag{8.4a}$$

$$p_V(\theta) = \sin\theta \tag{8.4b}$$

For these functions Eqs. (8.2) and (8.3) are readily verified.

Distance probability density functions

The distance x_V is the distance from a point to the nearest central axis of a worm burrow. The function $s_V(x_V)$ is the distance probability density of x_V. It describes the volume fractions soil at different distances from the burrow system and can be used to describe the structure of the burrow system in diffusion models (cf. Chapter 7). For test points in a cross section, however, only distances x_S to the nearest burrow intersection can be measured. When the burrows are not vertical, the measured distances will be too large. It is important therefore to know how the probability density function $s_S(x_S)$, which can be measured in a plane, is related to $s_V(x_V)$.

If the burrow system consists of long straight burrows with a random position, the relation between $s_S(x_S)$ and $s_V(x_V)$ is very simple. The functions have exactly the same form:

$$s_V(x_V) = 2\pi L_V x_V \mathrm{e}^{-\pi L_V x_V^2} \tag{8.5}$$

$$s_S(x_S) = 2\pi L_S x_S \mathrm{e}^{-\pi L_S x_S^2} \tag{8.6}$$

The distance probability density function $s_V(x_V)$ depends on L_V only. The value of L_V can be determined, for instance, from a measured value of L_S and the ratio L_V/L_S derived from measured polar angles with Eq. (8.3). The randomness of the burrow spacing can be verified by comparing a measured function $s_S(x_S)$ with Eq. (8.6).

Equation (8.5) was derived by Ogston (1958) for an isotropic system. In fact, he derived an expression for rods with a finite length. Here, (infinitely) long lines are considered and Ogston's expression has been simplified. As mentioned also by Barley (1970), Ogston's result remains valid for an anisotropic angular distribution. Hence, Eq. (8.5) in combination with a function $p_V(\theta)$ forms a complete description of a system of randomly located, long burrows.

From the function $s_V(x_V)$ a model system can be derived. If the presence or absence of sulfide depends on the distance x_V only, no model system is required, however. The function $s_V(x_V)$ directly leads to the light and dark fractions of the soil volume. Writing the threshold distance as d, the sulfide containing volume fraction is

$$v_{dark} = \int_d^\infty s_V(x)\,dx \tag{8.7}$$

Generation of a spatial model system

As explained already above, the nearest burrow intersection is not necessarily the intersection of the nearest burrow. This implies that the intersection of a cylinder representation of the soil does not lead to surface properties as function of the measurable distance x_S.

In the special case of random burrow locations and an oxidation model represented by Eq. (8.7), surface properties can be calculated by generating on a computer a system of randomly located lines, intersecting the system, and calculating the probability of anaerobiosis as function of the distance x_S. As the generation procedure is not entirely trivial it is described here in detail.

The system of lines is generated within a sphere with radius R and with its centre at the origin. Each line is specified by a position and an orientation. The orientation is given as a vector **d** of unit length, pointing in some direction. A direction vector **d** is determined by two angles, a polar angle θ and an azimuth angle φ. The position vector **h** points to an arbitrary point of the line. Once the line direction is known, there are only two degrees of freedom left for its position in space. A vector **d** and a vector **h** can therefore be generated from four random numbers. The generation of pairs (**h**,**d**) can be continued until a required number of lines or a required density is reached.

The used random numbers should be uniformly distributed in the interval [0,1] and may be calculated by means of a pseudo random number generator (e.g. Bratley *et al.*, 1983). The four numbers required for a single pair (**h**,**d**) are written as r_1, r_2, r_3 and r_4.

If there is azimuthal symmetry, a value for the azimuth angle φ is found from the first random number in a trivial way:

$$\varphi = 2\pi r_1$$

In case of isotropy, the probability density of the polar angle θ is given above by Eq. (8.4b). A value of θ distributed according to that function is calculated with help of the cumulative distribution function $F(\theta)$ which is

$$F(\theta) \equiv \int_0^\theta p_V(\theta)\, d\theta = \int_0^\theta \sin\theta\, d\theta = 1 - \cos\theta \tag{8.8}$$

A value of θ is found then by inversion (Bratley *et al.*, 1983) which results in

$$\theta = F^{-1}(r_2) = \arccos(1 - r_2)$$

In case of anisotropy, a value of θ should be generated which is distributed according to any other function $p_V(\theta)$, for instance by using a series of measured probabilities. After generating the angles φ and θ, the direction vector **d** in cartesian coordinates becomes

$$\mathbf{d} = \begin{pmatrix} \sin\theta\, \cos\varphi \\ \sin\theta\, \sin\varphi \\ \cos\theta \end{pmatrix} \tag{8.9}$$

The positioning procedure should guarantee that lines with different orientations are distributed over the sphere in the same way. A position vector **h** is randomly chosen in a square perpendicular to the generated direction **d**. The area of that square is R^2, independently of **d**. Hence, the density resulting from N lines with a certain orientation will be equal to the density resulting from N lines with another orientation.

The plane through the origin and perpendicular to **d** has an orthonormal basis formed by the two vectors $\mathbf{e}_1$ and $\mathbf{e}_2$ given by:

$$\mathbf{e}_1 = \begin{pmatrix} \cos\varphi\, \cos\theta \\ \sin\varphi\, \cos\theta \\ -\sin\theta \end{pmatrix}, \quad \mathbf{e}_2 = \begin{pmatrix} -\sin\varphi \\ \cos\varphi \\ 0 \end{pmatrix} \tag{8.10}$$

The third and fourth random number are now used to get two coordinates of **h** with respect to this basis. The coordinates both lie in the interval $[-R,+R]$. **h** is formed then as a linear combination of $\mathbf{e}_1$ and $\mathbf{e}_2$ according to

$$\mathbf{h} = (1 - 2r_3)R\mathbf{e}_1 + (1 - 2r_4)R\mathbf{e}_2 \tag{8.11}$$

The position vector **h** may be rejected when it is not inside the sphere. In that case new numbers r_3 and r_4 have to be generated. Rejection is not necessary, however. The intersection of a generated line with the "horizontal" plane $z = 0$ is written as the vector **h'**. When **h'** exists it is found as

$$\mathbf{h}' = \mathbf{h} + \{(1 - 2r_3)R \tan\theta\}\,\mathbf{d} \tag{8.12}$$

The calculation of the spatial distance from a test point **t** to the line given by (**d**,**h**)

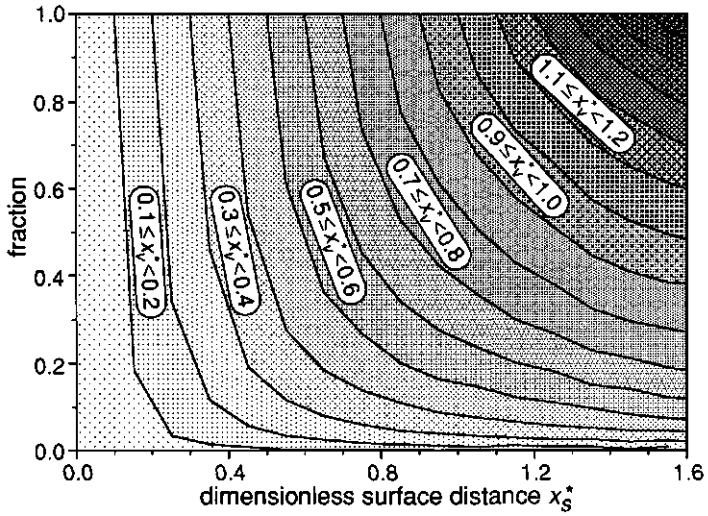

Figure 8.3. Test points with a certain dimensionless surface distance x_S^* ($= x_S\sqrt{\pi L_S}$, horizontal axis) lie at different spatial distances x_V^* ($= x_V\sqrt{\pi L_S}$) from the nearest burrow. Calculations have been made for an isotropic system randomly positioned straight lines.

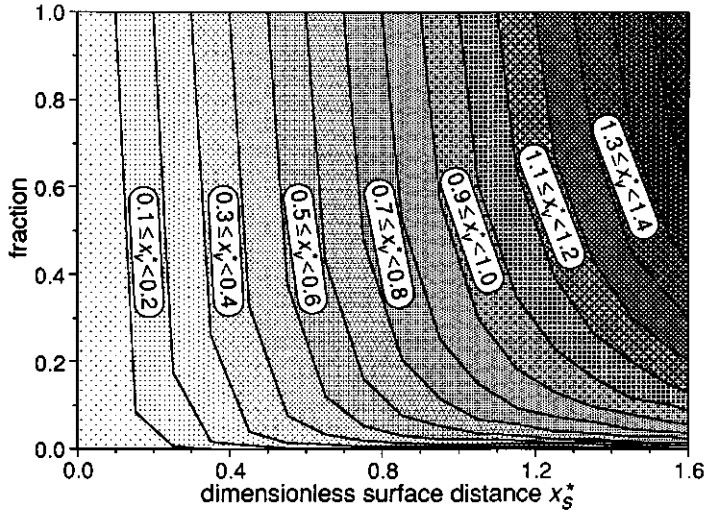

Figure 8.4. The same graph as Fig. 8.3, now based on the measured distribution of the polar angle θ (see Fig. 8.5). The preference for a vertical burrow orientation leads to a better correspondence between spatial and surface distances than in Fig. 8.3.

is simplified by the use of vector cross products. When the angle between two vectors **a** and **b** is α, the length of the cross product $\mathbf{a}\times\mathbf{b}$ is (e.g. Lang,1970)

$$\|\mathbf{a}\times\mathbf{b}\| = \|\mathbf{a}\|\,\|\mathbf{b}\|\,|\sin\alpha|$$

Using this property of vector cross products and $\|\mathbf{d}\|=1$, the distance from a line to a test point **t** becomes $\|(\mathbf{t}-\mathbf{h})\times\mathbf{d}\|$. If the test point lies in the plane $z=0$, the distance to a line intersection **h'** becomes $\|\mathbf{t}-\mathbf{h}'\|$.

After generating N vector pairs $(\mathbf{d}_i,\mathbf{h}_i)$ with $i=1\cdots N$, test points **t** are chosen in the plane $z=0$. The distance x_v from a test point **t** to the nearest line is

$$x_v = \min_i \|(\mathbf{t}-\mathbf{h}_i)\times\mathbf{d}_i\|$$

and the distance from the same test point to the nearest line intersection is found by calculating for all lines the intersection points **h'**. Then,

$$x_s = \min_i \|\mathbf{t}-\mathbf{h}'_i\|$$

Surface patterns

With the method described above, an isotropic system has been generated and a grid of test points has been chosen in the intersecting plane $z=0$. Figure 8.3 shows, as a function of x_s, the fractions of points with a distance x_v in a number of intervals. The distances have been made dimensionless according to

$$x_s^* = x_s\sqrt{\pi L_s}$$

$$x_v^* = x_v\sqrt{\pi L_s}$$

Note that the surface density L_s has been used to scale both the surface and the spatial distances. The graph demonstrates that, especially for a large surface distance, very different spatial distances occur.

Figure 8.4 has been calculated for the measured distribution of the polar angle θ, which expresses a preference for vertical burrows (see Fig. 8.5 below). The correspondence between surface and spatial distances is better than in Fig. 8.3. In case of vertical burrows the spatial distances would exactly correspond to surface distances and all curves would be vertical between 0 and 1.

EXPERIMENTS

Cross sections of clay prisms were made at a depth of about 6 cm using a steel wire with a diameter of 0.2 mm. The black and white photographs taken of

the surfaces have been digitized by a video camera. A digitized picture is a file consisting of 262,144 grey values organized as 512 lines of 512 pixels. Each grey value is a number between 0 and 255 (one byte). The sulfide containing, black parts of the surface appear in the file as pixels with a low grey value. Also the worm burrows themselves are dark spots. Some noise was removed from the image by applying a 5×5 median filter (Methir, 1975). No algorithm was developed for finding the positions of the worm burrows automatically. Instead, the positions of the burrows have been determined by hand using a plot of the digitized picture. Two black dots at a distance of 10 cm provide a reference length on all photographs.

The orientation of a worm burrow could be determined in the field by putting in a thin stick and measuring the angle between the stick and the (horizontal) cross-sectional surface. The result is easily converted to the angle θ between the burrow direction and a vertical line.

With help of the image files and burrow positions the relation between the 'color' of test points and their distance x_s to the nearest burrow intersection can be quantified. The burrow orientations are used to find spatial properties of the system from measured surface properties.

Orientation and distribution of burrows

482 measured angles were classified using 9 angle classes of equal width. For each class a probability $p_{i,s}$ has been calculated as the fraction of angles in that class ($i=1\cdots9$). Figure 8.5 shows the result as a histogram of probability densities (probabilities divided by the constant class width). The curve in Fig. 8.5 is a graph of the function $p_s(\theta)$ for an isotropic system (Eq. 8.4a). The difference between the histogram and the curve reflects the preference of the worms for vertical burrows.

From the surface probabilities $p_{i,s}$ the ratio L_v/L_s can be estimated as (cf. Eq. (8.3))

$$\frac{L_v}{L_s} = \sum_{i=1}^{9} \frac{p_{i,s}}{\cos\theta_i}$$

The midpoints of the classes have been used as angles θ_i. The result is a ratio 1.3 ± 0.1. This value is sensitive to the occurrence of angles close to 90^0 and the given inaccuracy of 0.1 is an estimate. Using this ratio L_v/L_s volume probabilities $p_{i,v}$ can be found from (cf. Eq. (8.2))

$$p_{i,v}(\theta) = \frac{1}{(L_v/L_s)} \frac{p_{i,s}(\theta)}{\cos\theta_i}$$

These probabilities have to be used to generate the above described spatial

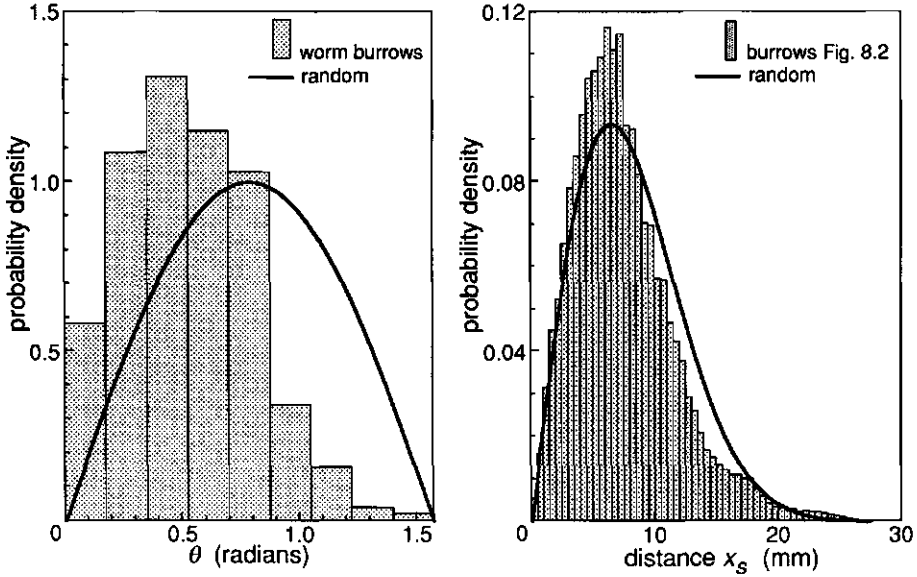

Figure 8.5. (left) Frequency distribution of the polar angle θ between a vertical line and a worm burrow appearing at an intersecting plane. The curve describes an isotropic system (Eq. (8.4a)). The histogram is based on 482 measured angles and reflects the preference of the worms for a vertical burrow orientation.

Figure 8.6. (right) The distribution of the surface distance x_S between a test point and the nearest burrow intersection. The histogram gives probability densities, measured for test points in the polygonal test area drawn in Fig. 8.1. The curve describes a random burrow position (Eq. (8.6) with $L_S = 0.38\ cm^{-2}$).

model of the burrow system.

A polygon drawn in the digitized image in Fig. 8.1 gives the area in which test points have been chosen. The burrow density L_S in the test area is $0.38\ cm^{-2}$. Using the average value for L_V/L_S above the estimated volume density L_V becomes $0.50\ cm^{-2}$.

Using the positions of the worm burrows, distance probabilities have been calculated by determining for each pixel in the test area the distance to the nearest burrow centre. The histogram in Fig. 8.6 shows the result. The curve refers to random burrow positions (Eq. (8.6) with $L_S = 0.38\ cm^{-2}$). The difference in shape between the histogram and the curve reflects a tendency towards a regular distribution of burrows. The statistical significance of this tendency has not been verified, but the same result has been found in other photographs. The deviation from random burrow positions has been neglected in the analysis of the oxidation pattern.

Sulfide oxidation

At first a criterion has to be found for classifying pixels of the image as either "dark"or "light" (oxidized). For the image in Fig. 8.1 the criterion is derived from the histogram of grey value frequencies in Fig. 8.7. The histogram shows a clear peak for low grey values. That peak represents the dark, sulfide containing parts of the surface. The grey value 75 at the right edge of the peak is chosen as the threshold value. Pixels with a smaller grey value are classified as dark and pixels with a larger grey value are classified as light.

Calculating the distances x_s for the pixels in the test area, also the dark or light nature of the pixels has been scored. That results in a fraction of light pixels as function of the distance x_s. Figure 8.8a shows a graph of the result. Many points with a distance below 2.5 mm are dark, simply because they are part of a worm burrow. Burrows with a radius above 2.5 mm are rare (the burrow radius measured in the field is 1.5 ± 0.3 mm) and from that distance on, the fraction of light, oxidized soil decreases and the fraction of dark, sulfide containing soil increases.

By combining the results of Figs. 8.6 and 8.8a, the light surface fraction can be calculated. It appears to be 47%. The surface fraction occupied by the burrows is about 2.5%, leading to a total oxic surface fraction of 50%. Since, for large samples, surface fractions are equal to volume fractions the estimated oxic volume fraction amounts also 50%.

This last number can be used to calculate a theoretical curve based on the assumption of a certain threshold distance above which all pixels are dark. For

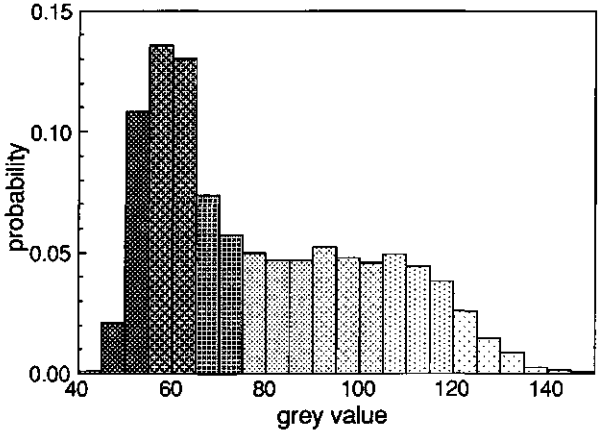

Figure 8.7. The grey value distribution of the pixels in the polygonal test area drawn in Fig. 8.1. The distinction between dark, sulfide containing soil and oxidized soil lies at a grey value of about 75.

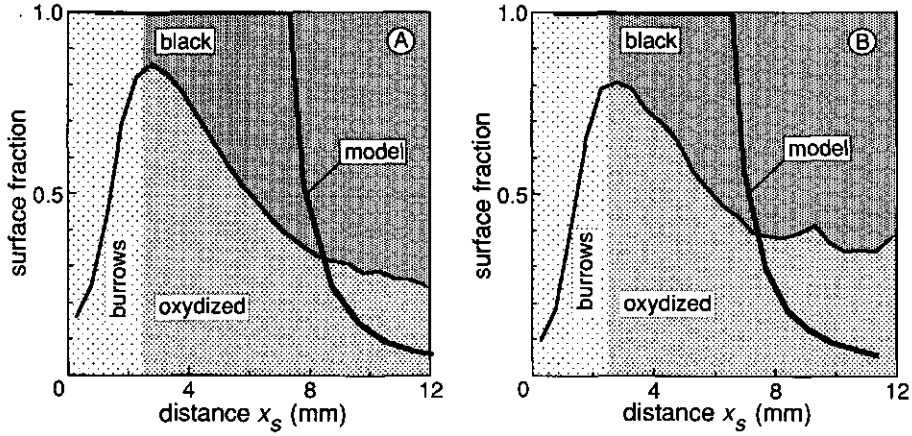

Figure 8.8. Test points at a distance x_s from the nearest burrow intersection have been classified as either dark or light (oxidized). Many pixels at distances below 2.5 mm are part of the (dark) burrows themselves. Above 2.5 mm, the fraction oxidized soil decreases with distance. The fat, steeply decreasing curve is the model result for randomly positioned straight lines (Fig. 8.4). (A) Result for the clod in Fig. 8.1 ; (B) The same a photograph of another clod.

an oxic volume fraction of 0.50, Eq. (8.6) leads to a threshold distance of 7.6 mm corresponding to a dimensionless distance of 0.83 according to Eq. (8.10). For a dimensionless distance of 0.8 a curve is available in Fig. 8.4, which has been adapted to the millimeter scale of Fig. 8.8a. Comparison of the theoretical and experimental curves in Fig. 8.8a shows that the rather slow decrease of the light fraction with distance cannot be explained from the fact that the burrows are not vertical. Accounting for the orientation of the burrows alone, a more steep decrease of the light fraction would be expected. Figure 8.8b shows a similar result derived for the cross section of another clay prism.

DISCUSSION

It is not difficult to list possible causes for the difference between the experimental and theoretical curves in Fig 8.8. When several worm burrows lie close together the entry distance for oxygen will be larger than for a single isolated burrow. The distinction between light and dark zones will not coincide then with a single threshold distance. This physical effect is observable in the field and is not accounted for in a model based on distances alone. The effect is probably small, however, a few tens of percents.

Other reasons all imply soil heterogeneity. The worm burrows have different diameters and may have different ages. Further, the physical properties of the soil matrix may be less constant than it looks like, especially under dry circumstances.

It is concluded that a fixed entry distance for oxygen leads only to a rough characterization of the system. This conclusion has been reached by comparing model results directly with field measurements. Improvement of the oxidation model requires more insight in the oxygen diffusion and sulfide oxidation.

Summary

Soil structure leads to a large spatial variability in conditions determining biological, chemical and physical processes taking place in the soil. In air-filled macropores close to the surface, for instance, usually plenty of oxygen is available. Inside a soil aggregate, however, the local oxygen demand may exceed the maximum possible flux. At such places the oxygen concentration drops to zero and anaerobic microorganisms become active. Some of these organisms are able to use nitrate as a source of oxygen, which leads to loss of fertilizer in agricultural soils.

Various models exist that describe oxygen diffusion, soil respiration, or even denitrification for a homogeneous soil aggregate with a spherical or cylindrical shape. It is not clear, however, how these processes have to be described for a structured soil. This thesis attempts to solve this problem. A theoretical method has been developed for the application of process models to an aggregated soil. Some experimental work has been done on oxygen diffusion and anaerobiosis in a cracked clayey soil. Finally, the developed theoretical method has been used to solve the problem of nutrient uptake by roots with a non-regular distribution.

Length scales in aggregated soil

Soil aggregates have complicated and different shapes; they occur in different sizes, and there are no two equal places in a soil. This means that different length scales are present in the soil structure. It appears that these length scales largely determine the result of a diffusion process and that aggregate shape is of minor importance. A diffusion model for a soil can thus be based on just the length scales occurring in the soil. This is done by solving the equations describing the diffusion proces for a simple model system consisting of either spheres, cylinders, or plane sheets with different radii (the radius of a plane sheet is half its thickness). The radii represent the various length scales occurring in the soil structure and the abundance of each scale (or radius) is expressed as a weight. It should be emphasized that the spheres, cylinders or plane sheets do not represent individual soil aggregates. The model system is not a geometrical simplification of the actual soil structure, but forms an abstract representation of the length scales in the soil structure. Technically, the weight belonging to a certain radius or length scale is equal to the volume fraction of the model system which is occupied by the spheres, cylinders or sheets with a certain radius.

Clearly, the abundance of a certain length scale cannot be measure directly.

The relevant lengths are closely related, however, to a distance distribution, which can be measured. For each point of the soil there is the distance to the nearest part of the inter-aggregate space, the distance to the nearest crack, for instance. The statistical distribution of this distance is used to characterize the soil structure. The real soil structure and the model system have identical distance distributions. This implies that the length scales on which diffusion takes place in the two systems are the same and that the process in the model system can thus be used as an approximate description of the process in the soil. For a certain soil structure different model systems can be derived, consisting either of spheres, cylinders or plane sheets. It has been verified that diffusion processes in the three model systems take place in approximately the same way. This demonstrates the shape-independence of diffusion processes. The (unknown) results for a real system with the same distance distribution as the three model systems, are likely to be somewhere between the results for the model systems.

The weights belonging to the radii of a model system are thus derived by requiring that the model system has the same distance distribution as the soil. When a certain radius (or length scale) does not occur in the soil, it has a zero weight. The equality of the distance distributions of the model system and the soil structure can be expressed mathematically as an equation with unknown weights. The weights are then found by solving this equation. In case of measured distances one may calculate "distance probabilities" as the fraction of the measured distances falling in a series of distinct distance classes. The equation for the weights of a model system then takes the form of N linear equations with N unknown weights. In theoretical calculations one may use continuous distance distributions, which lead to continuous weight functions.

Once the weights of a model system are found, the application of a diffusion model is straightforward. Depending on the type of model system, the equations of the applied diffusion model are solved for a spherical, a cylindrical or a plane geometry. The overall result for the soil is then found as the weighted sum of the results for the various radii in the model system.

The distances used to characterize a soil structure are distances in three-dimensional space. In practice, distances are more easily measured in the plane of a cross section of the soil. This plane shows cross sections of soil aggregates, together with parts of the inter-aggregate space, cracks or macropores. Then, for a large number of test points the distance to the nearest part of the inter-aggregate space is measured. These distances, however, are not equal to the true spatial distances belonging to the test points. For an isotropic soil structure, however, a model system consisting of cylinders can be obtained from the two-dimensional distances as well. As a start, the yet unknown model system is also made isotropic by assigning a random orientation to the cylinders. Then, instead of conserving the true distance distribution of the soil, the distribution as

observed in an intersecting plane can be conserved. In case of anisotropic systems this will not work and distances need to be measured in three dimensions.

Although the differences between the three types of model systems are small, the use of a cylinder system has a few advantages. The cylindrical shape represents a compromise between the shape of spheres and of plane sheets. Results of a diffusion process in a cylinder model system are always between the results for a sphere system and for a plane sheet system. Furthermore, the use of discrete distance intervals leads to a mathematical problem in deriving a sphere model system from measured distances. This problem is much smaller for a cylinder system and absent for plane sheets. Plane sheets, however, cannot be derived from cross-sectional distances, whereas an isotropic system of cylinders can be derived from a cross section of an isotropic soil.

When a soil sample consists of a small number of soil aggregates only, the measured distance distribution will not be representative for the soil. This leads to errors in the weights of the model system and, finally, in the result of a diffusion model. For a model of oxygen diffusion, this effect has been investigated by simulating the whole process of sampling, deriving a model soil and calculating an anoxic fraction. It appears that especially the prediction of small anoxic fractions requires accurate geometrical data (large sample sizes). As long as the soil structure is isotropic, there is hardly a difference between the results obtained with two-dimensional distances measured in a cross section, and the results for true three-dimensional distances. The loss of information by cross sectioning is negligible. This means that distance measurements in three dimensions, although necessary in case of anisotropy, do not solve problems related to a too small sample size.

Oxygen diffusion

The diffusion coefficient used in a diffusion model for a soil aggregate needs to be a coefficient for diffusion on the aggregate scale and not a coefficient measured on the scale of a vertical profile. With an oxygen electrode, the diffusivity of oxygen can be measured on a millimeter scale. The gas above a core sample is periodically changed from nitrogen to air and back. This leads to a concentration wave, which is measured as function of electrode depth, the distance from the electrode tip to the sample surface. The phase of the signal at a certain depth is shifted relative to the applied surface wave. This phase shift increases linearly with depth and the amplitude of the signal decreases exponentially with depth. For different Fourier components in the electrode signal, phase shifts are calculated. The diffusivity then follows from the increase in the phase shift per millimeter electrode depth. It is shown theoretically that the

phase shift is more suitable than signal amplitude for the derivation of a diffusivity. Moreover, phase shifts are easier to measure. The electrode does not require calibration, for instance, and signal drift is not a problem.

The oxygen diffusivity was measured for the clayey soil also used in the later field work. The air-filled porosity of the soil was about 5% and the diffusivity was 0.9×10^{-9} $m^2 s^{-1}$. This measured diffusivity is extremely low and corresponds with diffusion in water-saturated soil. This can be explained by the existence of small water-saturated zones in the clay soil. The diffusion coefficient for these zones is more than 100 times smaller than the macroscopic diffusion coefficients measured for whole core samples of the same soil. This demonstrates the large difference in soil properties on different size scales. The presence of water-saturated zones, with a size of several millimeters in an otherwise unsaturated soil, is relevant in describing gas transport and anaerobiosis.

Due to mechanical problems with the oxygen electrodes, the diffusivity on a centimeter scale could not be measured. On that scale, air-filled pores play a role in the transport, and the diffusion coefficient will be larger than in small saturated zones.

Another aspect of oxygen diffusion in a soil aggregate is studied theoretically. In case of uniform and zero-order soil respiration, the centre of an aggregate will become anoxic if the oxygen demand of the aggregate exceeds the maximum transport. Models exist which describe the steady-state of this process. The anoxic fraction is larger for a larger soil respiration, for a lower diffusion coefficient, and for a lower oxygen concentration at the surface. The anoxic zone is always located in the centre of the aggregate. Hence, when aggregates with different sizes or even different respiration rates occur in the soil, the probability of finding anoxic soil will increase with the distance from the aggregate surface.

This is not true for non-uniform soil aggregates. Local micro-biological activity in the soil may lead to small anoxic zones everywhere in an aggregate. In addition, a large local activity is consistent with a moderate overall respiration rate. The reason is that inactive soil may act as a barrier for oxygen transport between the surface and the active soil leading to a much lower oxygen flux than in case of soil activity at the aggregate surface. Since the total oxygen flow is equal to the overall soil respiration, also the respiration of a non-uniform aggregate is relatively low. The active zones stay largely anoxic and aerobic activity only takes place in the thin outer layers of the active zones.

For a plane geometry, a model of non-uniform activity can be kept simple. The overall respiration is calculated for a randomly located active zone. If a small portion of the soil is active, say 10%, the soil respiration may be several orders of magnitude smaller than the potential respiration of the active zone. Under these circumstances, the distribution of the anoxic soil almost coincides with the distribution of soil activity. There is not necessarily a relation between the

probability of anaerobiosis and the distance to the aggregate surface. When active soil occurs only near the surface, there will even be an inverse relation: anoxic soil occurs only near the surface and not in the centre.

The measured oxygen diffusivity and the theoretical work on non-uniform activity are combined with the results of field work carried out for a clayey soil. The aeration of this soil is studied by comparing the position of the cracks with the distribution of anoxic soil. Only a weak relation is found between the crack pattern and the distribution of anoxic soil. Locally, anoxic soil occurs even within 1 mm from a crack surface. Assuming that the soil is locally saturated with water, the measured macroscopic soil respiration would still allow a penetration depth of 10 mm. It is therefore concluded that the local activity exceeds the bulk respiration by at least a factor 100. As explained above, a non-uniform activity also explains the absence of a relation between the crack pattern and the distribution of anoxic soil. An important consequence of the presence of anoxic soil close to cracks is that denitrification may take place without diffusion of nitrate towards the inner parts of an aggregate. An anoxic "hot spot" may absorb dissolved nitrate from water passing through it.

The scale method applied to plant roots and worm burrows

The scale method is applied to roots with a non-regular distribution. Again, the actual calculations on (nutrient) diffusion are carried out for a model system instead of the real root system. The model system consists of soil cylinders with different radii, each with a root along its axis. The cylinder radii represent the length scales on which nutrient diffusion takes place in the system and a weight function expresses the relative abundance of each radius or length scale. The cylinders do not represent the soil around individual roots of the real root system. The nutrient uptake by the root system is calculated as a weighted sum of uptakes from the soil cylinders of the model system.

The weight function can be obtained from the statistical distribution of the distance from a point in the soil to the nearest root centre. Equations are given for deriving a continuous weight function from a continuous distance distribution, and for deriving a number of discrete weights from measured distances. The method is worked out for a zero-sink uptake model. Fractional uptakes calculated for random and clustered root distributions agree with electrical analogue data from the literature. In addition to its utility in describing root systems, the method can be applied to worm burrows, networks of blood capillaries, and similar systems.

The subject of the final chapter is the aeration of a homogeneous clay soil with worm burrows. Originally, the marine soil was entirely black due to the presence of sulfide. Around worm burrows the soil became oxidized resulting in a

light color. The pattern formed by the worm burrows and the dark and light soil has been recorded by making photographs of horizontal soil intersections. The photographs are analyzed with the help of a simple oxydation model made for randomly positioned burrows and accounting for the observed anisotropy of the burrow system. Assuming a constant distance over which oxygen has entered the soil, predictions can be made about the pattern of oxidized soil visible at an intersecting plane. These model results are compared with the photographs made in the field. The assumption of a fixed penetration distance does not explain the observed patterns. Other factors, such as differences in burrow diameter and burrow age play a role.

Samenvatting

De struktuur van een bodem leidt tot een grote ruimtelijke variabiliteit in omstandigheden die bepalend zijn voor het verloop van de biologische, chemische en fysische processen in de bodem. Bijvoorbeeld, in de met gas gevulde macroporiën dicht bij het bodemoppervlak zal gewoonlijk voldoende zuurstof aanwezig zijn. Binnen in een bodemaggregaat echter, kan de lokale behoefte aan zuurstof groter zijn dan de maximale aanvoer. Op zulke plaatsen daalt de zuurstofconcentratie naar nul en worden anaerobe micro-organismen aktief. Sommige van deze organismen zijn in staat om nitraat als zuurstofbron te gebruiken. Het nitraat wordt dan omgezet in stikstofoxiden of zelfs in gewoon stikstofgas. Dit proces, denitrifikatie, leidt op akkers en weiland tot het verlies van nitraatmeststof uit de bodem.

Er bestaan verschillende modellen die de zuurstofdiffusie, de bodemrespiratie en soms ook de denitrifikatie beschrijven voor een homogeen bodemaggregaat, dat de vorm heeft van een bol of cylinder. In het geval van een gestruktureerde grond echter, is het niet duidelijk hoe deze processen moeten worden beschreven. In dit proefschrift wordt gepoogd dat probleem op te lossen. Voor het toepassen van procesmodellen op een geaggregeerde bodem is een theoretische methode ontwikkeld. Er is tevens enig experimenteel werk gedaan aan zuurstofdiffusie en anaerobie in een scheurende kleigrond. De ontwikkelde theoretische methode is tenslotte ook gebruikt om de opname van nutrienten te berekenen voor een wortelstelsel met een onregelmatige verdeling van de wortels.

Lengteschalen in geaggregeerde grond

Vorm en grootte van bodemaggregaten zijn zeer variabel en er bestaan geen twee gelijke stukken grond. Dat betekent dat er verschillende lengteschalen in de bodemstruktuur aanwezig zijn. Het blijkt dat deze lengteschalen het resultaat van een diffusieproces grotendeels bepalen en dat de vorm van de aggregaten van weinig betekenis is. Een diffusiemodel voor de hele bodem kan daarom worden gebaseerd op alléén de lengteschalen die in de bodem voorkomen. Daartoe worden de vergelijkingen die het proces beschrijven opgelost voor een eenvoudig modelsysteem. Dat modelsysteem bestaat uit bollen, uit cylinders of uit vlakke platen. met verschillende stralen (de straal van een vlakke plaat is gelijk aan de helft van zijn dikte). De stralen stellen de lengteschalen voor die in het systeem voorkomen en het belang van elke schaal wordt uitgedrukt als een gewichtsfactor. Met nadruk wordt gesteld dat de bollen, cylinders of vlakke platen

niet gezien moeten worden als vereenvoudigde bodemaggreggregaten. Het modelsysteem is geen geometrische vereenvoudiging van de echte bodemstruktuur, maar vormt een meer abstracte voorstelling van de erin aanwezige lengteschalen. Technisch gezien is de gewichtsfactor die bij een bepaalde straal of lengteschaal behoort gelijk aan de volumefractie van het modelsysteem die wordt ingenomen door de bollen, cylinders of platen met die straal.

Het is duidelijk dat de mate waarin een bepaalde lengteschaal voorkomt geen meetbare grootheid is. De lengteschalen in de bodemstructuur zijn echter nauw verwant aan een afstandsverdeling die wèl kan worden gemeten. Voor elk punt van de bodem bestaat de afstand tot het dichtstbijzijnde deel van de ruimte tussen de aggregaten. Dat is bijvoorbeeld de afstand tot de dichtstbijzijnde scheur. De statistische verdeling van die afstand wordt gebruikt als karakteristiek van de bodemstructuur. De afstandsverdeling van de werkelijke bodemstructuur en die van het modelsysteem zijn identiek. Dat impliceert dat de lengteschalen waarop diffusieprocessen in de twee systemen plaats vinden gelijk zijn. Een beschrijving van een proces in het modelsysteem kan dan worden gebruikt als een benadering voor het verloop van hetzelfde proces in de bodem. Voor één bepaalde bodemstruktuur kunnen modelsystemen worden afgeleid die bestaan uit bollen, uit cylinders of uit vlakke platen. Het is nagegaan dat diffusieprocessen in de drie modelsystemen op ongeveer dezelfde wijze verlopen. Dat is het gevolg van het feit dat diffusieprocessen onafhankelijk zijn van de vorm van de objecten waarin ze plaats vinden. De (niet bekende) resultaten voor een bodem met dezelfde afstandsverdeling als de drie modelsystemen, liggen dan vermoedelijk ergens tussen de resultaten voor de modelsystemen in.

De bij een modelsysteem behorende gewichtsfactoren worden dus afgeleid uit de eis dat het modelsysteem dezelfde afstandsverdeling heeft als de bodem. De gelijkheid van de beide afstandsverdelingen kan mathematisch worden uitgedrukt als een vergelijking met onbekende gewichtsfactoren. De gewichtsfactoren worden dan gevonden door die vergelijking op te lossen. Inplaats van een continue afstandsverdeling kan men discrete kansen gebruiken, die horen bij een serie aan elkaar grenzende afstandsintervallen. Voor elk afstandsinterval wordt de bijbehorende kans berekend als de fractie van een groot aantal gemeten afstanden die valt in het betreffende interval. De vergelijking voor de gewichtsfactoren van het modelsysteem neemt in dat geval de vorm aan van N lineaire vergelijkingen met N onbekende gewichtsfactoren. In theoretische berekeningen is het meestal gemakkelijker om met een continue afstandsverdeling te werken. De gewichtsfactoren verschijnen dan als een continue gewichtsfunktie.

Als eenmaal de gewichtsfactoren zijn gevonden, dan is de procedure voor de toepassing van een diffusiemodel eenvoudig. Afhankelijk van het type modelsysteem, worden de vergelijkingen van het diffusiemodel opgelost voor een bol, een cylinder of een vlakke plaat. Het resultaat voor de bodem als geheel wordt

dan berekend als een gewogen som van de resultaten voor de verschillende lengteschalen.

De afstanden waarmee de bodemstruktuur wordt gekarakteriseerd, zijn afstanden in de driedimensionale ruimte. In de praktijk kunnen afstanden eenvoudig worden gemeten in het vlak van een doorsnede. Voor een groot aantal testpunten in het vlak wordt de afstand tot de dichtstbijzijnde scheur of macroporie bepaald. Deze afstanden zijn echter niet gelijk aan de driedimensionale afstanden die bij de testpunten behoren. Als de bodemstructuur isotroop is echter, dan kan uit de gemeten tweedimensionale afstanden een uit cylinders bestaand modelsysteem worden afgeleid. Eerst wordt het nog onbekende modelsysteem ook isotroop gemaakt door aan de cylinders willekeurig gekozen orientaties toe te kennen. Als behouden grootheid wordt dan de afstandsverdeling voor een doorsnede gebruikt in plaats van de afstandsverdeling van de volledige bodemstruktuur. Het is duidelijk dat dit niet zal werken in het geval van een anisotroop systeem. Dàn moeten driedimensionale afstanden worden gemeten.

Hoewel de verschillen tussen de drie typen modelsysteem klein zijn, heeft het gebruik van een cylindersysteem een paar voordelen. De cylindervorm vertegenwoordigt een compromis tussen een bol en een vlakke plaat. Het resultaat van een diffusieproces in een cylindrisch systeem ligt daarom altijd tussen de resultaten voor een bolvormig en een vlak systeem in. Verder leidt het gebruik van discrete afstandsintervallen tot een wiskundig probleem bij het berekenen van gewichtsfactoren voor bollen. Dit probleem is veel kleiner voor cylinders en voor vlakke platen is het afwezig. Vlakke platen, echter, kunnen weer niet worden afgeleid uit een doorsnede, terwijl een cylindersysteem wèl kan worden berekend uit afstanden in de doorsnede van een isotrope grond.

Als een monster uit slechts een klein aantal aggregaten bestaat, dan zal de gemeten afstandsverdeling niet representatief zijn voor de bodem. Dat leidt tot afwijkingen in de gewichtsfactoren van het modelsysteem. Die afwijkingen werken door in het resultaat van een diffusiemodel. Voor een model voor zuurstofdiffusie is dit onderzocht door middel van het simuleren van het hele proces van bemonstering, het bepalen van een afstandsverdeling, en het berekenen van een zuurstofloze fractie. Het blijkt dat het voorspellen van kleine zuurstofloze fracties relatief nauwkeurige geometrische gegevens vereist (grote monsters). Als de bodemstruktuur isotroop is, dan is er nauwelijks verschil tussen de resultaten voor een doorsnede en de resultaten voor een driedimensionaal monster. Het verlies aan informatie tengevolge van het gebruik van een doorsnede is dan verwaarloosbaar. Ofschoon afstandsmetingen in drie dimensies nodig zijn in het geval van anisotropie, vormen ze dus geen oplossing voor een te kleine monstergrootte.

Zuurstofdiffusie

De diffusiecoëfficient in een model voor een bodemaggregaat dient te worden gemeten op de aggregaatschaal en niet op de schaal van een vertikaal bodemprofiel. Met een zuurstofelektrode kan de diffusiviteit van zuurstof op millimeterschaal worden gemeten. De lucht boven een grondmonster wordt periodiek vervangen door stikstofgas. Dat levert aan het oppervlak van de grond een "concentratiegolf" op die zich voortplant in de grond. De periodieke concentratie wordt gemeten als funktie van de diepte van de zuurstofelektrode, waarbij de diepte dan gelijk is aan de afstand tussen de gevoelige top van de electrode en het grondoppervlak. De fase van het signaal verschoven ten opzichte van de golf aan het oppervlak. Deze faseverschuiving neemt lineair met de diepte toe en de amplitude van het periodiek signaal neemt exponentieel af met de diepte. Voor verschillende Fouriercomponenten van het elektrodesignaal wordt de faseverschuiving berekend en de diffusiviteit volgt dan uit de toename van de faseverschuiving per millimeter grond. Theoretisch wordt aangetoond dat de faseverschuiving geschikter is voor het bepalen van de diffusiviteit dan de amplitude van het signaal. Faseverschuivingen zijn bovendien eenvoudiger te meten. De elektrode hoeft bijvoorbeeld niet geijkt te worden en een langzaam verlopend signaal vormt geen probleem.

De diffusiviteit van zuurstof is gemeten voor monsters van dezelfde kleiige bodem, waarvoor later het veldwerk aan anaerobie is uitgevoerd. De met gas gevulde poriën namen ongeveer 5 % van het bodemvolume in en de diffusiviteit bedroeg 0.9×10^{-9} m^2s^{-1}. Deze gemeten diffusiviteit is extreem laag en kan worden verklaard met de aanwezigheid kleine, met water verzadigde gebieden in de grond. In deze gebieden is de diffusiecoëfficient meer dan 100 maal kleiner dan de macroscopische diffusiecoëfficient zoals die gemeten is voor ringmonsters van dezelfde grond. Dit laat zien dat bodemeigenschappen op verschillende schalen sterk van elkaar kunnen verschillen. De aanwezigheid van verzadigde gebieden met een grootte van enkele millimeters is relevant voor het beschrijven van het gastransport en anaerobie.

Als gevolg van mechanische problemen met de zuustofelektroden kon de diffusiviteit op een centimeterschaal helaas niet gemeten worden. Op die schaal spelen de met gas gevulde poriën weer een rol in het transport en de diffusiviteit zal groter zijn dan de lokale diffusiviteit in kleine verzadigde gebieden.

Een ander aspect van zuurstofdiffusie op aggregaatniveau is theoretisch bestudeerd. In het geval van een uniforme en nulde orde bodemrespiratie zal de kern van een bodemaggregaat zuurstofloos worden als de vraag naar zuurstof groter is dan het maximale transport. Er bestaan modellen voor het beschrijven van de stationaire toestand van een respirerend bodemaggregaat. De zuurstofloze fractie is groter bij een grotere aktiviteit in het aggregaat, bij een

kleinere diffusiecoëfficient en bij een lage zuurstofconcentratie aan de rand van het aggregaat. De zuurstofloze zone ligt altijd in het centrum van het aggregaat. Voor een mengsel van aggregaten met verschillende grootten zal de kans dat een willekeurig punt zuurstofloos is toenemen met de afstand van dat punt tot de rand van het aggregaat.

Dat is niet langer het geval als de aktiviteit van een bodemaggregaat niet overal gelijk is. Lokale aktiviteit op een willekeurige plaats in een bodemaggregaat kan leiden tot een zuurstofloos gebied. Een grote lokale aktiviteit blijkt bovendien consistent met een relatief geringe bodemrespiratie. De reden daarvan is dat niet aktieve grond functioneert als een weerstand voor zuurstoftransport tussen het oppervlak en de aktieve grond. Dat leidt tot een veel kleiner zuurstoftransport dan bij gelijke aktiviteit aan het oppervlak. De totale respiratie is dan relatief klein, omdat die nu eenmaal gelijk is aan het totale zuurstoftransport. De aktieve zones blijven dus grotendeels zuurstofloos en aerobe aktiviteit vindt alleen plaats in de dunne lagen aan de buitenkant van die zones.

In het geval van een vlakke geometrie kan een model voor niet uniforme aktiviteit eenvoudig worden gehouden. De respiratie van een vlak bodemaggregaat is berekend voor het geval van één aktieve zone met een willekeurig gekozen positie. Als slechts een klein deel van de grond aktief is, 10 % bijvoorbeeld, dan kan de bodemrespiratie enkele orden van grootte kleiner zijn dan de potentiële respiratie van de aktieve zone. Onder deze omstandigheden valt de verdeling van zuurstofloze grond nagenoeg samen met de verdeling van de aktieve grond in de bodem. Er bestaat dan niet noodzakelijkerwijs een relatie tussen de kans dat een bepaald punt zuurstofloos is en de afstand van dat punt tot het aggregaatoppervlak. Als aktieve grond alléén aan het oppervlak voorkomt, dan zal er zelfs een negatief verband bestaan: alléén aan het oppervlak kan zuurstofloosheid optreden.

De gemeten diffusiviteit en het theoretisch werk aan niet uniforme aktiviteit zijn gebruikt bij de interpretatie van de resultaten van veldwerk dat is uitgevoerd voor een kleiige bodem. De aeratie van deze bodem is bestudeerd door de plaats van de scheuren te vergelijken met de verspreiding van zuurstofloze grond. Er blijkt slechts een zwak verband te bestaan tussen het scheurenpatroon en de verdeling van anaerobie. Op verscheidene plaatsen komt zuurstofloze grond voor op minder dan 1 mm van een scheur. Zelfs voor verzadigde grond laat de gemeten bodemrespiratie nog een indringingsdiepte van 10 mm toe. Dat betekent dat de lokale aktiviteit tenminste een factor 100 hoger is dan de gemiddelde bodemrespiratie. Zoals hierboven uiteengezet verklaart een niet uniforme aktiviteit ook het ontbreken van een verband tussen het scheurenpatroon en de verspreiding van zuurstofloze grond. Een belangrijke consequentie van de aanwezigheid van zuurstofloze grond dichtbij scheuren is dat denitrifikatie kan plaatsvinden zónder diffusie van nitraat naar het centrum van een bodem-

aggregaat. Een zuurstofloze plek kan nitraat absorberen uit water dat dóór die plek stroomt.

De schaalmethode voor wortelstelsels en wormgangen

De schaalmethode is ook toegepast op het probleem van diffusie van nutrienten naar onregelmatig verspreide wortels. De eigenlijke berekeningen aan het diffusieproces worden weer uitgevoerd voor een modelsysteem inplaats van voor het echte wortelstelsel. Het modelsysteem bestaat cylinders met verschillende stralen. Elke cylinder bestaat uit grond en heeft een wortel langs de as. De cylinderstralen stellen weer de lengteschalen voor waarop de diffusie van nutrienten in het systeem plaats vindt en een gewichtsfunktie beschrijft het relatieve belang van elke straal of lengteschaal. De cylinders stellen dus niet de grond rondom individuele wortels voor. De opname van nutrienten door het hele wortelstelsel wordt berekend als een gewogen som van de resultaten voor de afzonderlijke cylinders van het modelsysteem.

De gewichtsfunktie wordt verkregen uit de statistische verdeling van de afstand van een punt van de bodem naar de dichtstbijzijnde wortelas. Vergelijkingen worden afgeleid voor het berekenen van een continue gewichtsfunktie uit een continue afstandsverdeling en voor het berekenen van een aantal discrete gewichten uit gemeten afstanden. De methode is toegepast op een model voor nutrientenopname dat uitgaat van een concentratie van nul aan het wortelоppervlak. Dat is een limietsituatie voor een wortelstelsel dat op elk moment zijn opname maximaliseert. Opnamen berekend voor random en geclusterede wortelverdelingen komen overeen met de resultaten uit de literatuur, die zijn verkregen met een elektrisch analogon. Behalve op wortelstelsels kan de ontwikkelde methode worden toegepast op wormgangen, bloedcapillairen en systemen met een gelijksoortige struktuur.

Het laatste hoofdstuk gaat over de aeratie van een homogene kleibodem met wormgangen, gelegen op de kwelder langs de dijk van Schiermonnikoog. Oorspronkelijk is de grond als gevolg van het aanwezige sulfide helemaal zwart geweest. Rondom de wormgangen is de grond echter geoxideerd en heeft een lichtere kleur gekregen. Op een horizontale doorsnede is een patroon van wormgangen, donkere grond en lichte grond goed zichtbaar. De gefotografeerde verdeling is geanalyseerd met behulp van een eenvoudig oxidatiemodel, dat is gemaakt voor random verdeelde gangen en dat rekening houdt met de waargenomen anisotropie van het systeem. Als wordt aangenomen dat de zuurstof over een vaste diepte in de grond is binnengedrongen, dan kan een voorspelling worden gemaakt over het patroon van wormgangen en geoxideerde grond dat verschijnt op een horizontale doorsnede. De resultaten van dat model

zijn vergeleken met waargenomen patronen. Het blijkt dat de aanname van een vaste indringingsdiepte niet realistisch is en dat andere factoren een rol spelen zoals verschillen in diameter en ouderdom tussen de wormgangen.

References

Abramowitz, M. and I. Stegun. 1970. Handbook of mathematical functions. Dover Publications, New York. 1046 pp.

Allmaras, R.R., R.E. Burwell, W.B. Voorhees and W.E. Larson. 1965. Aggregate size distribution in the row zone of tillage experiments. Soil Sci.Soc.Am.Proc.29:645–650.

Arah, J.R.M. and K.A. Smith. 1989. Steady–state denitrification in aggregated soils: a mathematical model. J. Soil Sci. 40:139–149.

Bakker, J.W., F.R.Boone and P.Boekel. 1987. Diffusie van gassen in grond en zuurstofdiffusiecoefficienten in Nederlandse akkerbouwgronden. Rapport 20, Instituut voor Cultuurtechniek en Waterhuishouding. Wageningen. 44 pp.

Bakker, J.W. and A.P.Hidding. 1970. The influence of soil structure and air content on gas diffusion in soils. Neth. J. Agric. Sci. 18:37-48.

Baldwin, J.P., P.B. Tinker and P.H. Nye. 1972. Uptake of solutes by multiple root systems from soil. II. The theoretical effects of rooting density and pattern on uptake of nutrients from soil. Plant and Soil 36:693-708.

Baldwin, J.P., P.H. Nye and P.B. Tinker. 1973. Uptake of solutes by multiple root systems from soil. III. A model for calculating the solute uptake by a randomly dispersed root system developing in a finite volume of soil. Plant and Soil 38:621-635.

Barber, S.A. 1962. A diffusion and mass-flow concept of soil nutrient availability. Soil Sci. 93:39-49.

Barley, K.P., 1970. The configuration of the root system in relation to nutrient uptake. Adv. Agron. 22:159-201.

Benson, B.B. and D. Krause. 1980. The concentration and isotopic fractionation of gasses dissolved in freshwater in equilibrium with the atmosphre. 1. Oxygen.Limnol. Oceanogr. 25:662-671.

Bird, R.B., W.E. Stewart and E.N. Lightfoot. 1960. Transport phenomena. Wiley & Sons, New York. 780 pp.

Bouldin, D.R. 1961. Mathematical description of diffusion processes in the soil–plant system. Soil Sci Soc. Am. Proc. 25:476-480.

Bouwman, L.A., A. van Klinken, P. de Ruiter and L. Brussaard. 1990. Mutual effects between wheat plants and microbivorous rhizosphere nematodes as observed in experimental growth systems (in prep).

Bratley, P., B.L.Fox and L.E.Schrage. 1987. A guide to simulation. Springer–Verlag. New York. 397 pp.

Bronswijk, J.J.B. 1991. Magnitude, modeling and significance of swelling and shrinkage processes in clay soils. Doctoral Thesis. Wageningen Agricultural University. Wageningen. 145 pp.

Chatfield, C. 1975. *The analysis of time series, an introduction.* Chapman and Hall, London, 286 pp.

Crank, J. 1956. The mathematics of diffusion. Clarendon Press. Oxford. 414 pp.

Currie, J.A. 1961. Gaseous diffusion in aeration of aggregated soils. Soil Sci. 92:40–45.

De Bakker , H. and J. Schelling. 1966. Systeem van bodemclassificatie voor Nederland : de hogere niveaus. Pudoc. Wageningen. 217 pp.

Delesse, M.A. 1847. Procédé mécanique pour déterminer la composition des roches.

C.R.Acad.Sci. (Paris) 25:544.
De Visser, C. 1958. Rapport van de bedrijfskartering van ' De Bouwing' in Randwijk. Stichting voor Bodemkartering. 5pp.
Diggle, P.J. 1978. On parameter estimation for spatial point processes. J. R. Statist. Soc. 40:178-181.
Diggle, P.J. 1983. Statistical analysis of spatial point patterns. Academic Press, London. 148 pp.
Gardner, W.R. 1956. Representation of soil aggregate–size distribution by a logarithmic–normal distribution. Soil Sci.Soc.Am.Proc.20:151–153.
Gilbert, E.N. 1962. Random subdivisions of space into crystals. Ann. Math. Stat. 33:958-972.
Glinski, J. and W. Stepniewski, 1985. Soil aeration and its role for plants. CRC Press. Boca Raton. Florida. 229 pp.
Grable, A.R. ,1966. Soil aeration and plant growth. Adv. Agron. 18:57-106.
Greenwood, D.J. 1961. The effect of oxygen concentration on the decomposition of organic materials in soil. Plant Soil 14:360–376.
Hogg, R.V. and A.T. Craig. 1978. Introduction to mathematical statistics. Macmillan Publishing Co., New York. 438 pp.
Koorevaar, P., G.Menelik and C.Dirksen. 1983. Elements of soil physics. Elsevier. Amsterdam. 228 pp.
Lang, S. 1970. Linear algebra. Addison–Wesley Publishing Company. Reading, Massachusetts. 400 pp.
Leffelaar, P.A. 1987. Dynamics of partial anaerobiosis, denitrification and water in a soil aggregate: simulation. Soil Sci. 146:427–444.
Methir, P.M. 1975. Computer processing of remotely sensed images. John Wiley & Sons. New York.
Nye, P.H. and P.B. Tinker. 1977. Solute movement in the soil-root system. Blackwell Scientific Publications, Oxford. 342 pp.
Ogston, A.G. 1958. The spaces in a uniform random suspension of fibres. Trans. Faraday Soc. 54:1754-1757.
Olsen, S.R. and W.D. Kemper. 1968. Movement of nutrients to plant roots. Adv. Agron. 20:91-151.
Press, W.H., B.P.Flannery, S.A.Teukolsky and W.T.Vetterling. 1986. Numerical Recipes, the art of scientific computing. Cambridge University Press. 818 pp.
Rappoldt, C. 1990. The application of diffusion models to an aggregated soil. Soil Science 150: 645-661.
Revsbech, N.P., Jørgensen, B.B., Blackburn, T.H. and Y.Cohen. 1983. Micro–electrode studies of the photosynthesis and O2, H2O and pH profiles of a microbial mat. Limnol.Oceanogr. 28:1062-1074.
Rolston, D.E. 1986. Gas diffusivity. In: Arnold Klute (Ed.) Methods of soil analysis, Part 1, Physical and mineralogical methods. American Society of Agronomy. Madison. 1188 pp.
Rowell, D.L., M.W. Martin and P.H. Nye. 1967. The measurement and mechanism of ion diffusion in soils. III. The effect of moisture content and soil solution concentration on the self-diffusion of ions in soils. J. Soil Sci. 18:204-222.
Sanders, F.E., P.B. Tinker and P.H. Nye. 1970. Uptake of solutes by multiple root systems from soil. I. An electrical analog of diffusion to root systems. Plant Soil 34: 453-466.
Seech, A.G. and E.G. Beauchamp. Denitrification in soil aggregates of different sizes. Soil Sci. Soc. Am. J. 52:1616-1621.
Scheid, F. 1968. Theory and problems of numerical analysis. 1968.

McGraw–Hill Book Company, New York. 422 pp.
Soil Survey Staff. 1951. Soil survey manual. US Dept. Agric. Handbook 18. Washington.
Soil Survey Staff. 1975. Soil taxonomy; a basic system of soil classification for making and interpreting soil surveys. Agric. Handbook 436. Soil Conservation Service. US Dept. Agric. Washington.
Smith, K.A. 1977. Soil aeration. Soil Sci. 123:284–291.
Stichting voor Bodemkartering, 1973. Bodemkaart van Nederland schaal 1:50 000. Toelichting bij de kaartbladen 39 West Rhenen en 39 Oost Rhenen. Wageningen. 193 pp.
Tardieu, F. 1989. Root system responses to soil structural properties: micro– and macro–scale. In: W.E. Larsen et al. (eds.), Mechanics and related processes in structured agricultural soils, Kluwer Academic Publishers.
Weibel, E.R. 1979. Stereological methods, Volume 1, Practical methods for biological morphometry. Academic Press. London.
Willigen, P. de and M. van Noordwijk. 1987. Roots, plant production and nutrient use efficiency. PhD thesis Agricultural University Wageningen, the Netherlands.
Youngs E.G. and W.R. Gardner. 1963. A problem of diffusion in the infinite hollow cylinder. Soil Sci. Soc. Amer. Proc. 27:475-476.

Curriculum vitae

Cornelis Rappoldt werd geboren op 27 februari 1954 te Naarden. Na het behalen van het diploma HBS-B in 1971 aan het Willem de Zwijgerlyceum te Bussum, begon hij met een studie natuurkunde aan de Rijksuniversiteit te Utrecht. Na vervulling van de dienstplicht werd in 1983 het doctoraal examen afgelegd met als hoofdvak experimentele natuurkunde en als bijvakken wiskunde en theoretische ecologie. In het kader van het hoofdvak werd 6 maanden gewerkt op de vakgroep Vaste Stof Fysica aan het bouwen van een opstelling voor para-electrische resonantie en 12 maanden op de vakgroep Theoretische Teeltkunde in Wageningen aan een onderwerp over de verspreiding van schimmelsporen in gewassen. Voor het bijvak theoretische ecologie werd gewerkt aan niche theorie.

In oktober 1985 trad hij in dienst van de Stichting Onderzoek Wereldvoedselvoorziening en werkte aan een model voor gewasgroei, in het bijzonder aan de statistische verdeling van regenval in het groeiseizoen. Vanaf augustus 1986 tot februari 1990 was hij als promotieassistent verbonden aan de vakgroep Theoretische Productie Ecologie van de Landbouwuniversiteit voor het verrichten van onderzoek aan het transport van zuurstof en water in gestruktureerde grond. Vanaf maart 1990 werkt hij op het Instituut voor Bodemvruchtbaarheid te Haren op de afdeling Bodemfysica.